NASA Contractor Report 2948

Pressure Distributions for the GA(W)-2 Airfoil With 20% Aileron, 25% Slotted Flap and 30% Fowler Flap

W. H. Wentz, Jr., and K. A. Fiscko

FOR EARLY DOMESTIC DISSEMINATION

NASA

NASA Contractor Report 2948

Pressure Distributions for the GA(W)-2 Airfoil With 20% Aileron, 25% Slotted Flap and 30% Fowler Flap

W. H. Wentz, Jr., and K. A. Fiscko
Wichita State University
Wichita, Kansas

NASA

National Aeronautics
and Space Administration

**Scientific and Technical
Information Office**

1978

FOR EARLY DOMESTIC DISSEMINATION

Because of its significant early commercial potential, this information, which has been developed under a U.S. Government program, is being disseminated within the United States in advance of general publication. This information may be duplicated and and used by the recipient with the express limitation that it not be published. Release of this information to other domestic parties by the recipient shall be made subject to these limitations. Foreign release may be made only with prior NASA approval and appropriate export licenses. This legend shall be marked on any reproduction of this information in whole or in part.

Date for general release: February 1980.

SUMMARY

Surface pressure distributions have been measured for the 13% thick GA(W)-2 airfoil section fitted with 20% aileron, 25% slotted flap and 30% Fowler flap. All tests were conducted at a Reynolds number of 2.2×10^6 and a Mach number of 0.13. Pressure distribution and force and moment coefficient measurements are compared with theoretical results for a number of cases. Agreement between theory and experiment is generally good for low angles of attack and small flap deflections. For high angles and large flap deflections where regions of separation are present, the theory is inadequate. Theoretical drag predictions are poor for all flap-extended cases.

INTRODUCTION

This report documents experimental surface pressure distributions for the GA(W)-2 airfoil section fitted with 20% aileron, 25% slotted flap, and 30% Fowler flap. Pressure distributions and aerodynamic characteristics of the basic GA(W)-2 airfoil section have been reported earlier (ref. 1). Wind tunnel force measurements of the airfoil with high-lift and control devices including optimizations of flap settings have been conducted at WSU, and the results of that research have been reported in ref. 2.

Theoretical computer calculations of pressure distributions using the methods of refs. 3 and 4 are presented for a number of cases. The purpose of the present research is to determine actual pressure distributions for the new airfoil with high-lift and control devices, and to compare both experimental pressure distributions and overall aerodynamic force and moment results with theoretical predictions.

SYMBOLS

Dimensional quantities are given in both International (SI) Units and U.S. Customary Units. Measurements were made in U.S. Customary Units. Conversion factors between the various units may be found in ref. 5. The symbols used in the present report are defined as follows:

c Airfoil reference chord (flap nested)

c_d Coefficient of drag, section drag/(c x dynamic pressure)

c_ℓ Coefficient of lift, section lift/(c x dynamic pressure)

c_m Pitching moment coefficient, section moment about .25c/(c^2 x dynamic pressure)

c_{m_a} Airfoil forward section moment coefficient, moment about leading edge/(c^2 x dynamic pressure)

c_{m_f} Flap moment coefficient, moment about leading edge/ (c^2 x dynamic pressure)

c_{n_a} Airfoil forward section normal force coefficient, normal force/ (c x dynamic pressure)

$c_{n_{ai}}$ Aileron normal force coefficient, normal force/ (c x dynamic pressure)

c_{n_f} Flap normal force coefficient, normal force/ (c x dynamic pressure)

c_p Coefficient of pressure, $(p - p_{\infty})$/dynamic pressure

ℓ_c Flap cove length

p Pressure

x Coordinate along airfoil chord

z Coordinate normal to airfoil chord

α Angle of attack, degrees

δ Rotation of control surface from nested position, degrees. (Trailing edge down is positive.)

Subscripts

a   Airfoil forward element

ai   Aileron

f   Flap

p   Pivot point for flap

∞ Free-stream conditions

APPARATUS AND TEST METHODS

Model Description

The GA(W)-2 airfoil section is a 13% maximum thickness air-foil section derived from the 17% GA(W)-1 section (ref. 6). For tests in the WSU two-dimensional facility, models are sized with 91.4 cm (36 inch) span and 61.0 cm (24 inch) chord. All models were equipped with 1.07 mm (0.042 inch) diameter pressure taps.

2

Model geometric details and flap pivot locations are given in figure 1.

Instrumentation

Pressure measurements were made using as many as 96 pressure channels multiplexed into 4 pressure transducers through a series of pressure switches. The unbonded-strain gage type transducers are connected to precision digital strain indicators for conversion from analog to digital data. The digital data are recorded on punch cards for off-line processing through the WSU Digital Computing Center. System resolution is ±2.4 newtons/meter^2 (0.05 psf) which corresponds to ±0.2% of dynamic pressure for the present tests. Figure 2 shows a pressure measurement schematic.

Test Procedure

All tests were conducted at a Reynolds number of 2.2 x 10^6 and Mach number of 0.13. Transition strips consisting of 2.5 mm (.10 inch) wide strips of #80 carborundum grit were applied to the upper surface at 5% chord and to the lower surface at 10% chord. All pressure data have been converted to coefficient form. Tunnel dynamic pressure has been corrected for solid and wake blockage, and model angle of attack has been corrected for induced effects, using the linear correction methods of ref. 7. Surface pressure measurements were integrated numerically to calculate component normal force coefficients, and moment coefficients about the component leading edge or hingeline.

Wind Tunnel

The WSU Walter Beech Wind Tunnel is a closed return tunnel with atmospheric test section static pressure. With two-dimensional inserts installed the test section is 0.91 m x 2.13 m (3 ft x 7 ft). Complete description of the insert and calibration details are given in ref. 8.

THEORETICAL METHODS

For selected cases, studies have been conducted to determine theoretical pressure distributions and overall force coefficients for comparison with the experimental measurements. These theoretical studies were conducted utilizing sophisticated computing routines which include boundary layer effects. For the flap-nested configuration, the computations utilized the programs of refs. 3 and 4. The principal difference between these programs is that ref. 4 includes a drag computation by the Squire-Young method (see ref. 9), but is restricted to single-element analysis. The flap-extended configurations were analyzed by the program of ref. 3, which is capable of analyzing multi-element configurations, but does not utilize the Squire-Young drag computation.

As discussed in ref. 10, for improved simulation of pressures near the airfoil trailing edge of flap-extended configurations, the lower surface flow was assumed to separate at the entrance to the flap cove and reattach ahead of the slot lip. This technique for modeling involves using an effective cove shape derived by assuming a straight line from cove entrance to the 75% cove location, as shown in the sketch which follows:
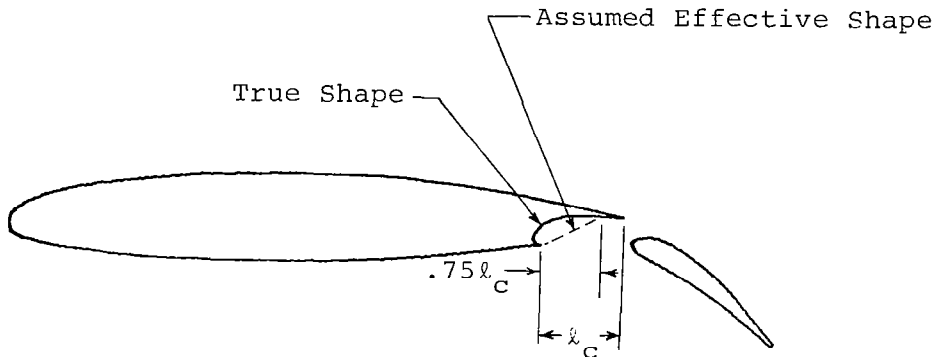
Sketch A - Flap Cove Theoretical Modeling

4

EXPERIMENTAL AND THEORETICAL RESULTS

Flap Nested

For the flap-nested configuration, data from the present
tests are compared with NASA data from ref. 1 and theoretical
results in figure 3. The two sets of experimental data show
good agreement at all angles up to 14°. At 18°, the NASA data
show more scatter than the WSU data, indicating a somewhat
less stable separation. Agreement between experiment and
theory is good for cases with little or no separation ($\alpha < 14°$).
For cases with separation ahead of .9 x/c, the theory is sub-
stantially in error.

20% Aileron

Pressure distributions with 20% aileron with 0.5% gap are
shown in figure 4 for aileron deflections from -60° to +60° and a
nominal angle of attack range of -8° to 16°. These data show
trends very similar to the pressure distribution results reported
earlier (ref. 10) for an aileron applied to the GA(W)-1 airfoil
section. For large aileron deflections ($\delta_a \geq 20°$) separated flow
on the suction side of the aileron is indicated, as evidenced
by a region of constant pressure. Because separation is ordi-
narily present for moderate and high aileron deflection, no
theoretical studies were conducted with aileron.

25% Slotted Flap

Experimental force characteristics for optimum flap settings
as reported in ref. 2 are shown in figure 5, along with theoret-
ical force characteristics for selected cases. The experimental
c_ℓ vs. α curve for 35° flap shows an increase in slope just prior
to stalling, an indication of flow improvement just prior to mas-
sive separation. During optimization force studies with 35° and
40° flap deflections, many non-linearities in force characteristics

were observed. This non-linear behavior is interpreted as evidence of separation over some portion of the airfoil or flap at virtually every angle of attack for these flap deflections. It is seen that the improvement in c_ℓ values between 30° and 35° flap is quite small, and the performance with 40° flap is essentially the same as 35° flap.

For the flap-nested case, the methods of refs. 3 and 4 are compared in figure 5. These data show that the Squire-Young drag computation routine of ref. 4 provides considerable improvement in drag prediction.

For angles of attack less than 10° and flap deflections less than 30°, theoretical lift and pitching moment agree reasonably well with experiment. For higher angles of attack and flap deflections the agreement becomes progressively poorer. These trends are attributed to inadequate theoretical modeling for situations with nearly-separated or partially-separated boundary layers. The theoretical drag predictions are poor for all flap-extended cases. The theory is very inconsistent, even predicting a reduction in drag as flap deflection is increased in some instances.

Theoretical pressure distributions are presented in figures 6 through 9. The results of these theoretical studies compare quite favorably with experiment for angles of attack below stall, and lower flap deflections. For higher angles of attack or flap deflection angles, the agreement becomes progressively poorer.

Detailed experimental pressure distributions for this configuration for optimum flap settings are presented in figure 10. For flap deflections up to 20°, the pressure data indicate attached flow for angles of attack up to 12°. For 30° flap deflection, flow separation on the flap is indicated at 16.2° angle of attack, and a large step in pressure is indicated on the airfoil upper surface. This condition is beyond $c_{\ell max}$ as indicated by the force data of figure 5. The apparent jump in pressure at about 20% chord is attributed to an unsteady flow situation with

6

intermittent separation, and is believed to be associated with the slow-scan method of pressure recording utilized for these tests.

For 35° flap, the flap flow tends to separate at the trailing edge at the lower angles of attack. At higher angles, the flap flow improves.

The situation with 40° flap is very similar to 35° flap. In this case, the flap is evidently fully attached only at 12.2°, and re-separates at 14.4°. These observations for 35° and 40° flap correlate very well with trends observed in the force measurements.

30% Fowler Flap

Results of optimum force tests for this flap from ref. 2 are shown in figure 11, along with theoretical results for selected cases. As with 25% flap, the theory significantly over-predicts lift at high angles of attack and high flap deflections.

Close comparison of the flap-nested data from the 25% and 30% flap models (figures 5 and 11) shows that the 30% flap model provides slightly more lift at low angles than the 25% flap model, even though $c_{\ell max}$ and stalling angle are unchanged. The 30% flap model had a clean, continuous upper surface while the 25% model had a slight step at the spoiler trailing edge, and four spoiler hinges which created small protuberances at four span-wise stations. The differences in aerodynamic data are attributed to these geometric variations.

Experimental pressure distributions are compared with theory in figures 12 through 15. Again, the principal disparities occur at high angles and large flap deflections.

Detailed experimental pressure distributions for various flap settings are shown in figure 16. For flap deflections up to 30°, the distributions indicate attached flow on both airfoil and flap for all but the highest angles of attack. For 35° and 40° flap deflections the distributions indicate separation

7

on the flap at most angles of attack. At the post-stall ($\alpha = 12.3°$) condition, separation is indicated over the aft half of the flap, and the airfoil forward section pressure shows a jump indicating an unstable pressure distribution as discussed with the 25% flap.

CONCLUSIONS

1. Pressure distributions for the GA(W)-2 airfoil with 20% aileron show trends similar to the GA(W)-1 airfoil with aileron.

2. Lift and pitching moment predictions from theory agree reasonably well with experimental measurements for α less than 10° and flap deflections less than 35°. For cases with nearly separated or partially separated boundary layers, present theories are inadequate.

3. Drag prediction using the Squire-Young formulation is adequate for single-element airfoils without separation. The multi-element drag computation is poor for all cases.

4. Pressure distributions for the GA(W)-2 airfoil with 25% and 30% flaps show good agreement with theory at low angles and small flap deflections, but poor agreement for high angle or large flap deflection cases which involve flow separation.

REFERENCES

1. McGhee, R.J.; Beasley, W.D. and Somers, D.M.: Low-Speed Aerodynamic Characteristics of a 13-Percent-Thick Airfoil Section Designed for General Aviation Applications. NASA TMX-72697.

2. Wentz, W.H., Jr.: Wind Tunnel Tests of the GA(W)-2 Airfoil with 20% Aileron, 25% Slotted Flap, 30% Fowler Flap, and 10% Slot-Lip Spoiler. NASA CR-145139, 1977.

3. Stevens, W.A.; Goradia, S.H. and Braden, J.A.: Mathematical Model for Two-Dimensional Multi-Component Airfoils in Viscous Flow. NASA CR-1843, 1971.

4. NASA Langley Research Staff: Viscous Flow Single-Element Airfoil Analysis Computing Routine (Program AIRFOIL), 1976.

5. Mechtly, E.A.: The International System of Units - Physical Constants and Conversion Factors (Revised). NASA SP-7012, 1969.

6. McGhee, R.J. and Beasley, W.D.: Low-Speed Aerodynamic Characteristics of a 17-Percent-Thick Airfoil Section Designed for General Aviation Applications. NASA TND-7428, 1973.

7. Pope, A. and Harper, J.J.: Low-Speed Wind Tunnel Testing, John Wiley and Sons, 1966.

8. Siew, R.J.: Calibration of a Two-Dimensional Insert for the WSU 7' x 10' Wind Tunnel, AR 73-2, Wichita State University, 1973.

9. Schlichting, H.: Boundary Layer Theory. McGraw-Hill Book Co., Sixth edition, 1968.

10. Wentz, W.H., Jr.; Seetharam, H.C. and Fiscko, K.A.: Force and Pressure Tests of the GA(W)-1 Airfoil with a 20% Aileron and Pressure Tests with a 30% Fowler Flap. NASA CR-2833, 1977.
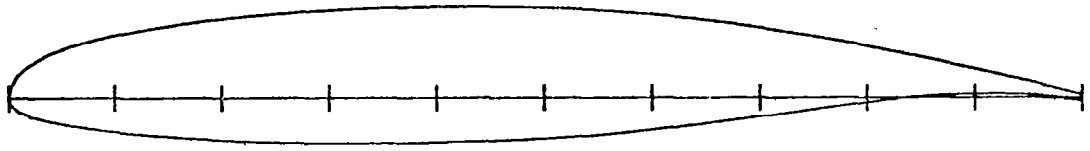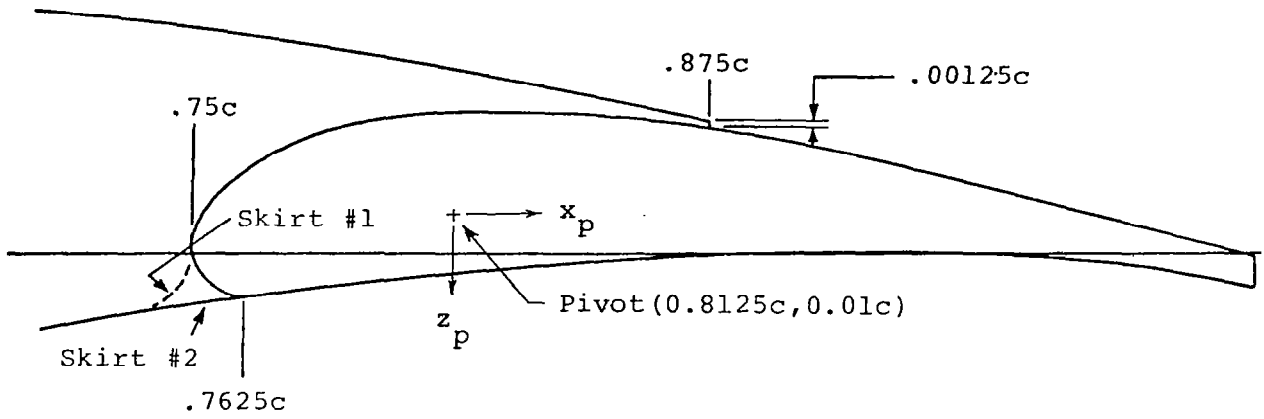
UPPER SURFACE		LOWER SURFACE	
x/c	z/c	x/c	z/c
0.0000	0.0000	0.0000	0.0000
.0020	.0103	.0020	-.0066
.0050	.0163	.0050	-.0097
.0125	.0246	.0125	-.0144
.0250	.0336	.0250	-.0188
.0375	.0400	.0375	-.0223
.0500	.0451	.0500	-.0250
.0750	.0528	.0750	-.0294
.1000	.0588	.1000	-.0328
.1250	.0637	.1250	-.0357
.1500	.0677	.1500	-.0380
.1750	.0712	.1750	-.0398
.2000	.0742	.2000	-.0415
.2500	.0788	.2500	-.0438
.3000	.0820	.3000	-.0449
.3500	.0840	.3500	-.0452
.4000	.0849	.4000	-.0449
.4500	.0846	.4500	-.0437
.5000	.0833	.5000	-.0417
.5500	.0807	.5500	-.0386
.5750	.0789	.5750	-.0362
.6000	.0767	.6000	-.0337
.6250	.0739	.6250	-.0307
.6500	.0708	.6500	-.0276
.6750	.0672	.6750	-.0243
.7000	.0633	.7000	-.0210
.7250	.0591	.7250	-.0175
.7500	.0545	.7500	-.0143
.7750	.0497	.7750	-.0110
.8000	.0447	.8000	-.0078
.8250	.0395	.8250	-.0051
.8500	.0341	.8500	-.0028
.8750	.0285	.8750	-.0012
.9000	.0228	.9000	.0000
.9250	.0170	.9250	.0001
.9500	.0110	.9500	-.0007
.9750	.0049	.9750	-.0028
1.0000	-.0015	1.0000	-.0071

(a) Basic GA(W)-2 Airfoil.

Figure 1 - Geometry.

0.005c

$r_1 = 0.0263c$

$r_2 = 0.0313c$

Chord Line

r_1

r_2

0.0184c

0.20c
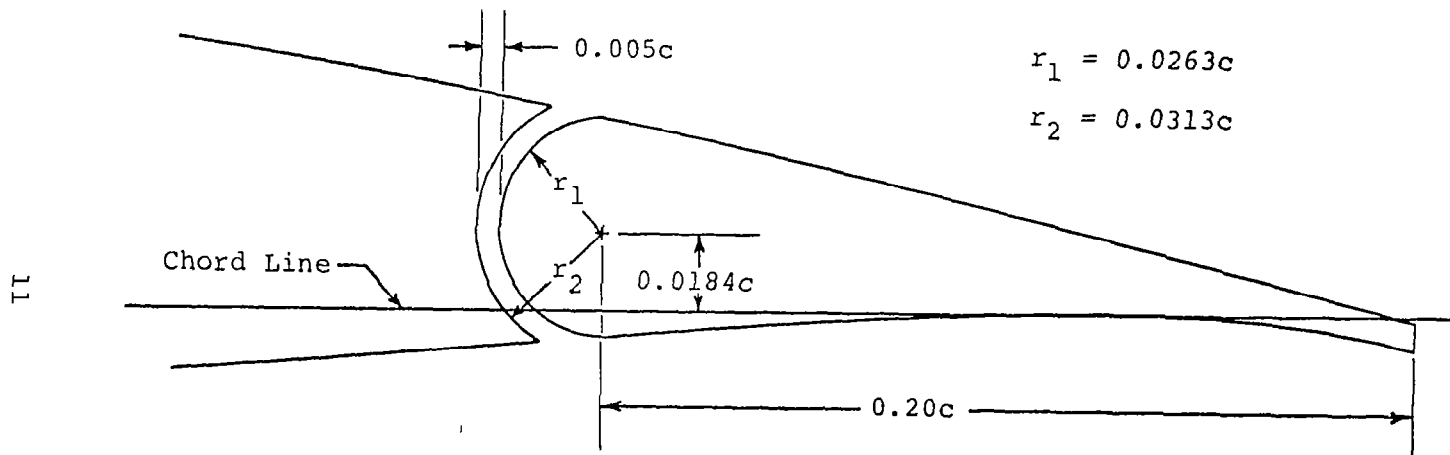
(b) 20% Aileron.

Figure 1 - Continued.

Flap Upper Surface

x/c	z/c
0.7500	−0.0010
.7531	0.0072
.7562	.0109
.7593	.0138
.7625	.0164
.7750	.0234
.7875	.0276
.8000	.0298
.8125	.0307
.8250	.0308
.8375	.0306
.8500	.0302
.8625	.0288
.8742	.0271
.8875	.0250
.8992	.0229

Nose Radius = 0.012c

Nose Radius Location
(x/c,z/c) = (0.762c,−0.00087c)
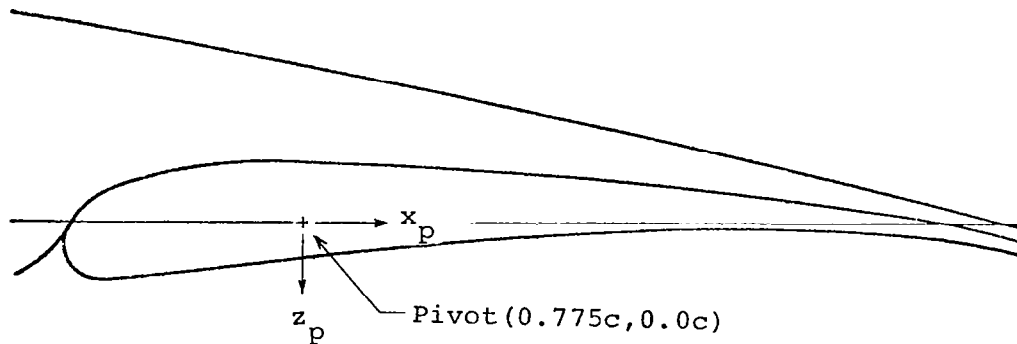
Note: Remainder of flap
contour matches basic airfoil.

Skirt #1

Radius = 0.012c

Location (x/c,z/c) = (0.738c,−0.00087c)

(c) 25% Slotted Flap.

Figure 1 — Continued.

12

Pivot(0.775c,0.0c)

Skirt			Flap Upper Surface	
x/c	z/c		x/c	z/c
.675	−.0231		.700	−.0069
.680	−.0215		.705	.0030
.685	−.0204		.710	.0075
.690	−.0158		.720	.0119
.700	−.0105		.740	.0171
.705	.0030		.760	.0194
			.775	.0190
			.800	.0184
			.825	.0172
			.850	.0156
			.875	.0137
			.900	.0114
			.925	.0086
			.950	.0051
			.975	.0014
			1.000	−.0044

Nose Radius = 0.0117c

Nose Radius Location (x/c,z/c) = (0.7119c,−0.0071c)

Note: Remainder of Flap contour matches basic airfoil.

(d) 30% Fowler Flap.

Figure 1 - Continued.

13

Airfoil with
Pressure Tubes

Model

96 Pressure Tubes ⟶

24 Pressure Tubes ⟶

4 Pressure Switches

| S1 | S2 | S3 | S4 |

Pressure Data System

Pressure Tube

4 Pressure Transducers

| T1 | T2 | T3 | T4 |

Electrical Signal

4-Channel
Digital Strain Indicator

| #1 | #2 | #3 | #4 |

Analog to Digital
and Recording

Card
Punch

Punch

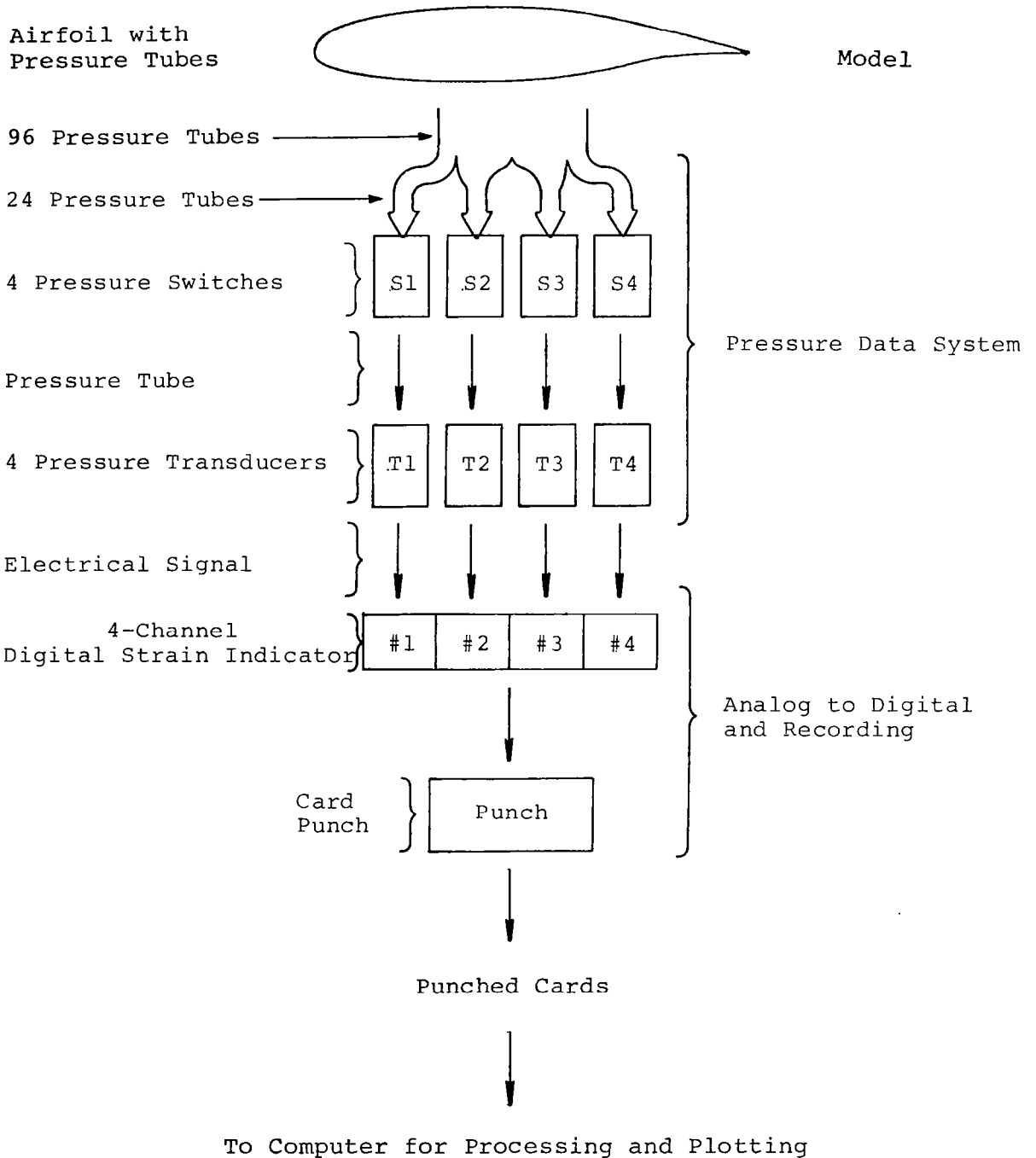Punched Cards

To Computer for Processing and Plotting

Figure 2 - Pressure Measurement System Schematic.

14

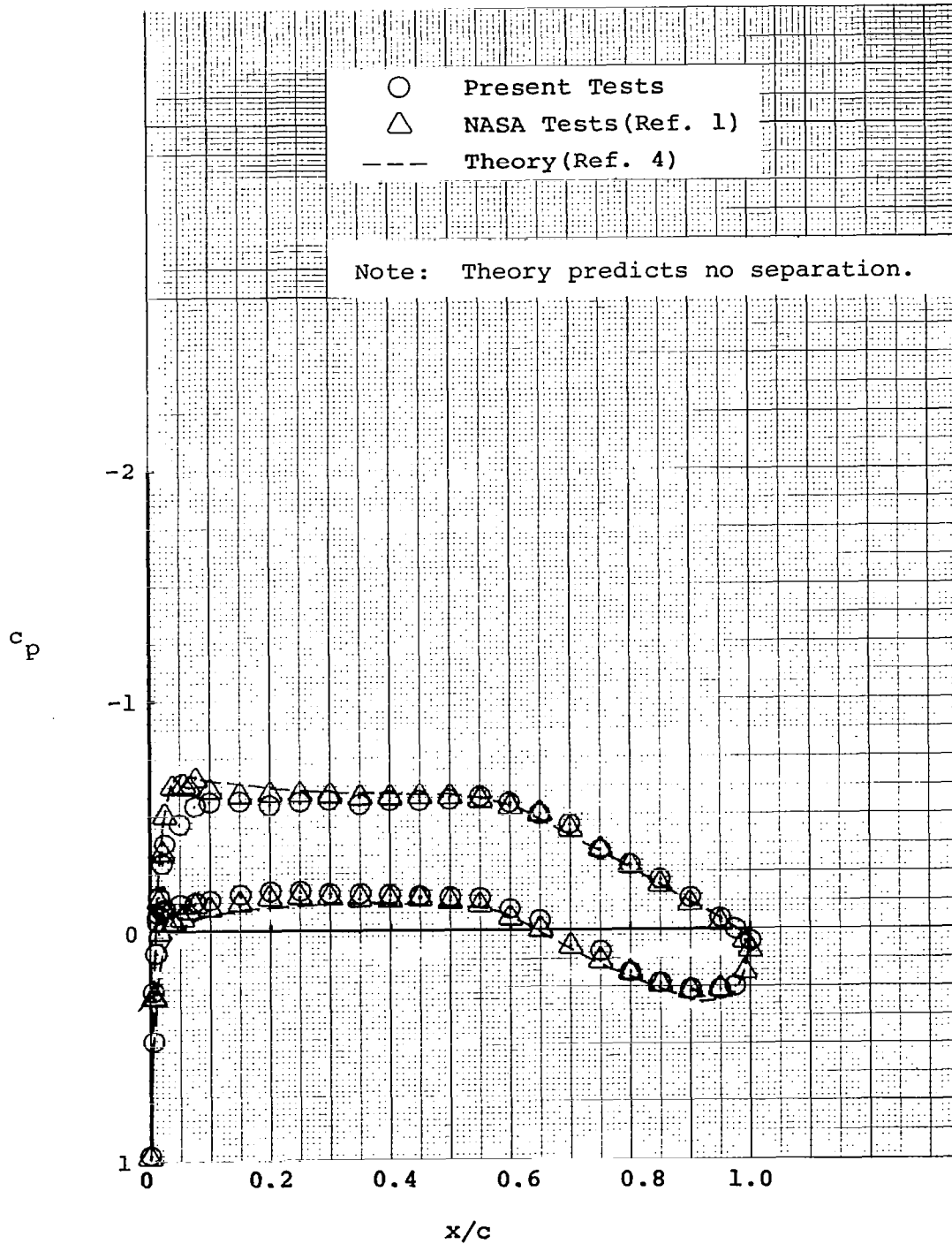(a) $\alpha \approx 0°$

Figure 3 - Comparisons of Pressure Measurements with Theory
and NASA experiments.

15

(b) $\alpha \simeq 8°$

Figure 3 - Continued.

16

(c) $\alpha \approx 10°$

Figure 3 - Continued.

17

(d) $\alpha \approx 14°$

Present Tests
NASA Tests (Ref. 1)
Theory (Ref. 4)

Note: Theory predicts separation at $x/c = .81$ (upper surface).

c_p

x/c

Figure 3 - Continued.

18

(e) $\alpha \approx 18°$

○ Present Tests
△ NASA Tests (Ref. 1)
– – – Theory (Ref. 4)

Note: Theory predicts separation at
x/c = .67 (upper surface).
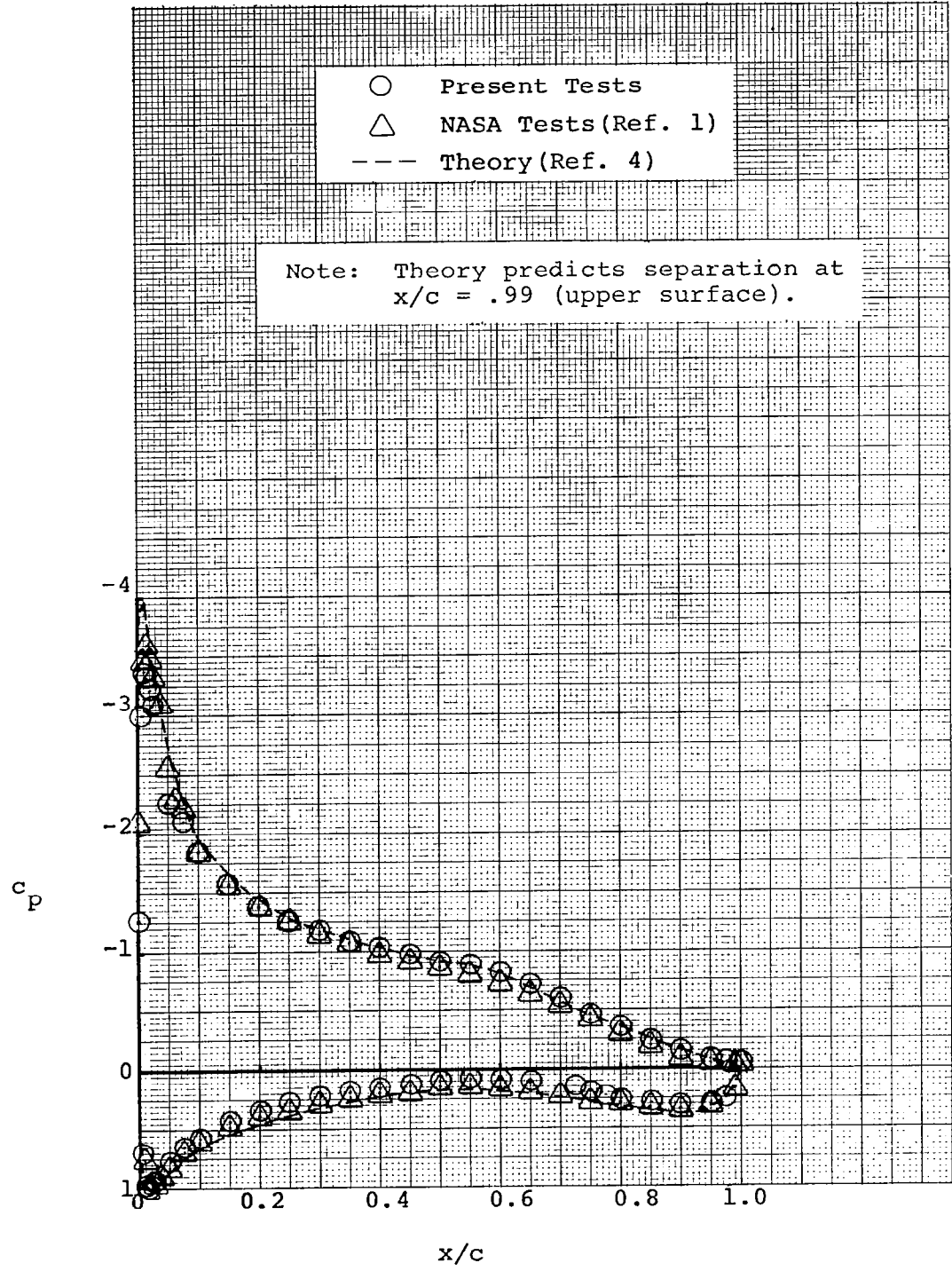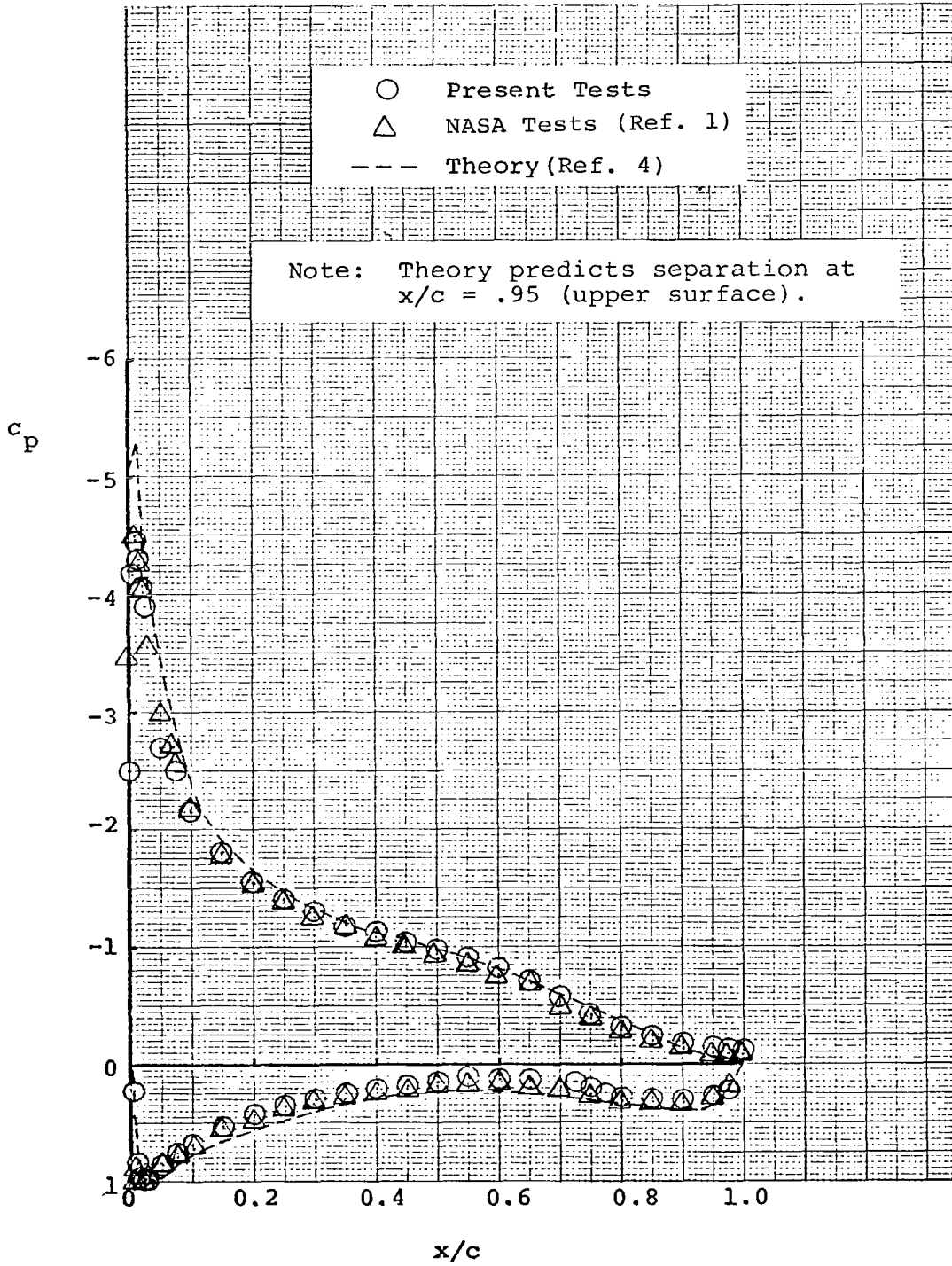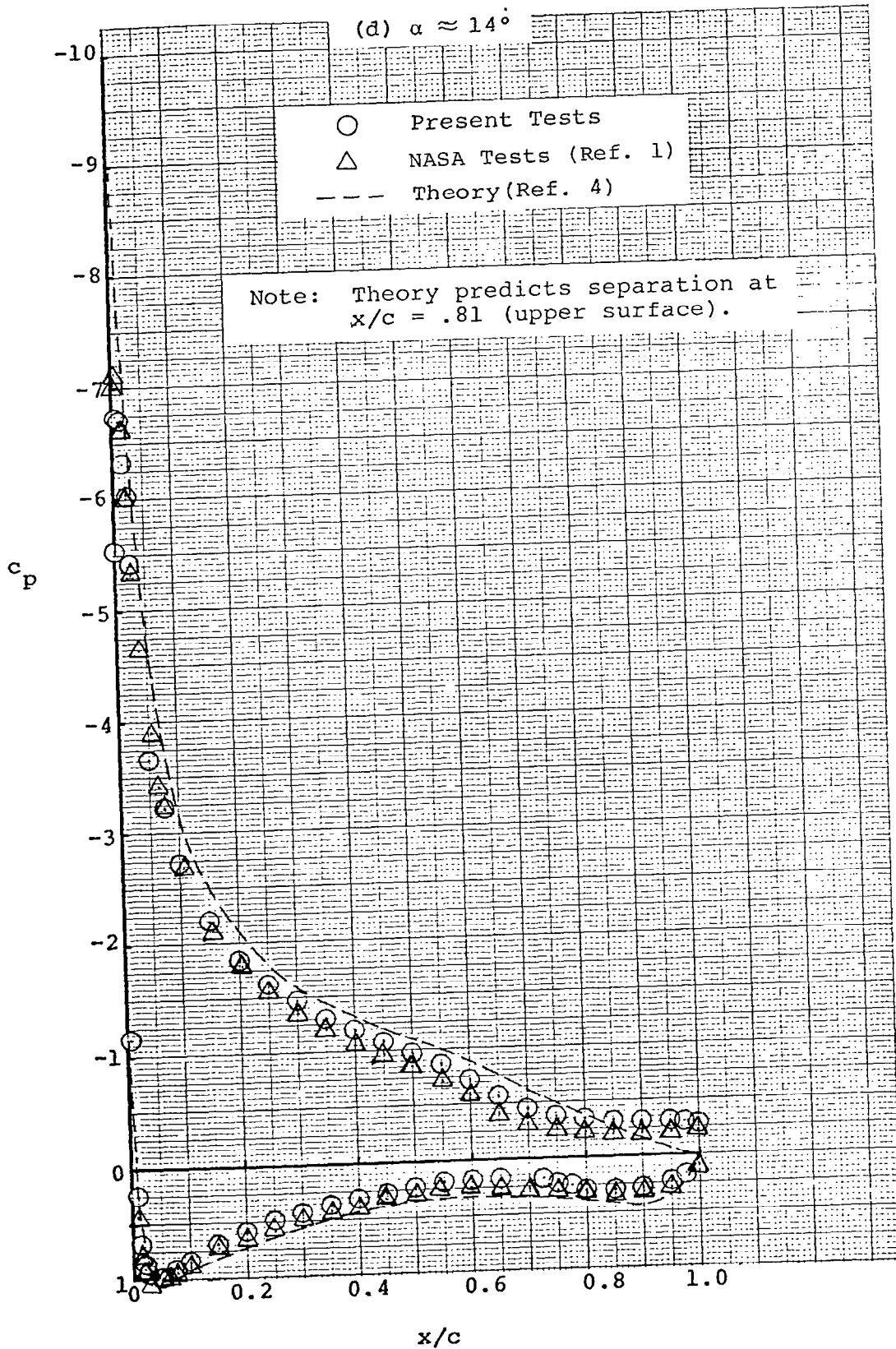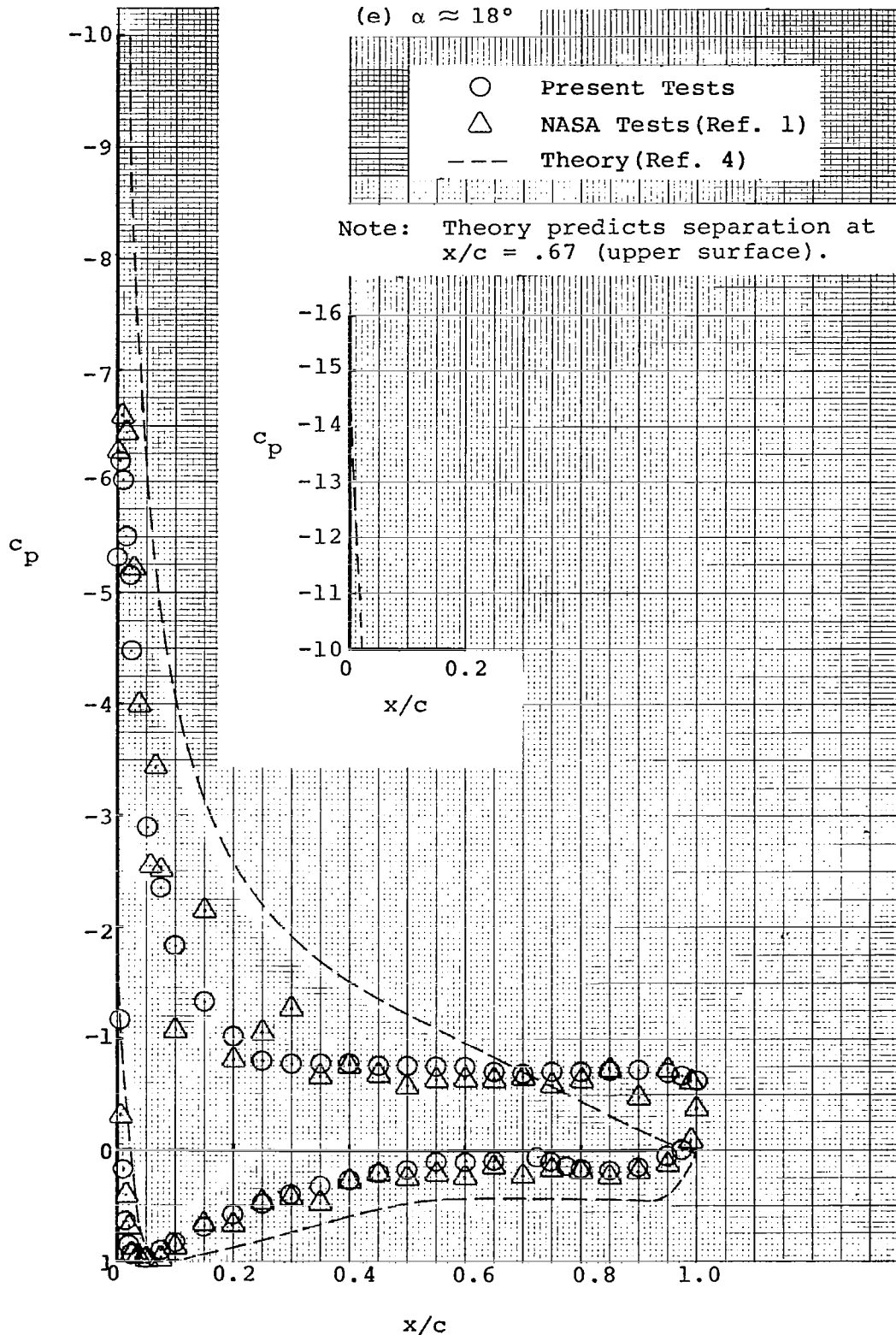
Figure 3 - Concluded.

(a) AILERON DEFLECTION = 0.0 DEGREES

MACH NO. = 0.13

REYNOLDS NO. = 2.2 E 06

SYMBOL	ALPHA	c_{n_a}	$c_{n_{ai}}$
+	-7.9°	-.55	.04
×	0.2°	.27	.09
▷	8.3°	1.08	.10
▼	12.4°	1.43	.11
◀	16.4°	1.64	.13

Flagged Symbols Denote
Lower Surface Pressures

-8.00

-7.00

-6.00

-5.00

C_P

-4.00

-3.00

-2.00

-1.00

0.00

1.00

X/C   0.80   1.00

Figure 4 - Pressure Distributions with 20% Aileron.
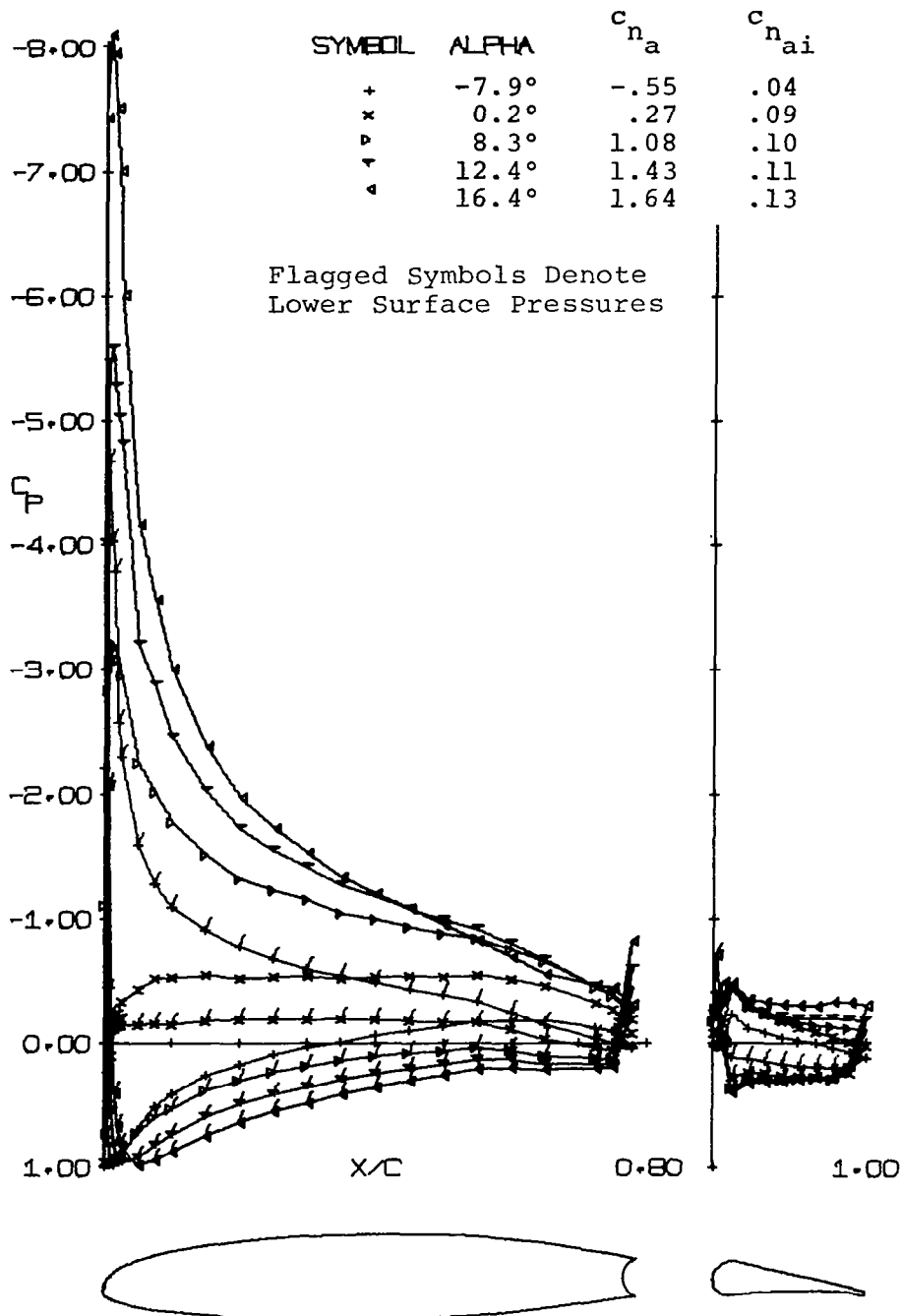
(b) AILERON DEFLECTION = 5.0 DEGREES

MACH NO. = 0.13

REYNOLDS NO. = 2.2 E 06

SYMBOL	ALPHA	c_{n_a}	$c_{n_{ai}}$
+	-7.9°	-.38	.09
×	0.2°	.45	.12
▷	8.3°	1.24	.13
▼	12.4°	1.61	.14
◁	16.4°	1.80	.15
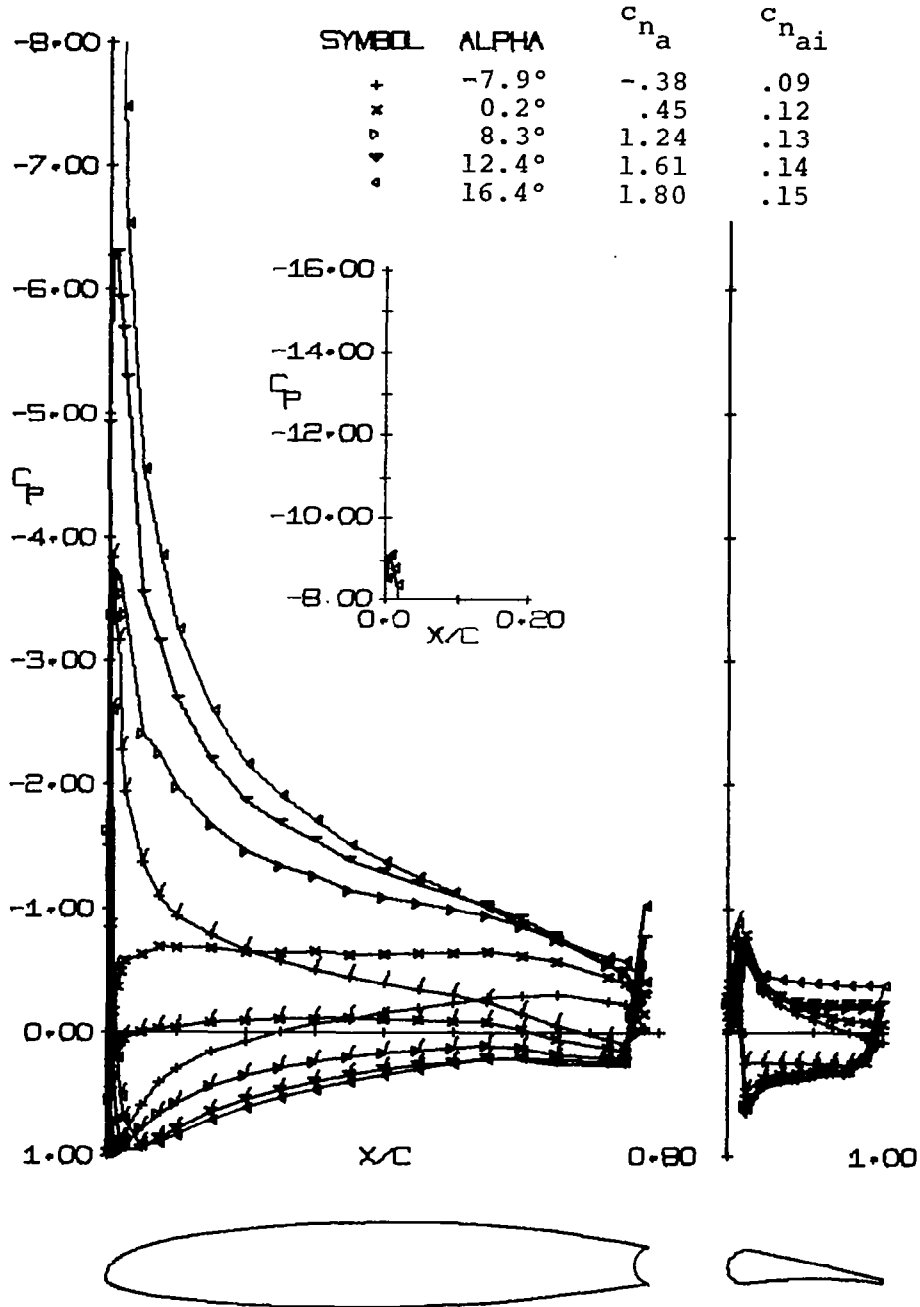
Figure 4 - Continued.

(c) AILERON DEFLECTION = 10.0 DEGREES

MACH NO. = 0.13

REYNOLDS NO. = 2.2 E 06

SYMBOL	ALPHA	c_{n_a}	$c_{n_{ai}}$
+	-7.9°	-.25	.11
×	0.2°	.59	.14
▷	8.3°	1.39	.16
▼	12.4°	1.77	.16
◀	16.4°	1.95	.18
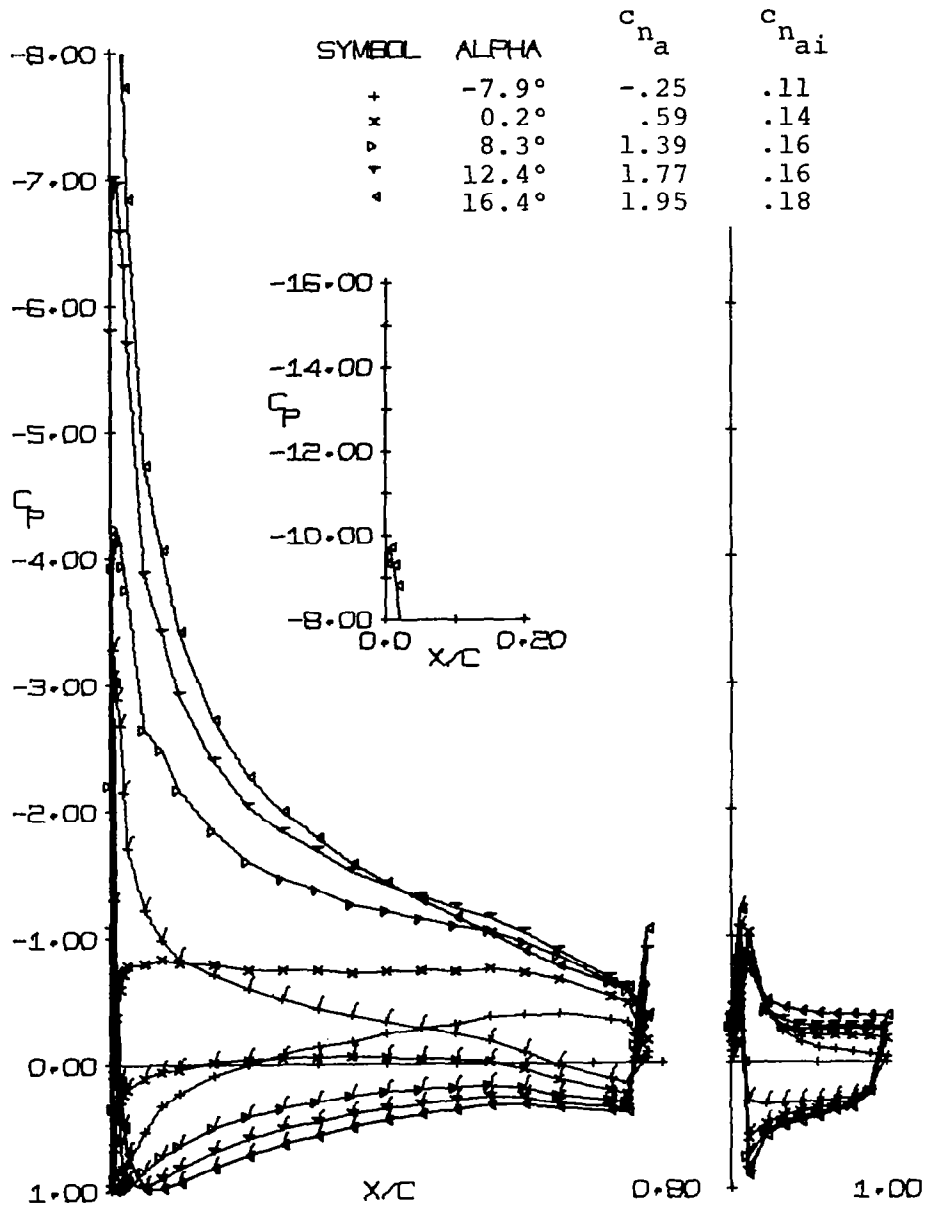
Figure 4 - Continued.

(d) AILERON DEFLECTION = 20.0 DEGREES
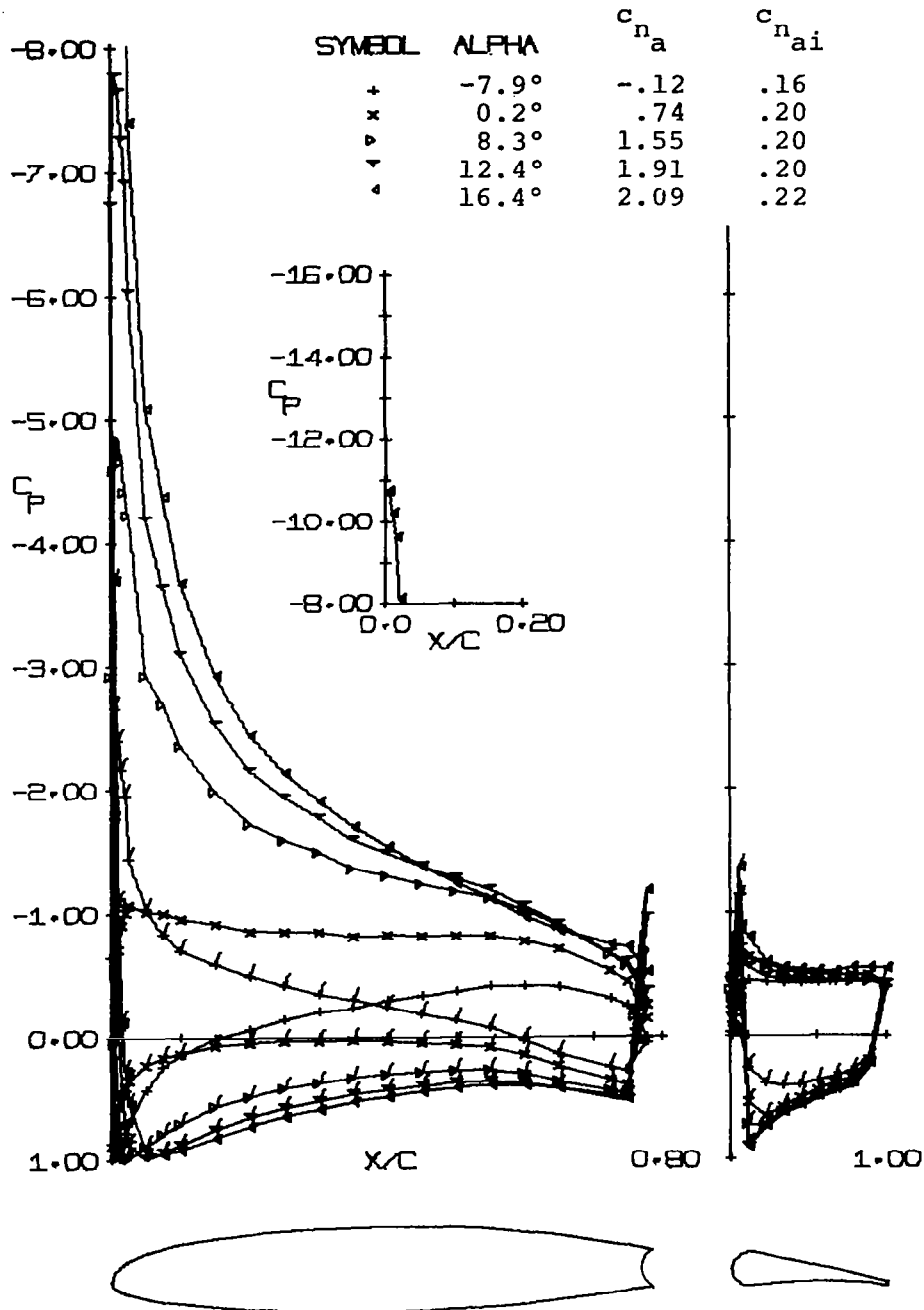
MACH NO. = 0.13

REYNOLDS NO. = 2.2 E 06

SYMBOL	ALPHA	c_{n_a}	$c_{n_{ai}}$
+	-7.9°	-.12	.16
×	0.2°	.74	.20
▷	8.3°	1.55	.20
▼	12.4°	1.91	.20
◀	16.4°	2.09	.22

-8.00
-7.00
-6.00
-5.00
C_P
-4.00
-3.00
-2.00
-1.00
0.00
1.00

-16.00
-14.00
C_P
-12.00
-10.00
-8.00

0.0   0.20

X/C

X/C   0.80   1.00

Figure 4 - Continued.

23

(e) AILERON DEFLECTION = 40.0 DEGREES

MACH NO. = 0.13

REYNOLDS NO. = 2.2 E 06

SYMBOL	ALPHA	c_{n_a}	$c_{n_{ai}}$
+	-7.9°	.27	.24
x	0.2°	1.12	.27
▶	8.3°	1.93	.26
▼	12.4°	2.27	.25
◀	16.4°	2.45	.23
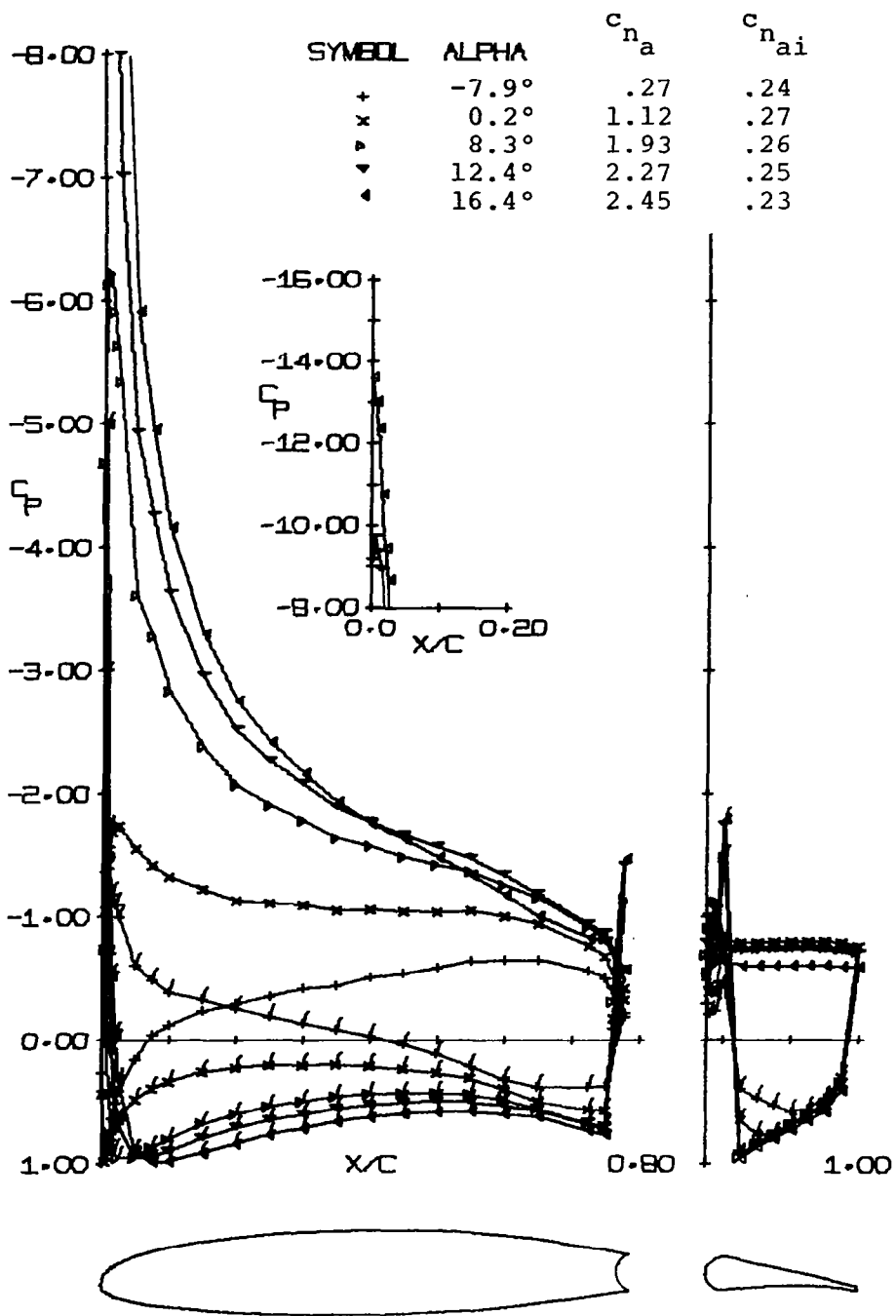
Figure 4 - Continued.

(f) AILERON DEFLECTION = 60.0 DEGREES
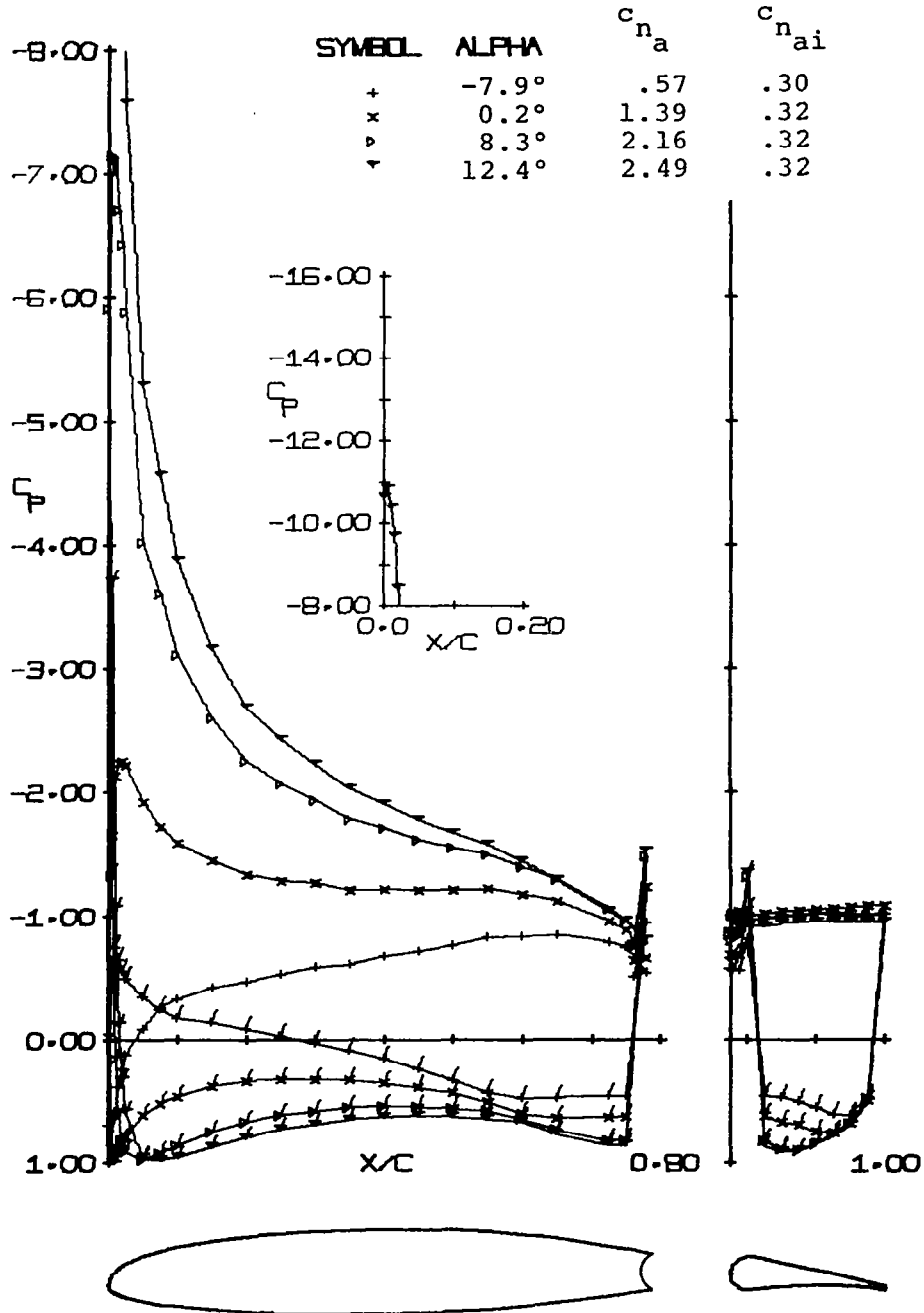
MACH NO. = 0.13

REYNOLDS NO. = 2.2 E 06

SYMBOL	ALPHA	c_{n_a}	$c_{n_{ai}}$
+	-7.9°	.57	.30
x	0.2°	1.39	.32
▷	8.3°	2.16	.32
▼	12.4°	2.49	.32

Figure 4 - Continued.

MACH NO. = 0.13

REYNOLDS NO. = 2.2 E 06

SYMBOL	ALPHA	c_{n_a}	$c_{n_{ai}}$
+	-7.9°	-.62	.00
×	0.2°	.09	.04
▷	8.3°	.92	.08
▼	12.4°	1.27	.09
◀	16.4°	1.50	.11
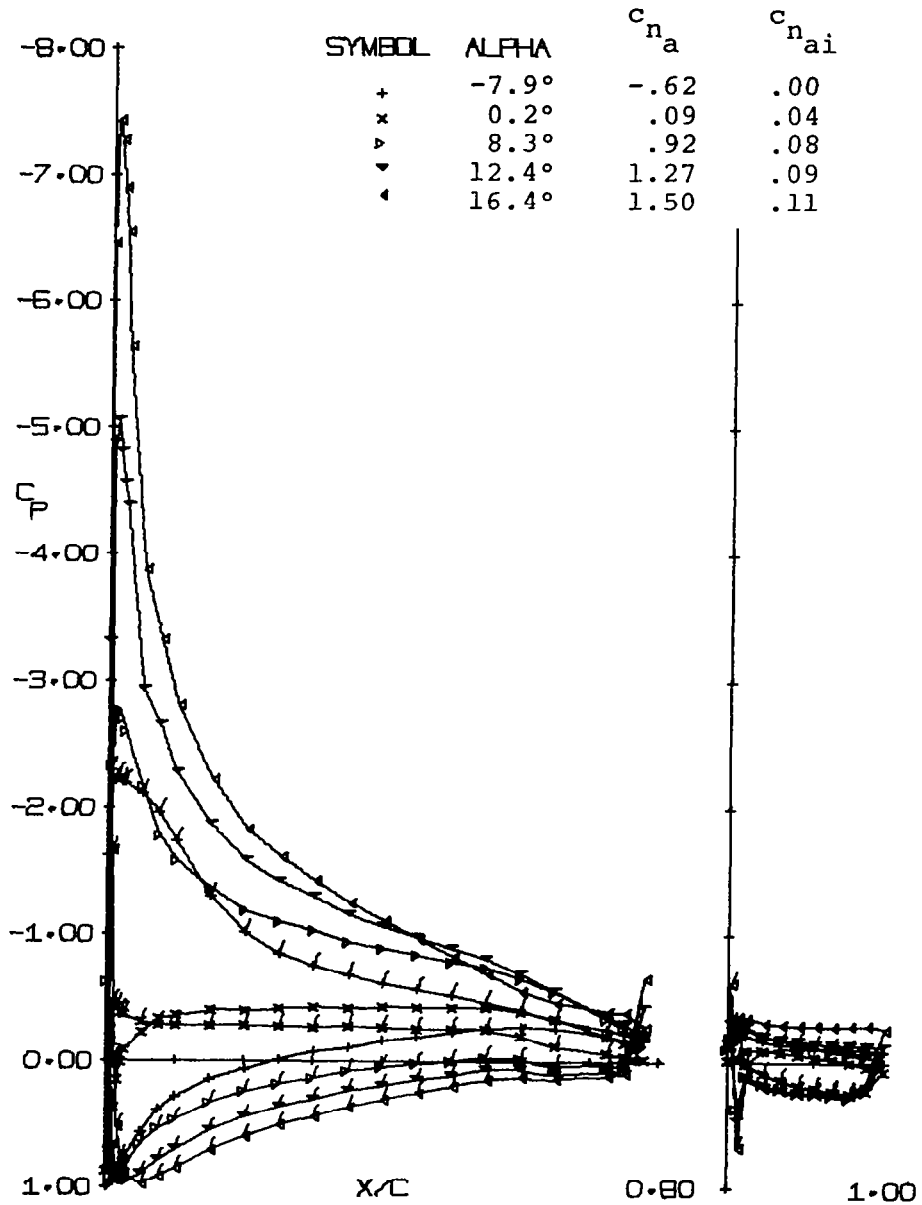
Figure 4 - Continued.

(h) AILERON DEFLECTION = -10.0 DEGREES
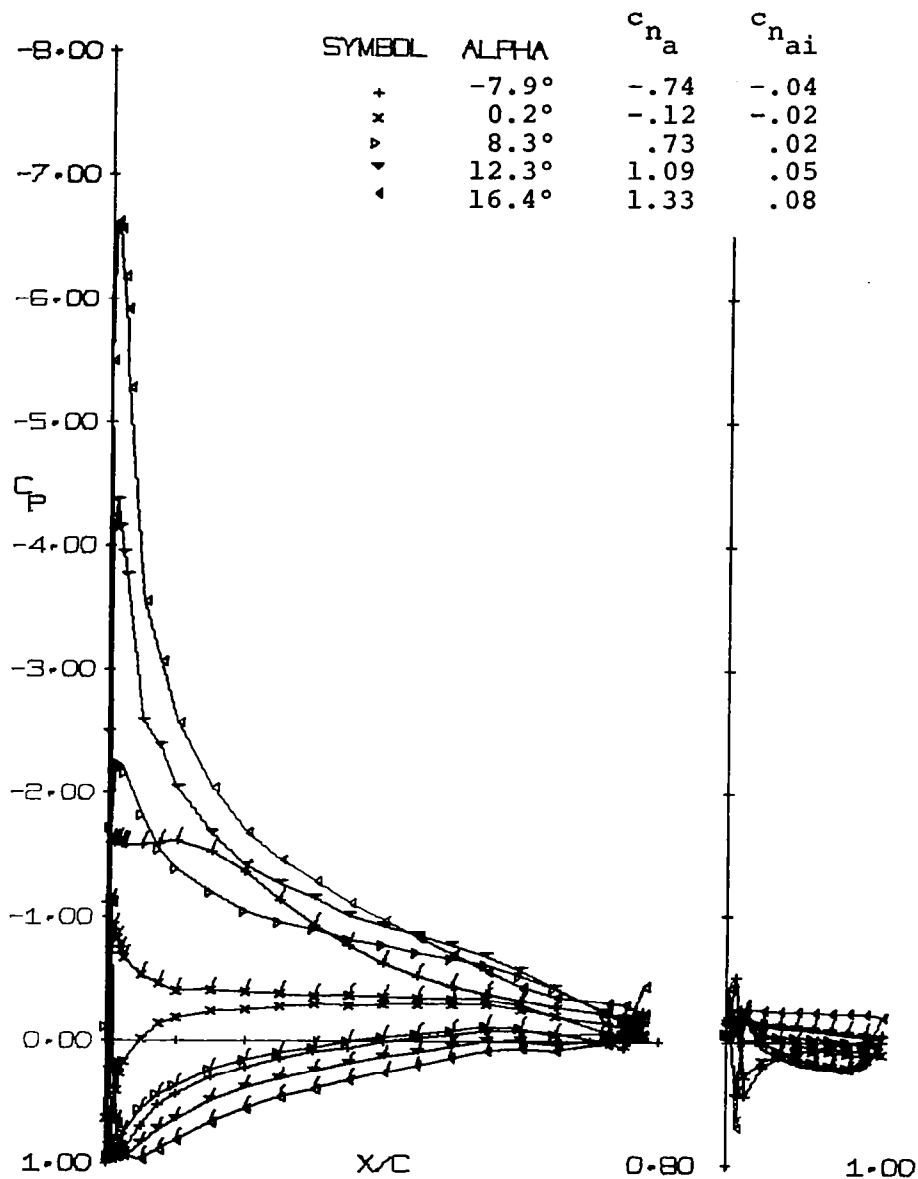
MACH NO. = 0.13

REYNOLDS NO. = 2.2 E 06

SYMBOL	ALPHA	c_{n_a}	$c_{n_{ai}}$
+	-7.9°	-.74	-.04
×	0.2°	-.12	-.02
▷	8.3°	.73	.02
▼	12.3°	1.09	.05
◀	16.4°	1.33	.08

Figure 4 - Continued.

27

(i) AILERON DEFLECTION = -20.0 DEGREES

MACH NO. = 0.13

REYNOLDS NO. = 2.2 E 06

SYMBOL	ALPHA	c_{n_a}	$c_{n_{ai}}$
▸	-7.9°	-.91	-.10
✗	0.2°	-.34	-.08
▹	8.3°	.40	-.09
▾	12.3°	.75	-.06
◂	16.4°	1.06	-.01

Figure 4 - Continued.

28

(j) AILERON DEFLECTION = -40.0 DEGREES

MACH NO. = 0.13

REYNOLDS NO. = 2.2 E 06

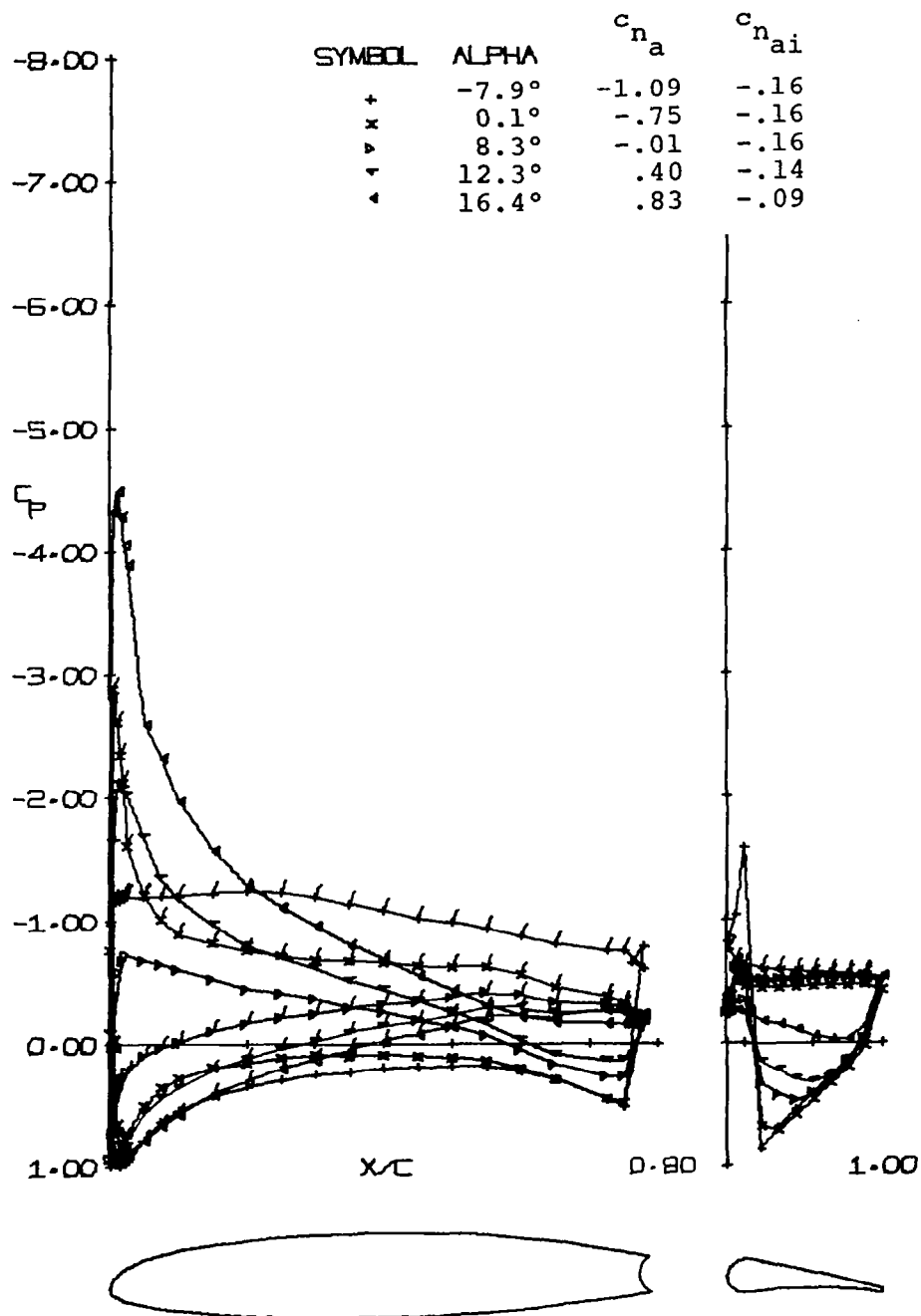| SYMBOL	ALPHA	c_{n_a}	$c_{n_{ai}}$
+	-7.9°	-1.09	-.16
×	0.1°	-.75	-.16
▷	8.3°	-.01	-.16
▽	12.3°	.40	-.14
◁	16.4°	.83	-.09
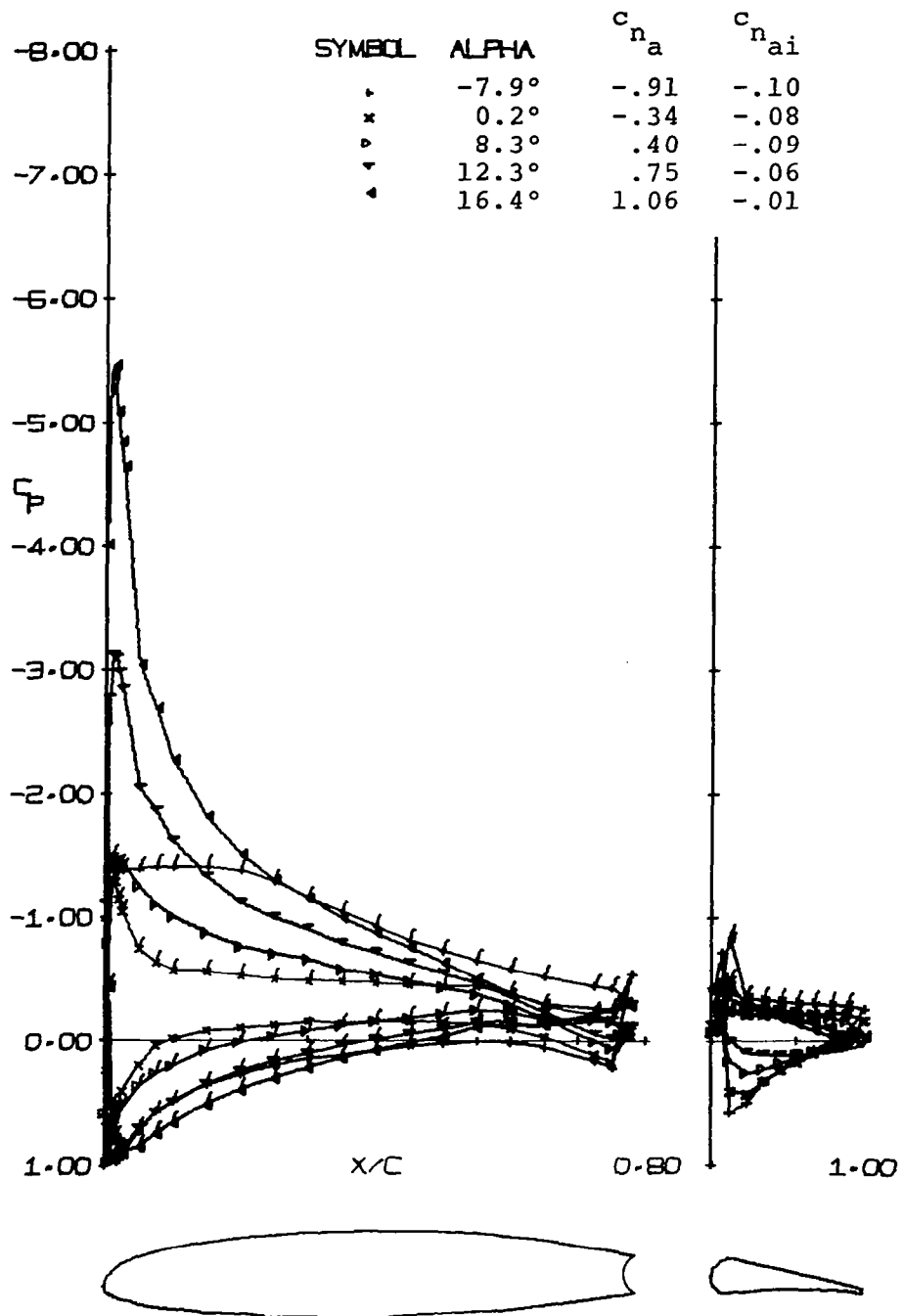
Figure 4 - Continued.

(k) AILERON DEFLECTION = -60.0 DEGREES
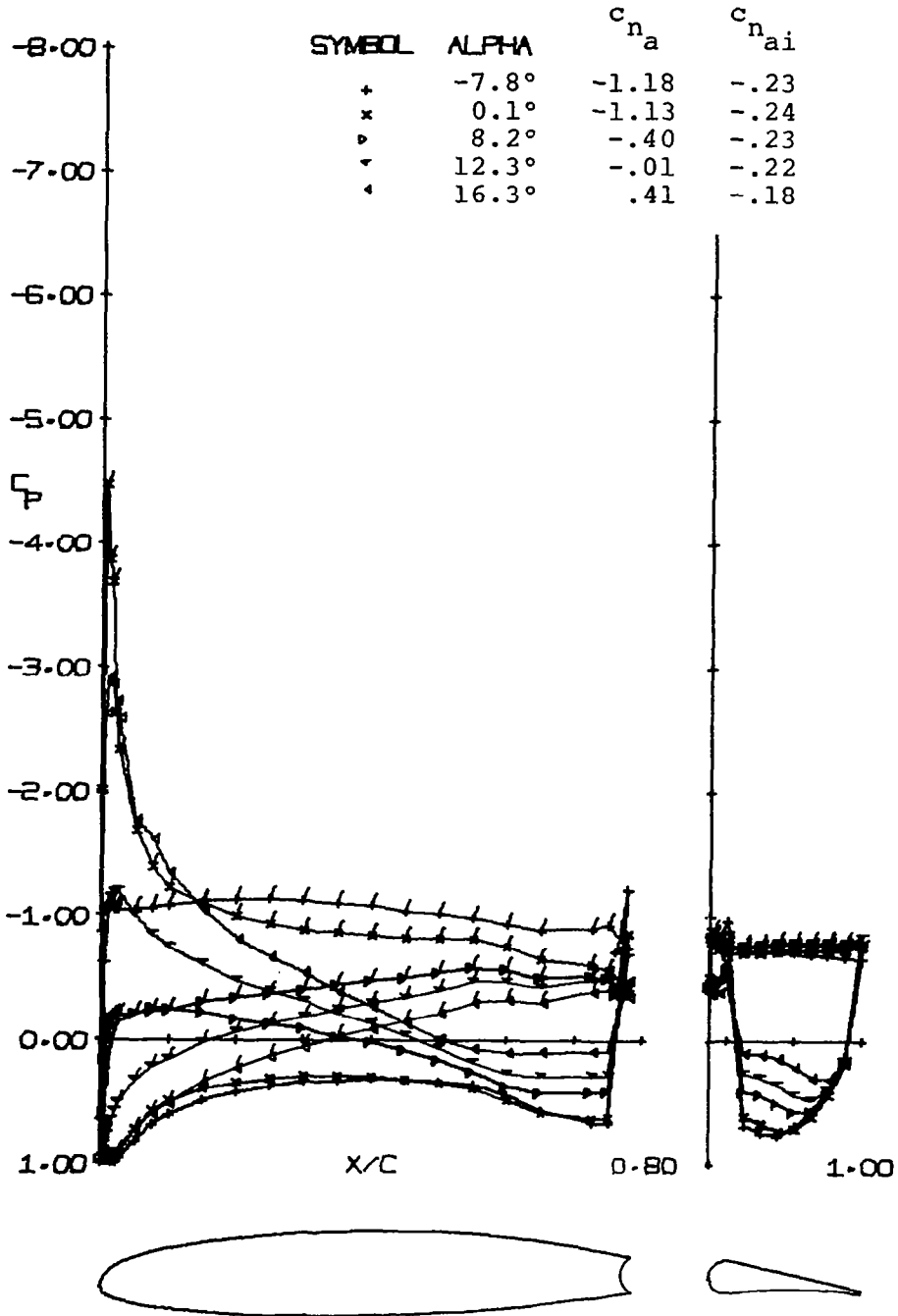
MACH NO. = 0.13

REYNOLDS NO. = 2.2 E 06

SYMBOL	ALPHA	c_{n_a}	$c_{n_{ai}}$
+	-7.8°	-1.18	-.23
×	0.1°	-1.13	-.24
▷	8.2°	-.40	-.23
▼	12.3°	-.01	-.22
◀	16.3°	.41	-.18

Figure 4 - Concluded.

30

Symbol	δ_f	$x_p(\%)$	$z_p(\%)$
◯	0°	0	0
△	10°	9.0	4.0
▷	20°	13.0	4.0
◇	30°	12.5	3.5
⬠	35°	13.0	2.5
⬡	40°	13.0	2.0

c_ℓ

Notes:
(1) Shaded symbols denote theoretical values using the method of Ref. 3.
(2) Flagged symbols from method of Ref. 4.
(3) See pressure distributions for computer predicted separation.
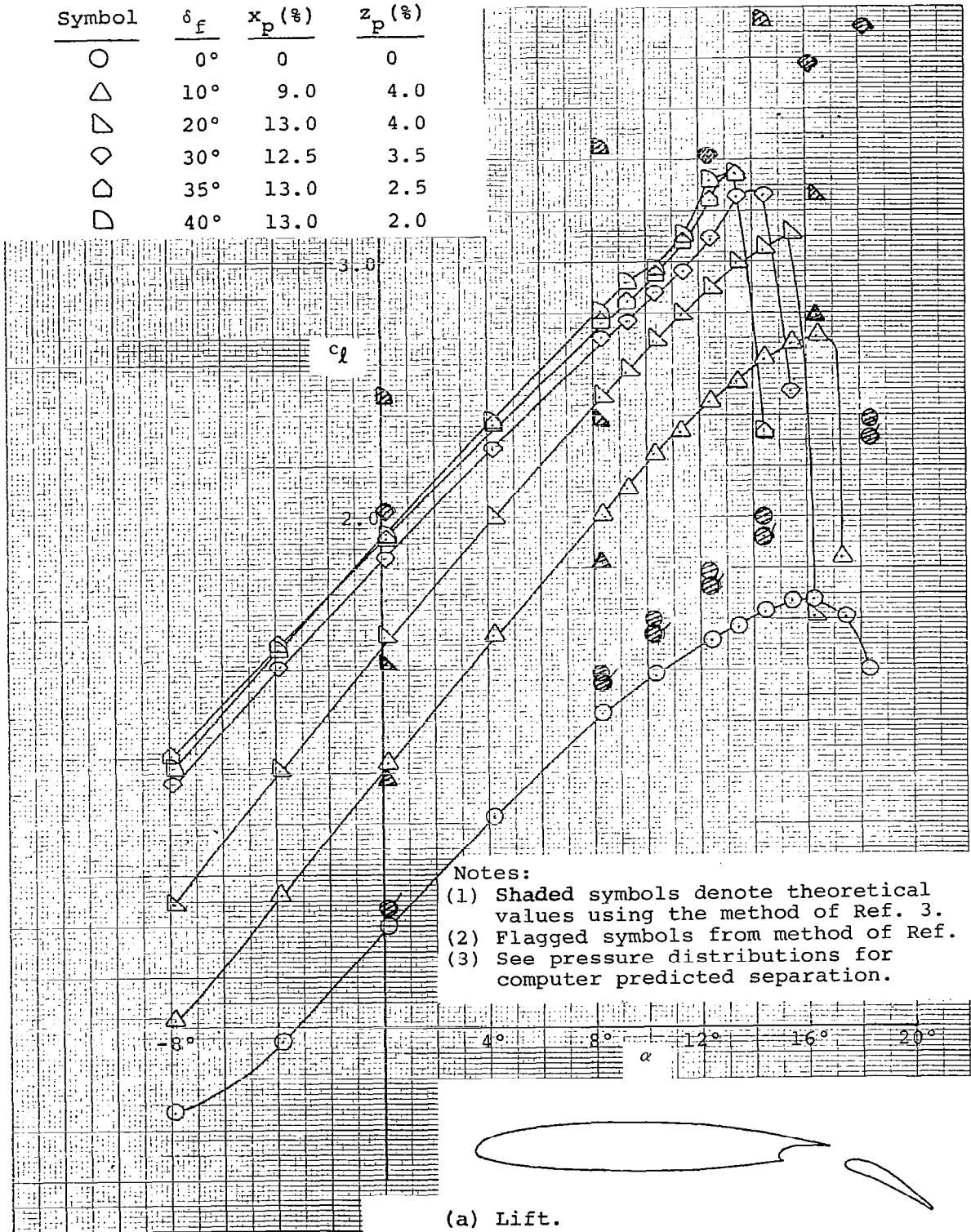
(a) Lift.

Figure 5 – Theoretical and Experimental Force Characteristics with 25% Slotted Flap.
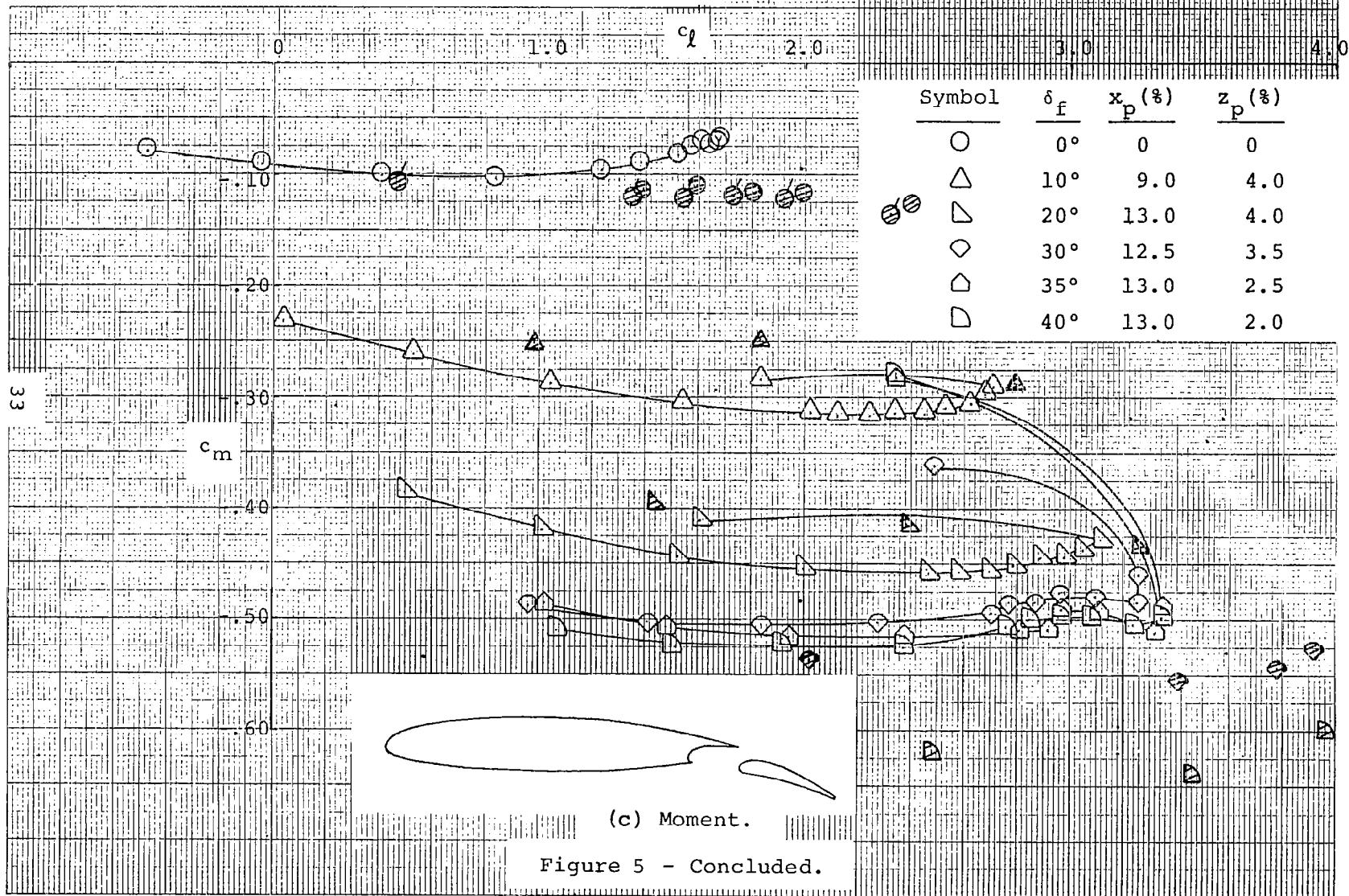
31

Notes: (1) Shaded symbols denote theoretical
            values using the method of Ref. 3.
        (2) Flagged symbols from method of Ref. 4.
        (3) See pressure distributions for
            computer predicted separation.

Symbol	δ_f	$x_p(\%)$	$z_p(\%)$
○	0°	0	0
△	10°	9.0	4.0
◁	20°	13.0	4.0
◇	30°	12.5	3.5
⬠	35°	13.0	2.5
⬡	40°	13.0	2.0

c_d

.15

.10

.05

0   1.0   2.0   3.0   4.0

c_ℓ
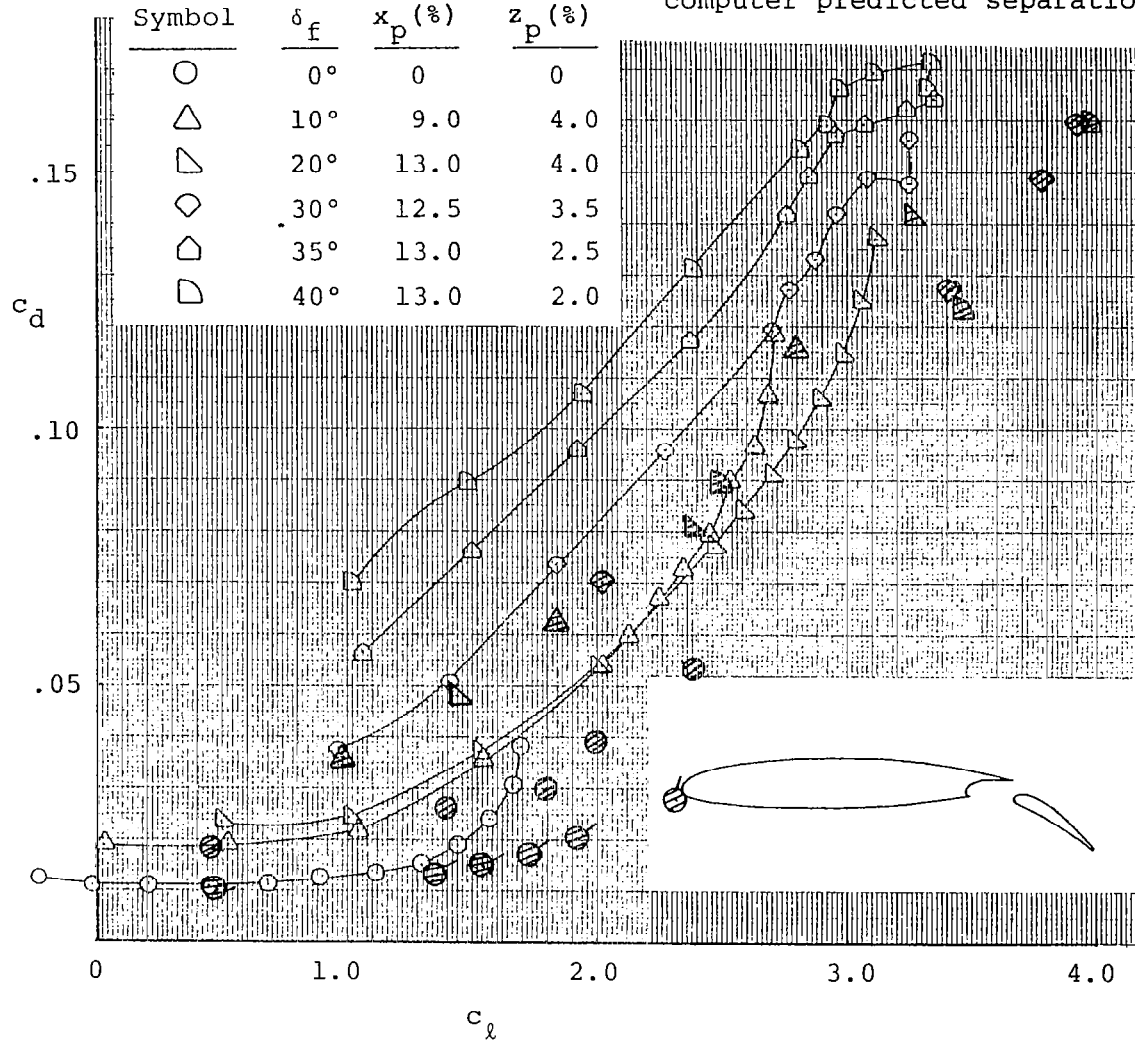
(b) Drag.

Figure 5 – Continued.

Notes: (1) Shaded symbols denote theoretical values using the method of Ref. 3.
(2) Flagged symbols from method of Ref. 4.
(3) See pressure distributions for computer predicted separation.

Symbol	δ_f	x_p(%)	z_p(%)
◯	0°	0	0
△	10°	9.0	4.0
◁	20°	13.0	4.0
◇	30°	12.5	3.5
⬠	35°	13.0	2.5
⬡	40°	13.0	2.0

(c) Moment.

Figure 5 - Concluded.

33

(a) α = 0.2°

Note: (1) Theory predicts no separation.
      (2) Confluent boundary layer error encountered.

○ Experiment
--- Theory (Ref. 3)

c_p

x/c

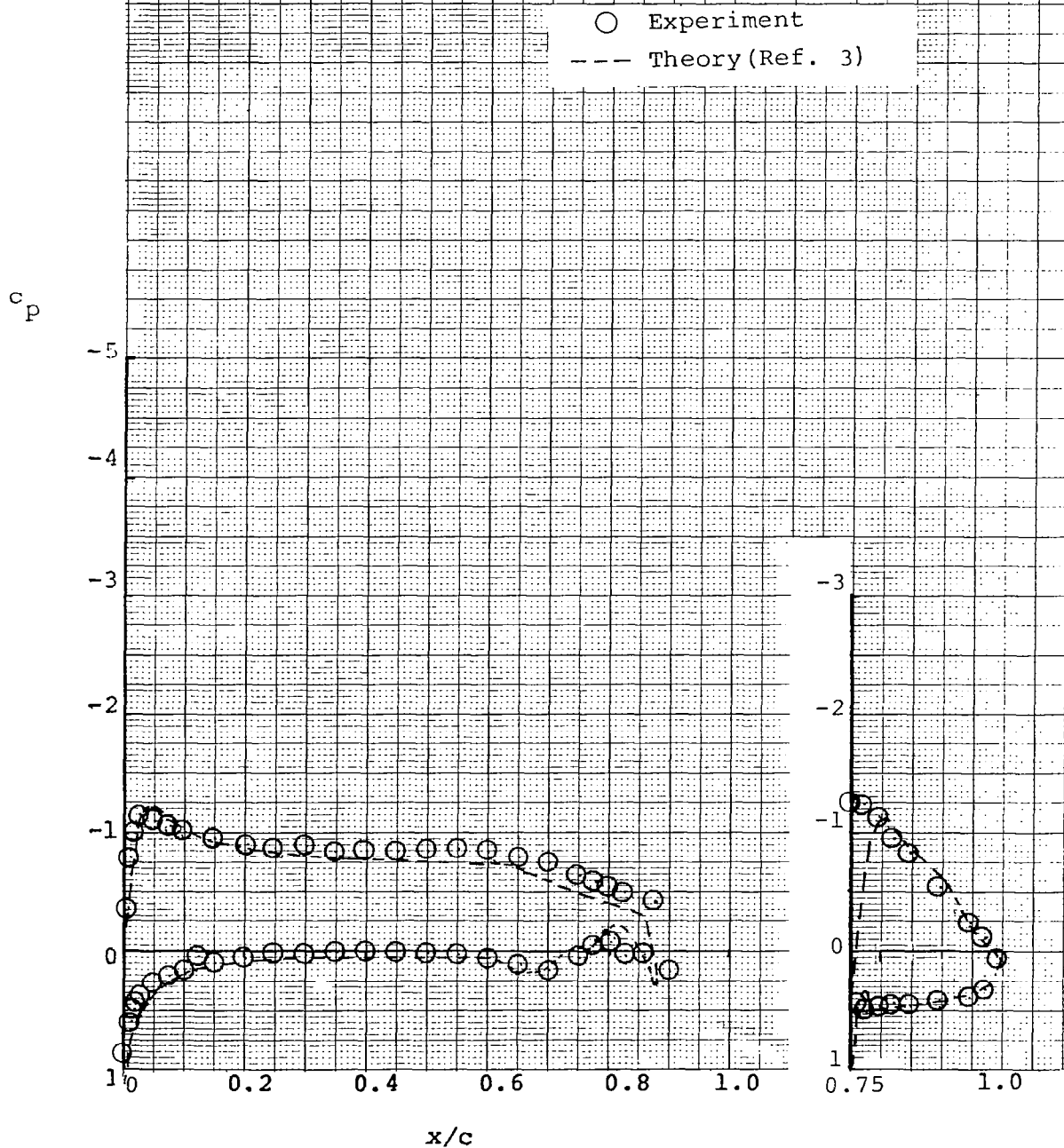Figure 6 - Pressure Distributions with
25% Slotted Flap, 10° Flap Deflection.

34

(b) $\alpha = 8.3°$

Note: (1) Theory predicts no separation.
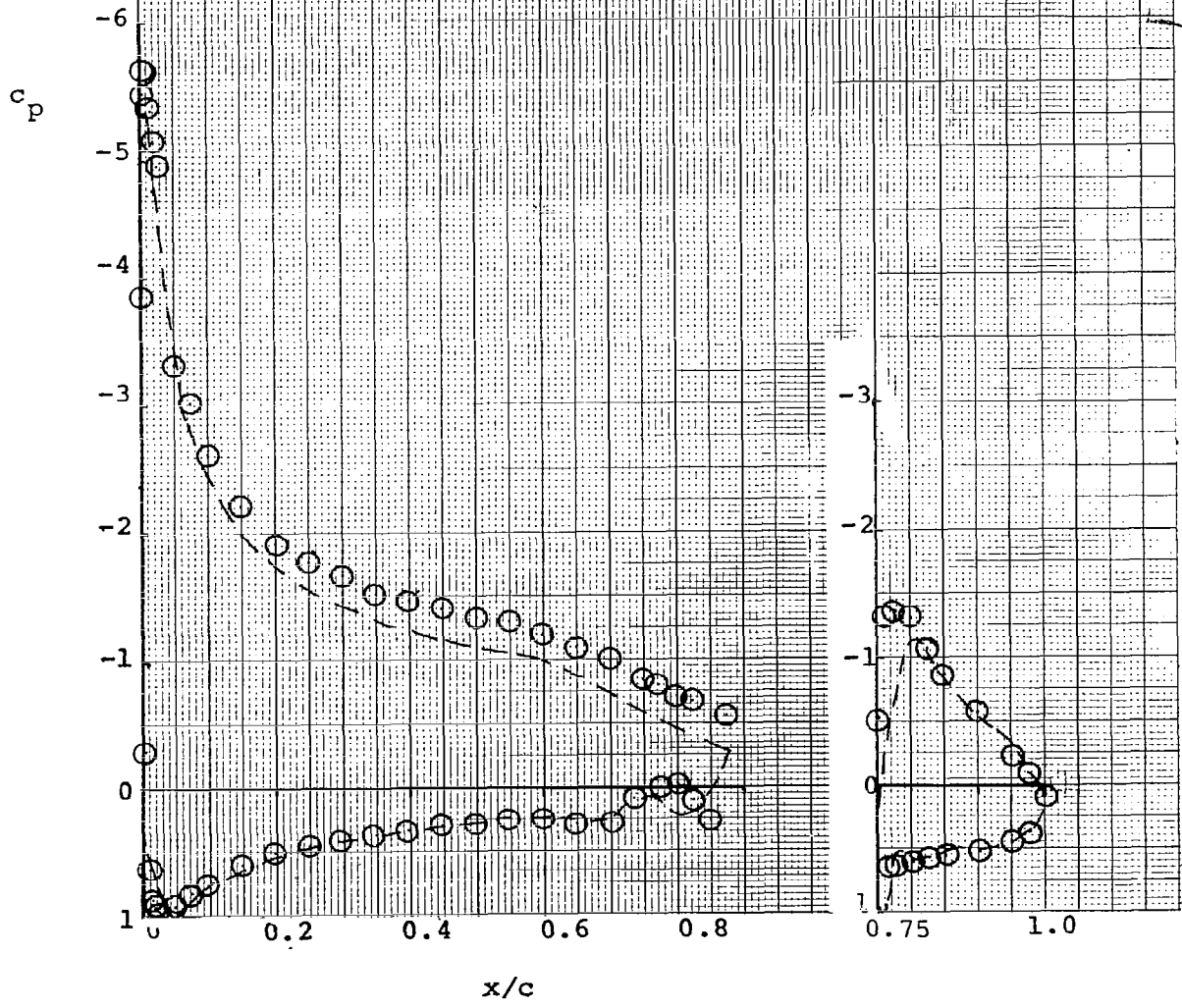(2) No confluent boundary layer error encountered.

○ Experiment
——— Theory (Ref. 3)
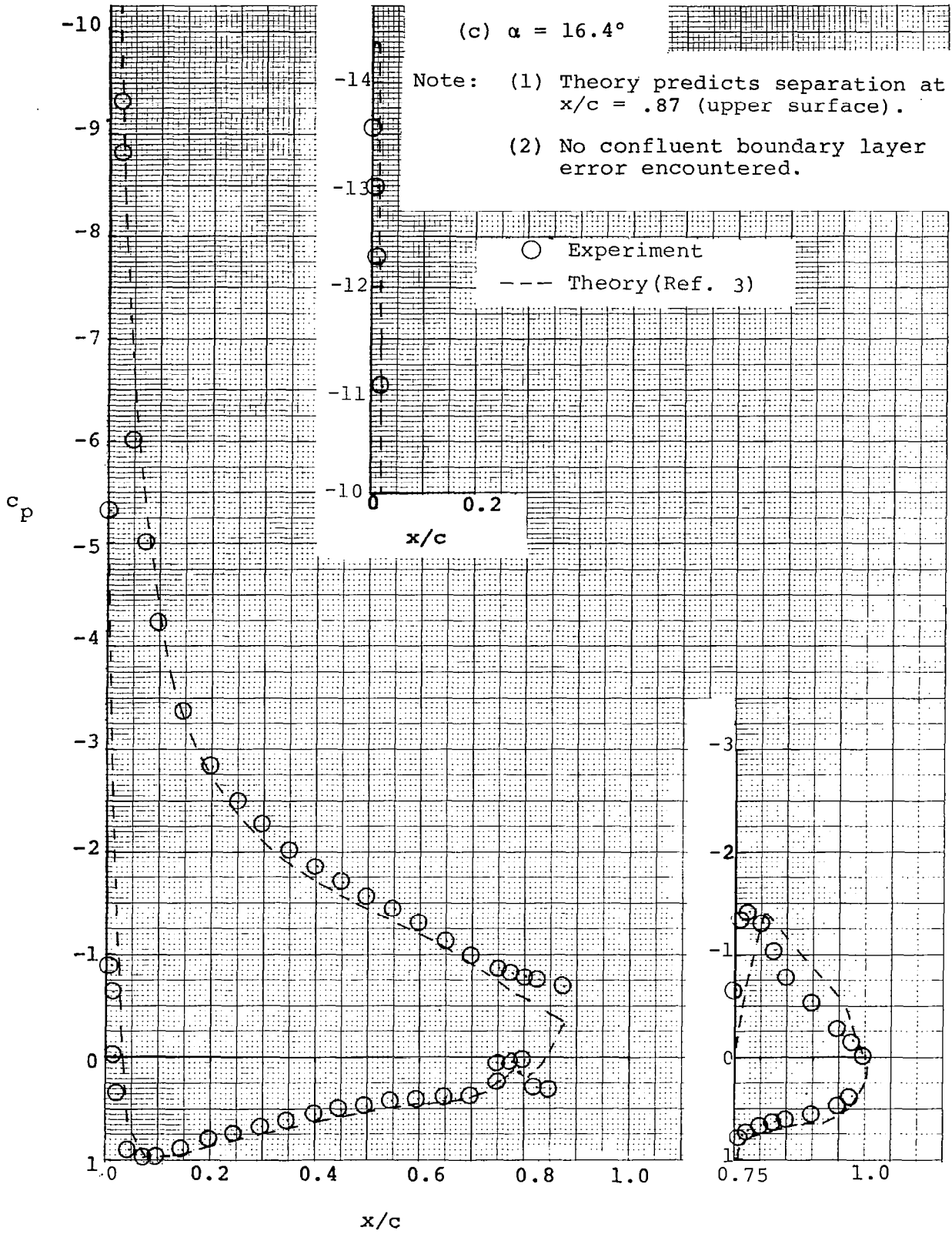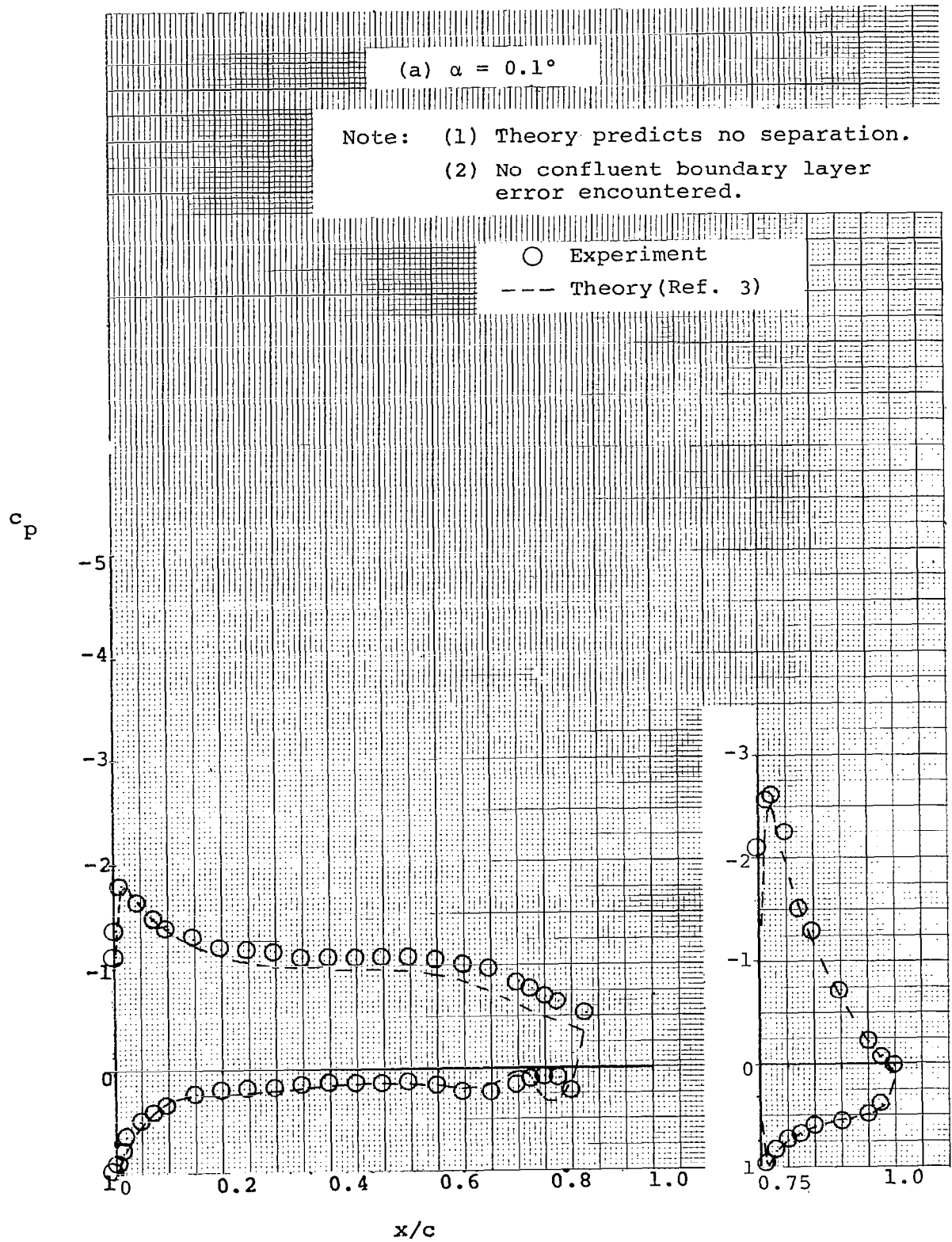
x/c

Figure 6 - Continued.
35

(c) α = 16.4°

Note: (1) Theory predicts separation at x/c = .87 (upper surface).

(2) No confluent boundary layer error encountered.

○ Experiment
——— Theory(Ref. 3)

x/c

Figure 6 - Concluded.

(a) $\alpha = 0.1°$

Note: (1) Theory predicts no separation.

(2) No confluent boundary layer error encountered.

○ Experiment

– – – Theory(Ref. 3)

c_p

x/c

Figure 7 – Pressure Distributions with 25% Slotted Flap, 20° Flap Deflection.

37

(b) α = 8.3°

Note: (1) Theory predicts no separation.
      (2) No confluent boundary layer error encountered.
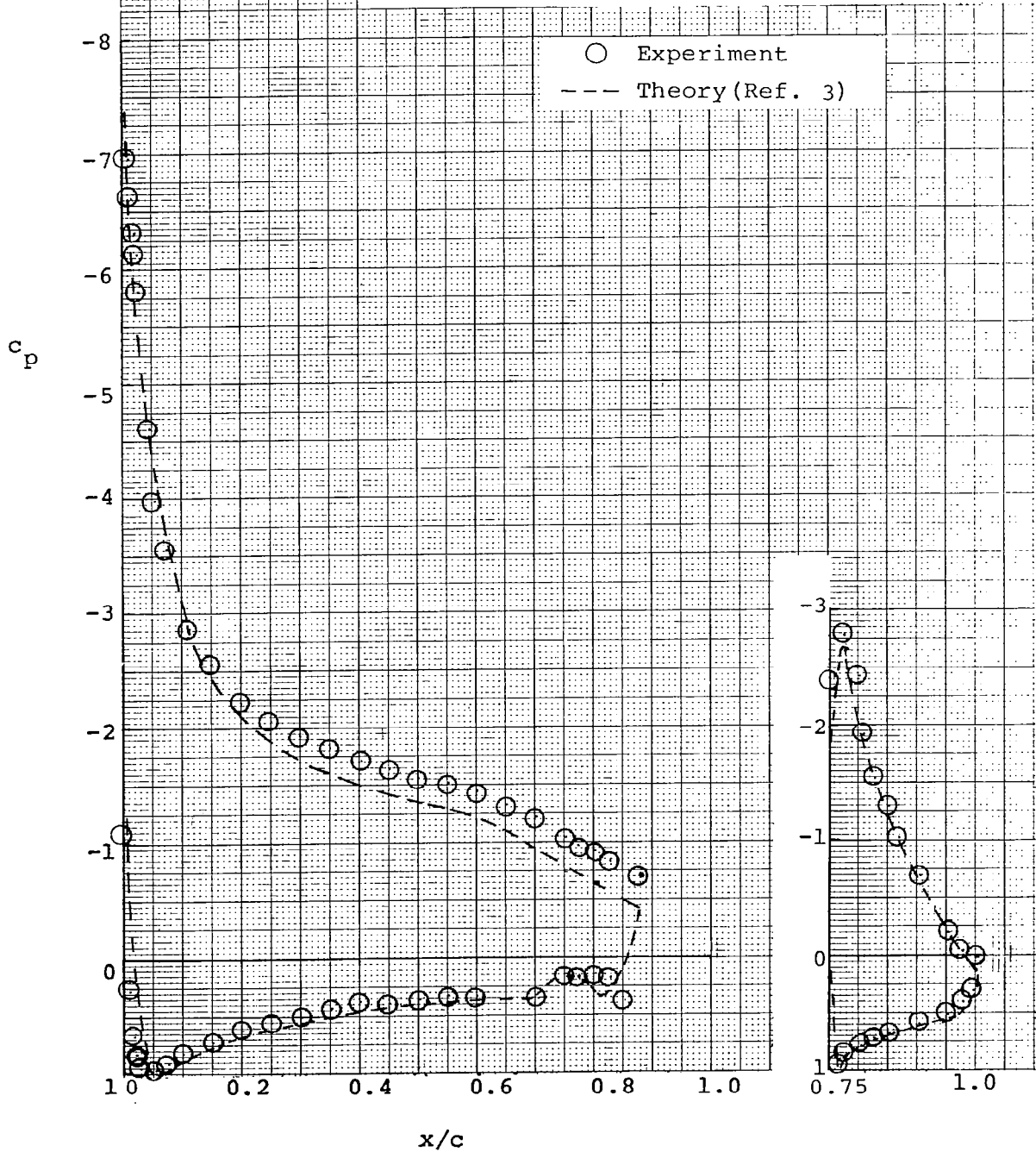
○   Experiment
--- Theory(Ref. 3)

x/c

Figure 7 - Continued.

38

(c) α = 16.4°

Note: (1) Theory predicts no separatio
(2) No confluent boundary layer
      error encountered.
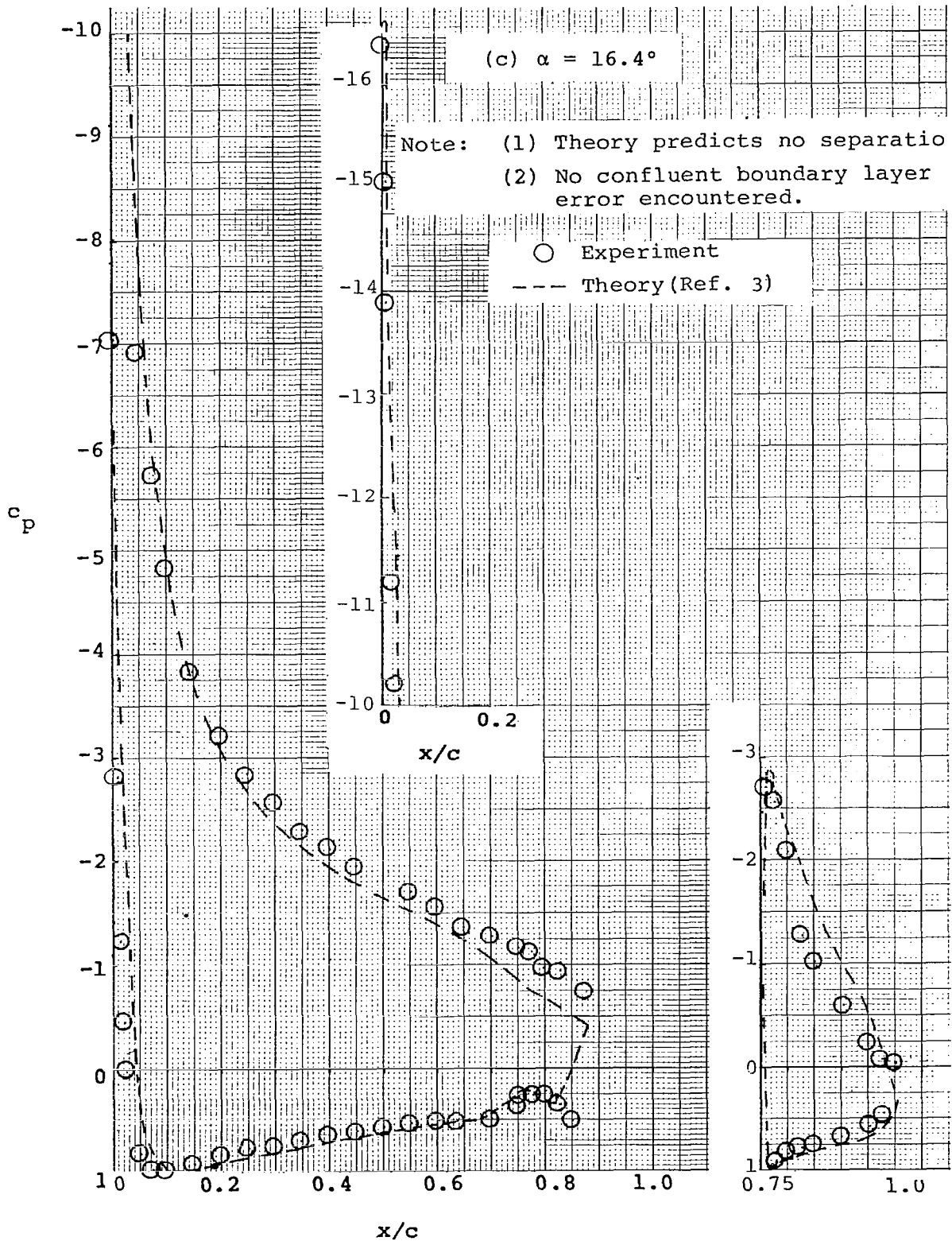
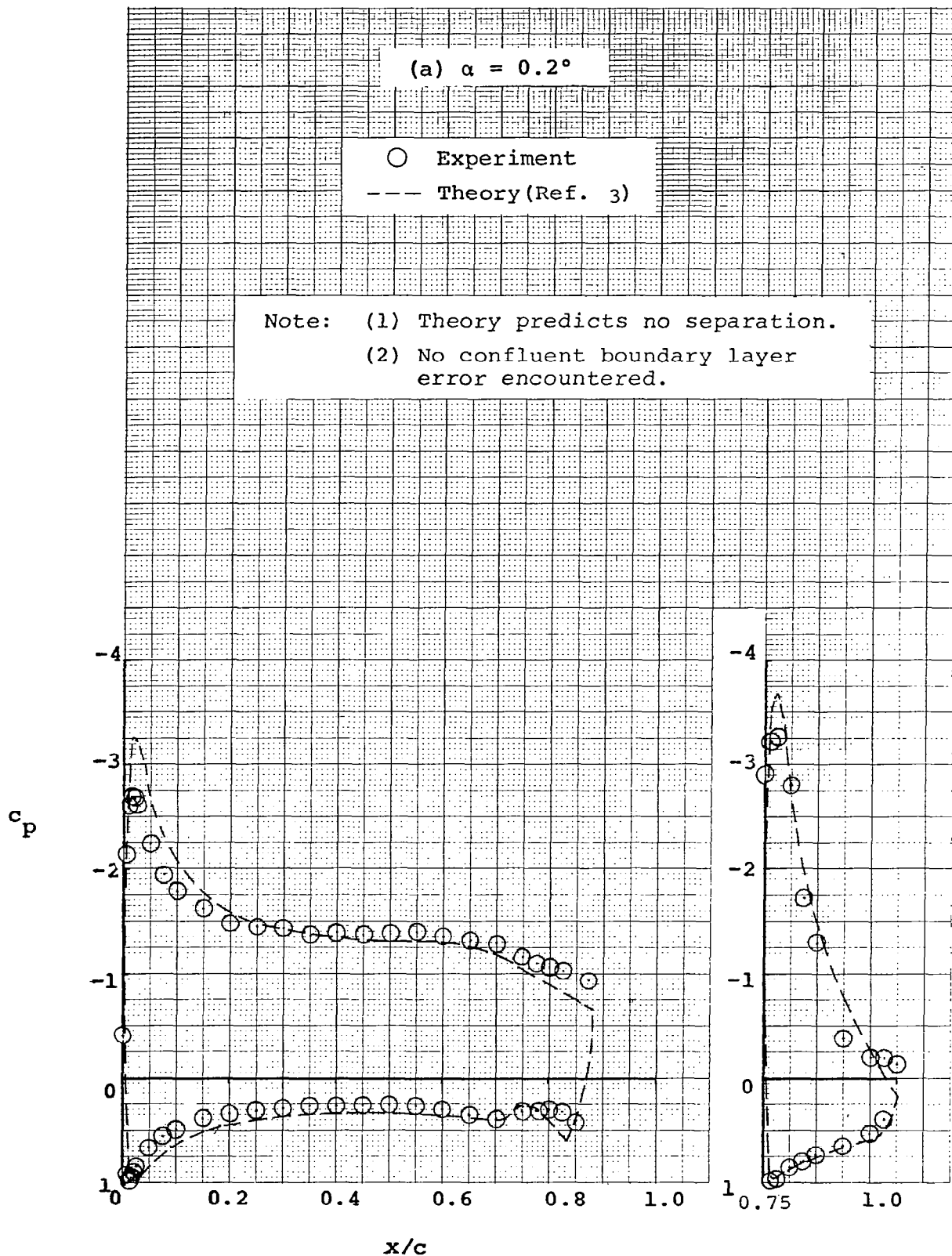◯ Experiment
--- Theory (Ref. 3)

Figure 7 - Concluded.

39

Figure 8 - Pressure Distributions with
25% Slotted Flap, 30° Flap Deflection.

40

(b) $\alpha = 8.3°$

Note: (1) Theory predicts no separation.
(2) No confluent boundary layer error encountered.

○ Experiment
––– Theory (Ref. 3)

c_p

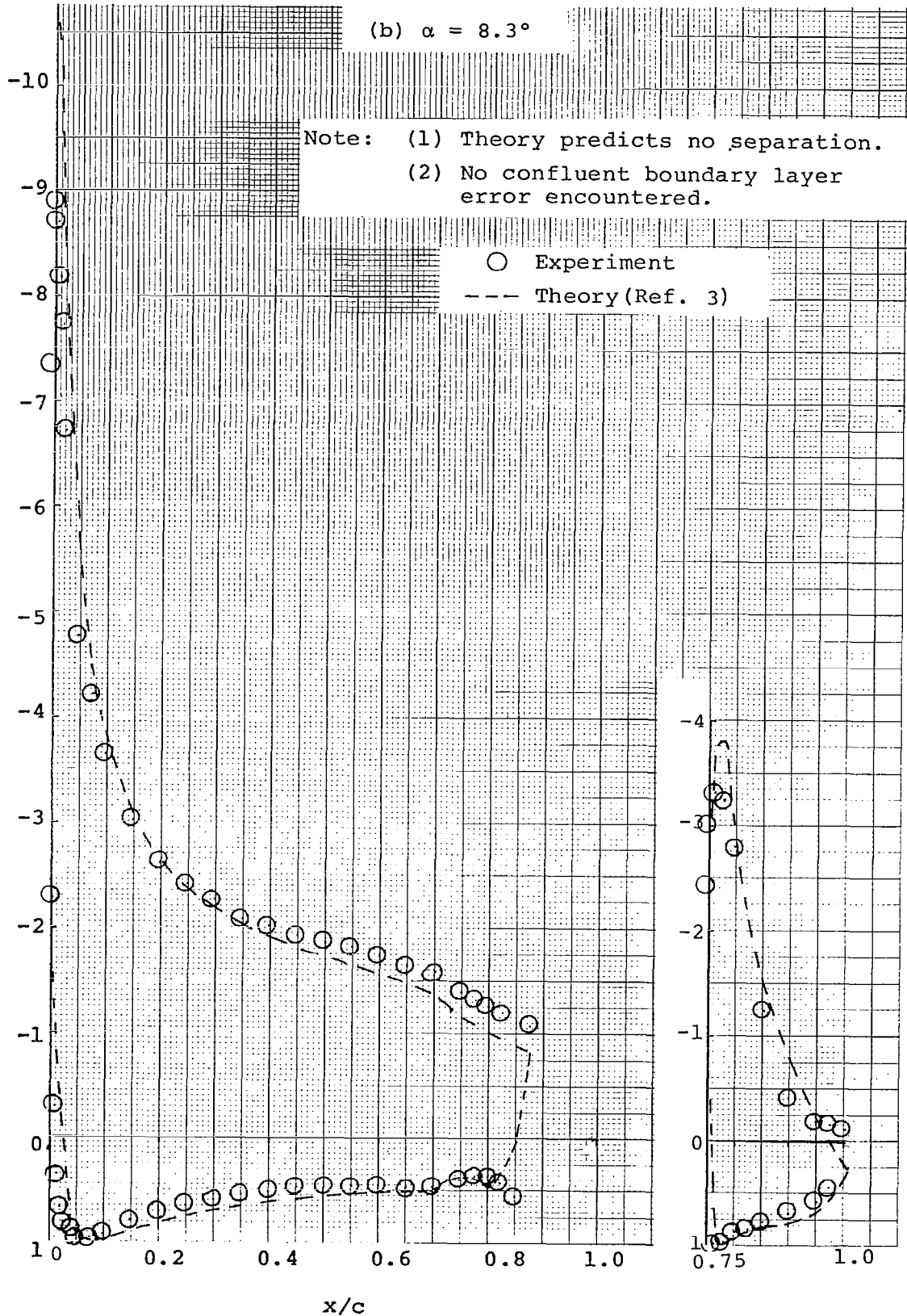x/c

Figure 8 – Continued.

41

(c) α = 12.4°

Note: (1) Theory predicts no separation.
(2) No confluent boundary layer
error encountered.

○ Experiment
--- Theory(Ref. 3)

Figure 8 - Continued.

42

Figure 8 - Concluded.

(a) α = 0.2°

Note: (1) Theory predicts no separation.

(2) Confluent boundary layer error encountered.

○ Experiment
--- Theory(Ref. 3)
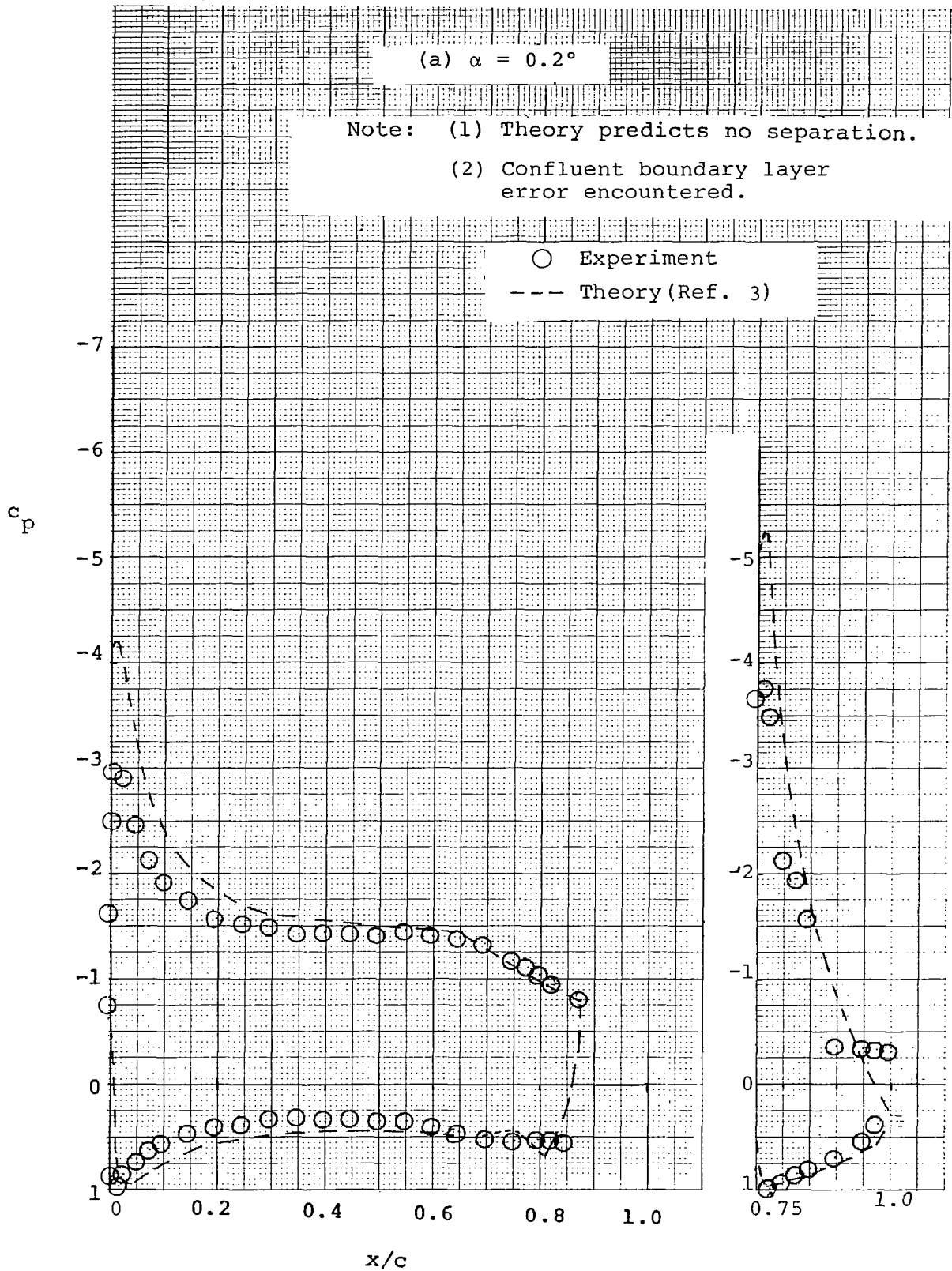
Figure 9 - Pressure Distributions with
25% Slotted Flap, 40° Flap Deflection.
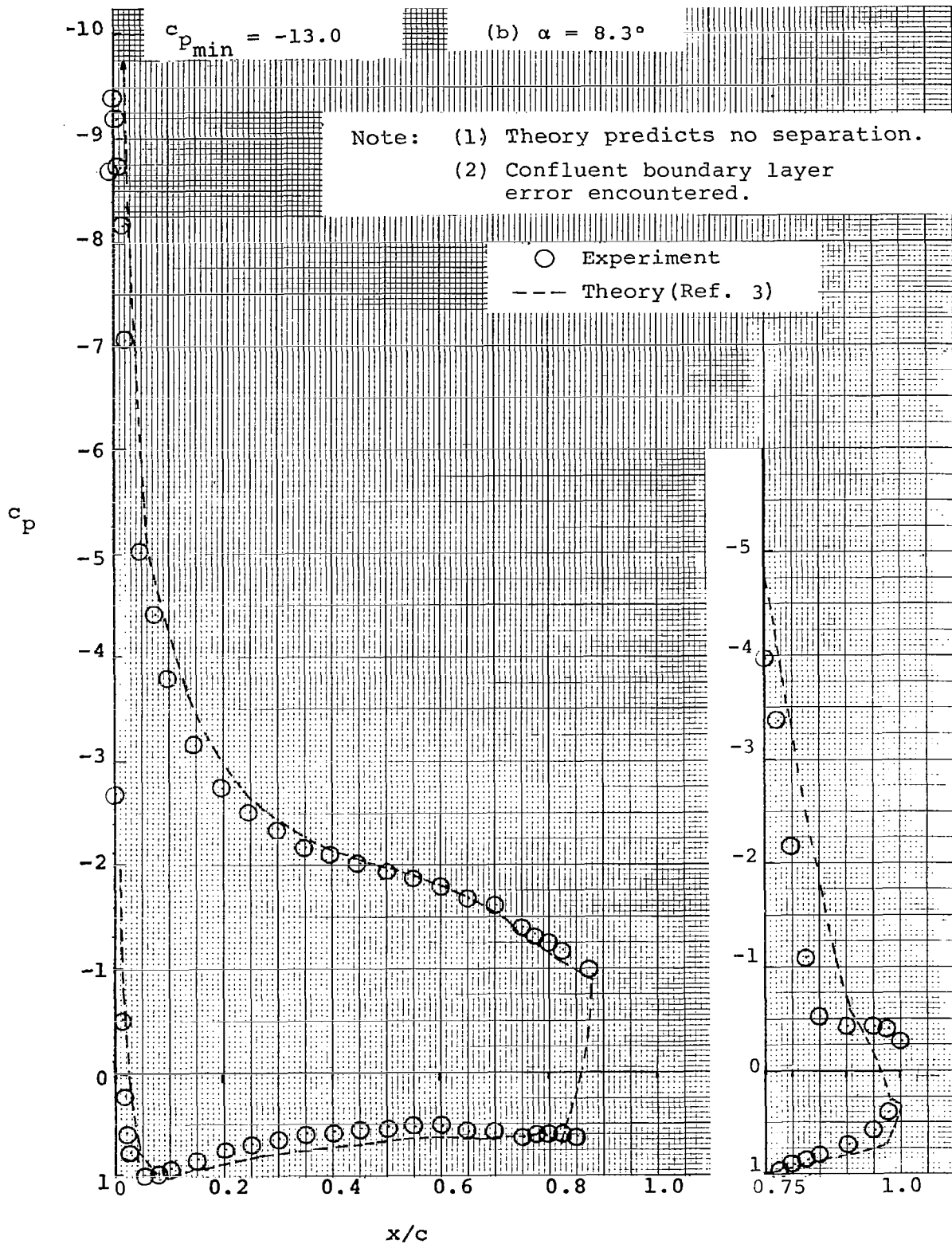
44

Figure 9 - Continued.
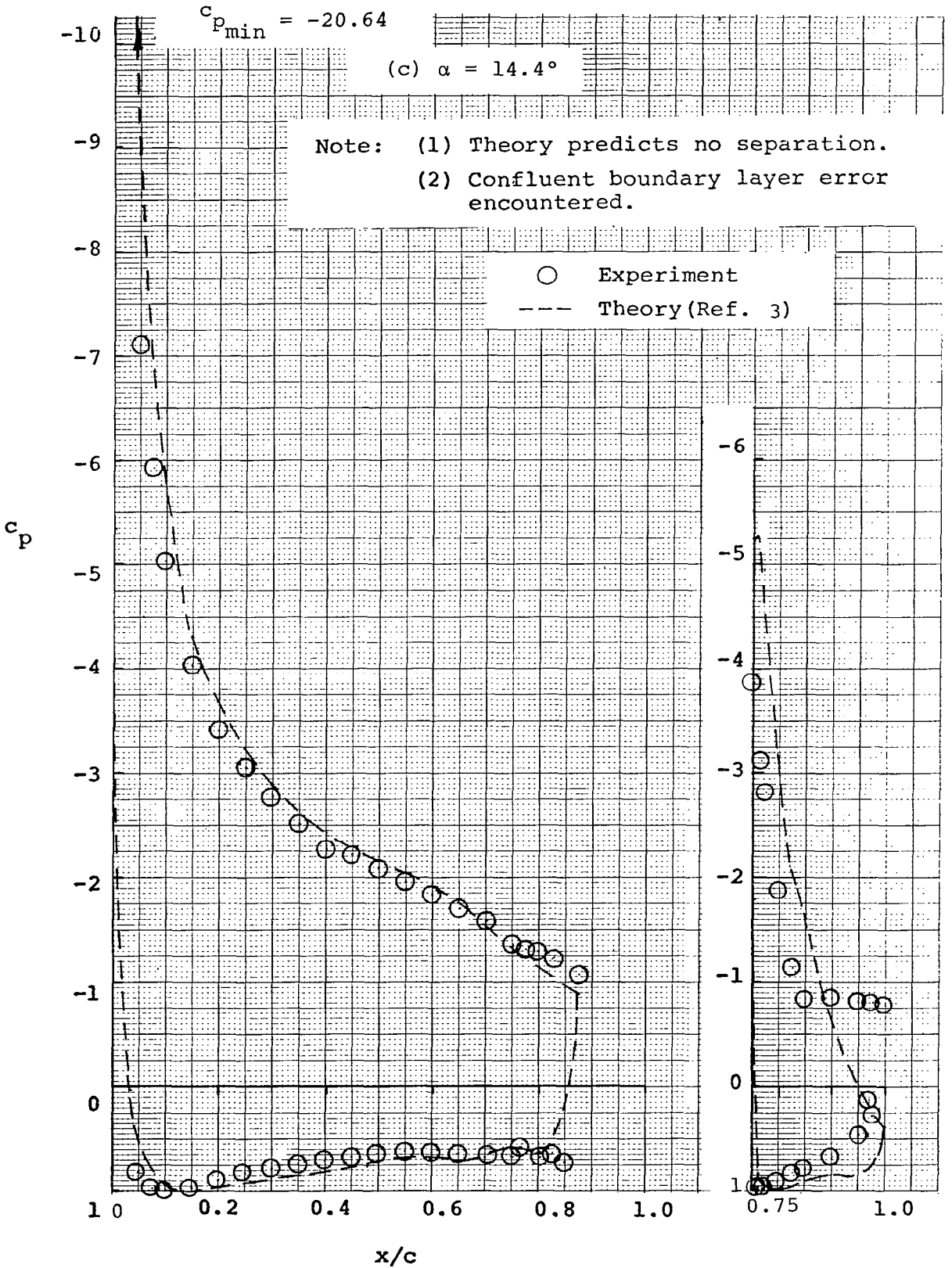
$c_{p_{min}} = -20.64$

(c) $\alpha = 14.4°$

Note: (1) Theory predicts no separation.
(2) Confluent boundary layer error encountered.

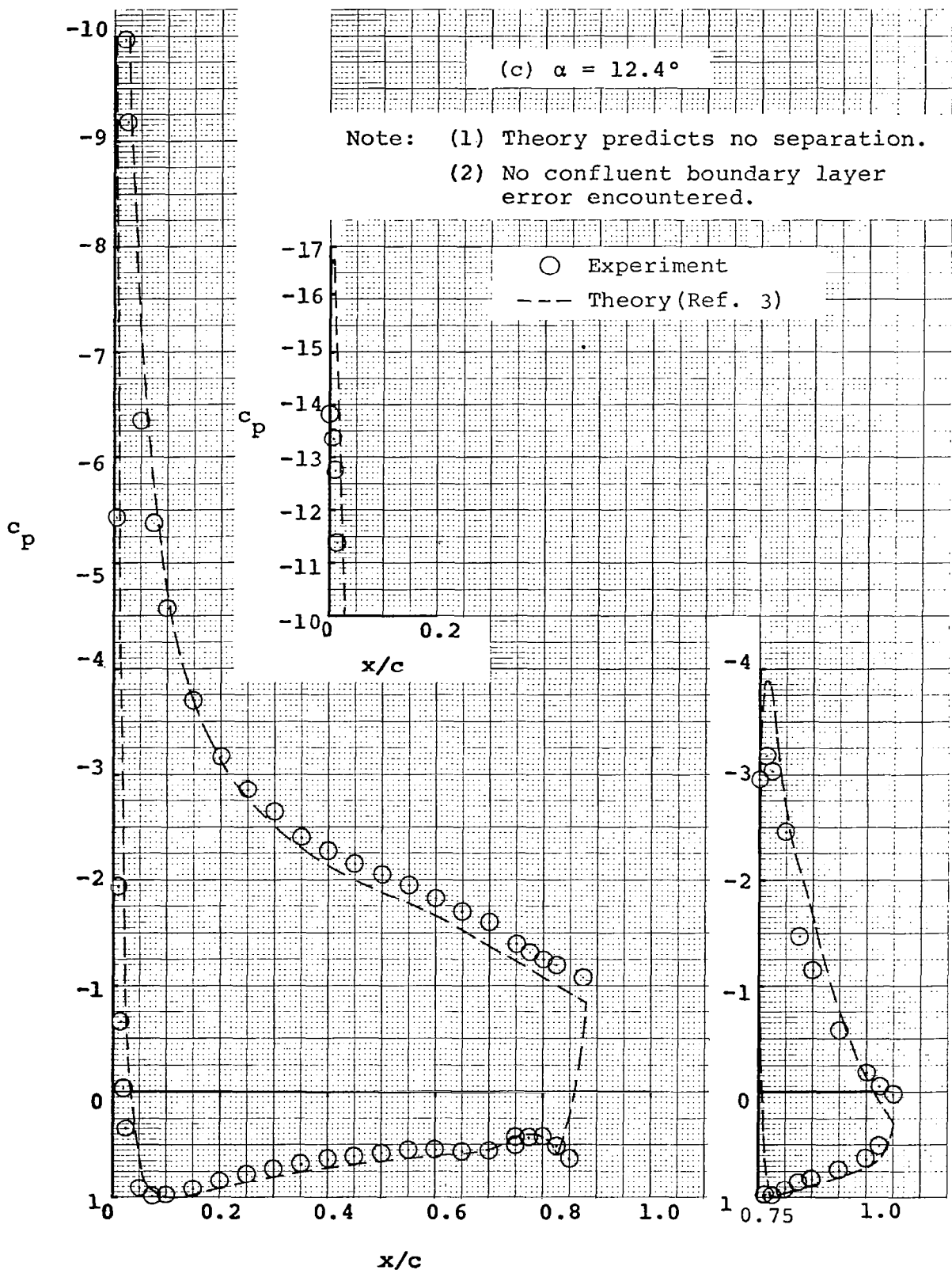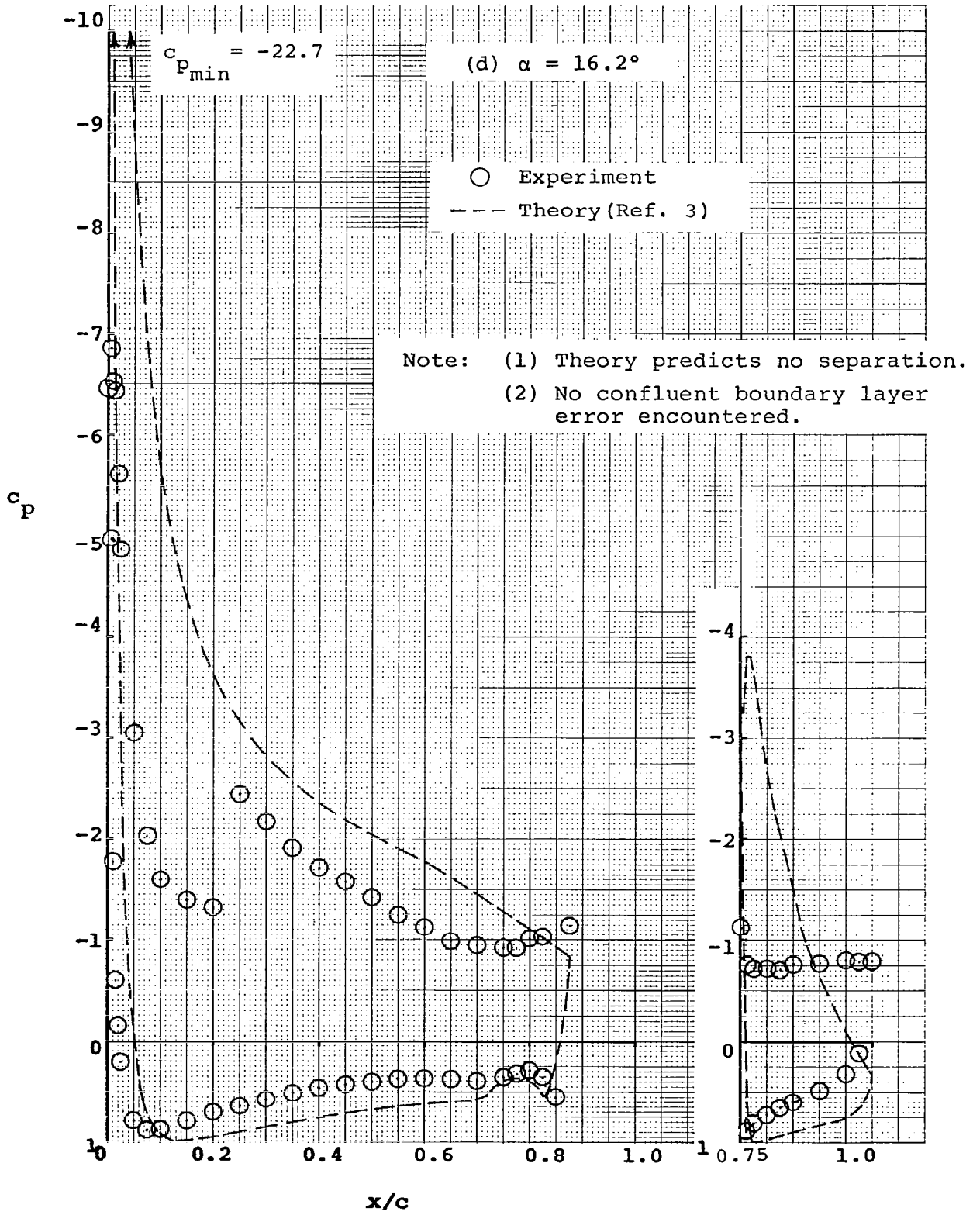○   Experiment
―――   Theory(Ref. 3)

x/c

Figure 9 - Concluded.
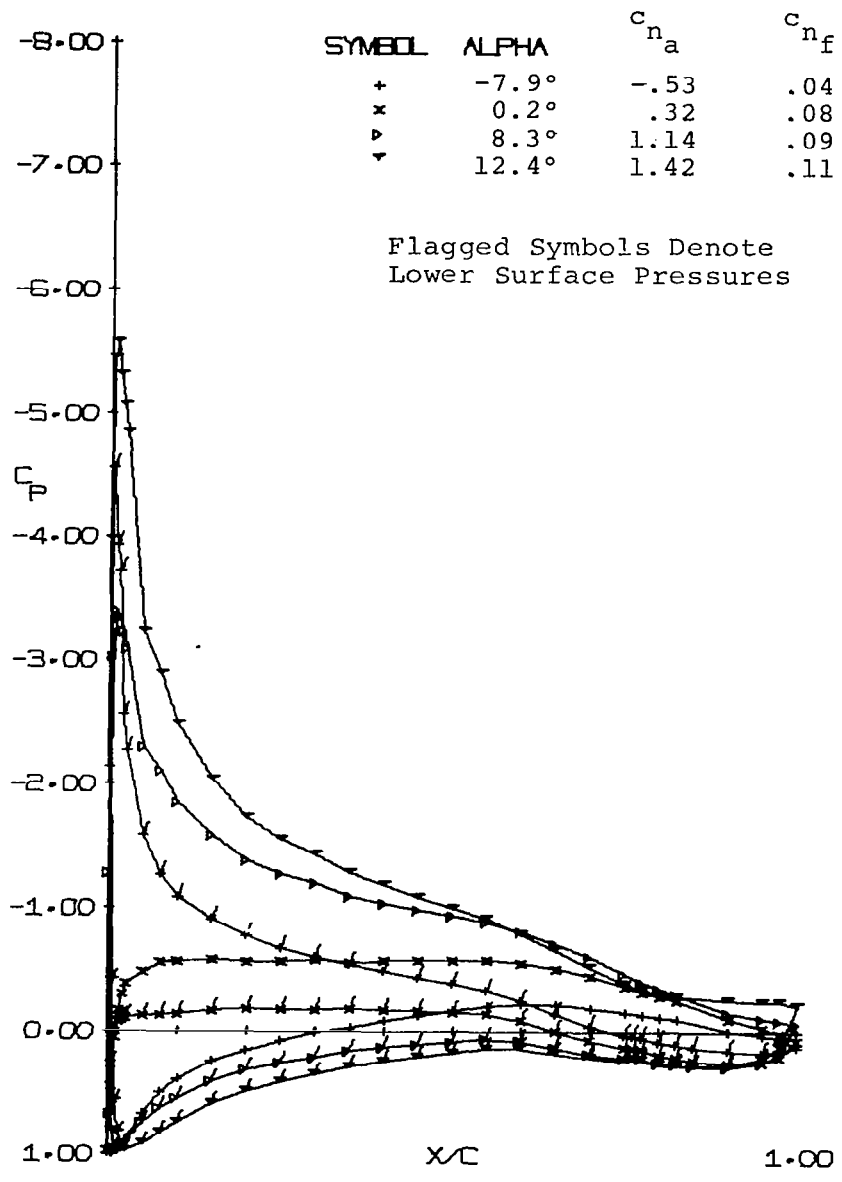
Figure 10 - Experimental Pressure Distributions with 25% Slotted Flap.

47

(b) FLAP DEFLECTION = 0.0 DEGREES, HIGH α'S

MACH NO. = 0.13

REYNOLDS NO. = 2.2 E 06

SYMBOL	ALPHA	c_{n_a}	c_{n_f}
+	8.3°	1.14	.09
×	12.4°	1.42	.11
▷	16.4°	1.55	.15
▽	18.3°	1.21	.18

C_p

-8.00
-7.00
-6.00
-5.00
-4.00
-3.00
-2.00
-1.00
0.00
1.00

X/C

1.00

Figure 10 - Continued.

48

(c) FLAP DEFLECTION = 10.0 DEGREES , LOW α'S

MACH NO. = 0.13

REYNOLDS NO. = 2.2 E 06

SYMBOL	ALPHA	c_{n_a}	c_{m_a}	c_{n_f}	c_{m_f}
+	-8.0°	-.19	-.045	.21	-.34
×	0.2°	.79	-.31	.27	-.42
ᴅ	8.3°	1.78	-.57	.30	-.47
▼	12.4°	2.22	-.68	.31	-.48

Figure 10 - Continued.

49

(d) FLAP DEFLECTION = 10.0 DEGREES, HIGH α'S

MACH NO. = 0.13

REYNOLDS NO. = 2.2 E 06

SYMBOL	ALPHA	c_{n_a}	c_{m_a}	c_{n_f}	c_{m_f}
+	8.3°	1.78	-.57	.30	-.47
×	12.4°	2.22	-.68	.31	-.48
▷	16.4°	2.49	-.73	.31	-.49
▼	18.2°	1.45	-.50	.41	-.68

Figure 10 - Continued.

MACH NO. = 0.13

REYNOLDS NO. = 2.2 E 06

SYMBOL	ALPHA	c_{n_a}	c_{m_a}	c_{n_f}	c_{m_f}
+	-8.0°	.13	-.16	.37	-.54
✗	0.1°	1.15	-.44	.42	-.59
▷	8.3°	2.12	-.70	.44	-.61
▾	12.3°	2.58	-.81	.44	-.61

Figure 10 - Continued.

51
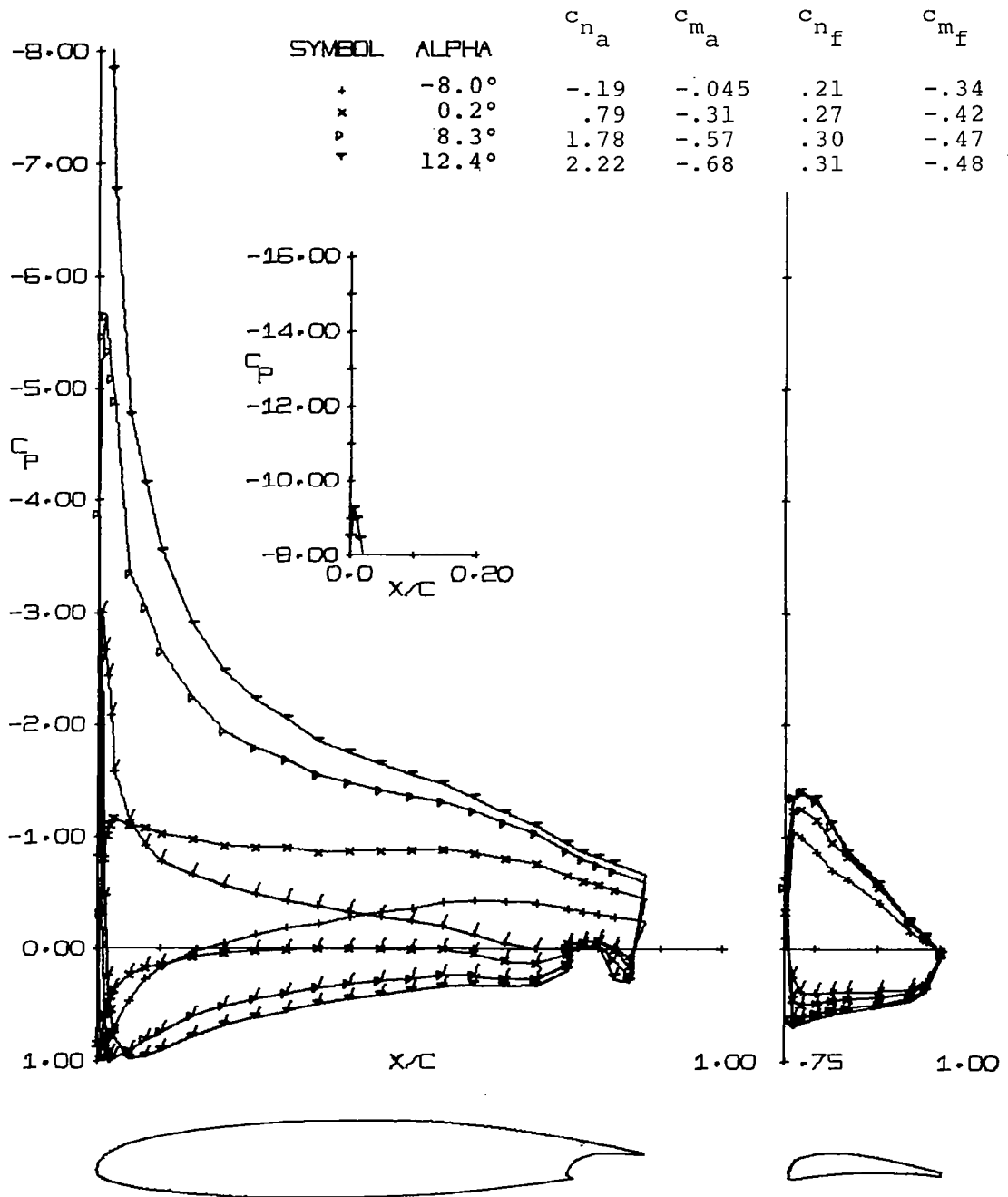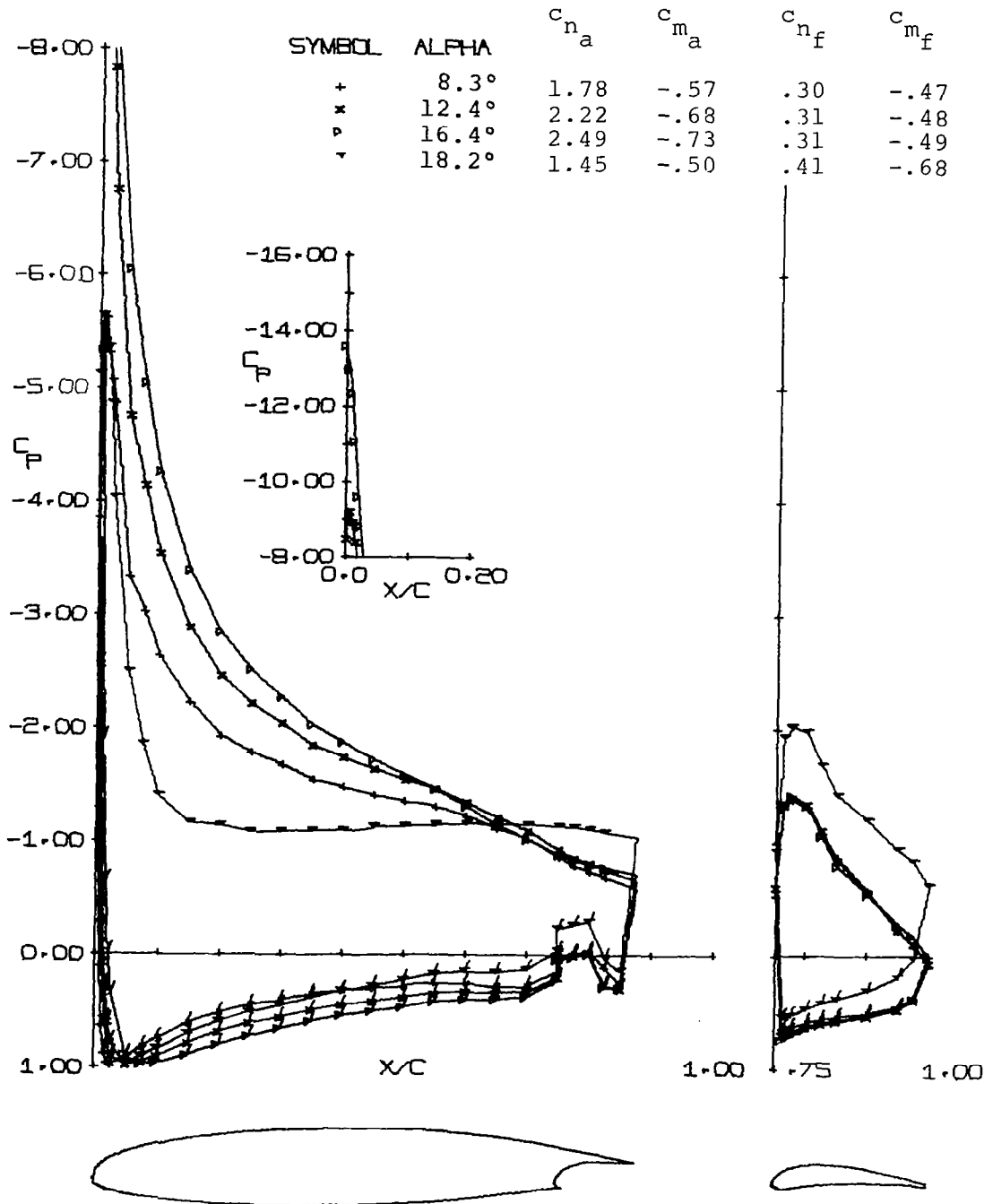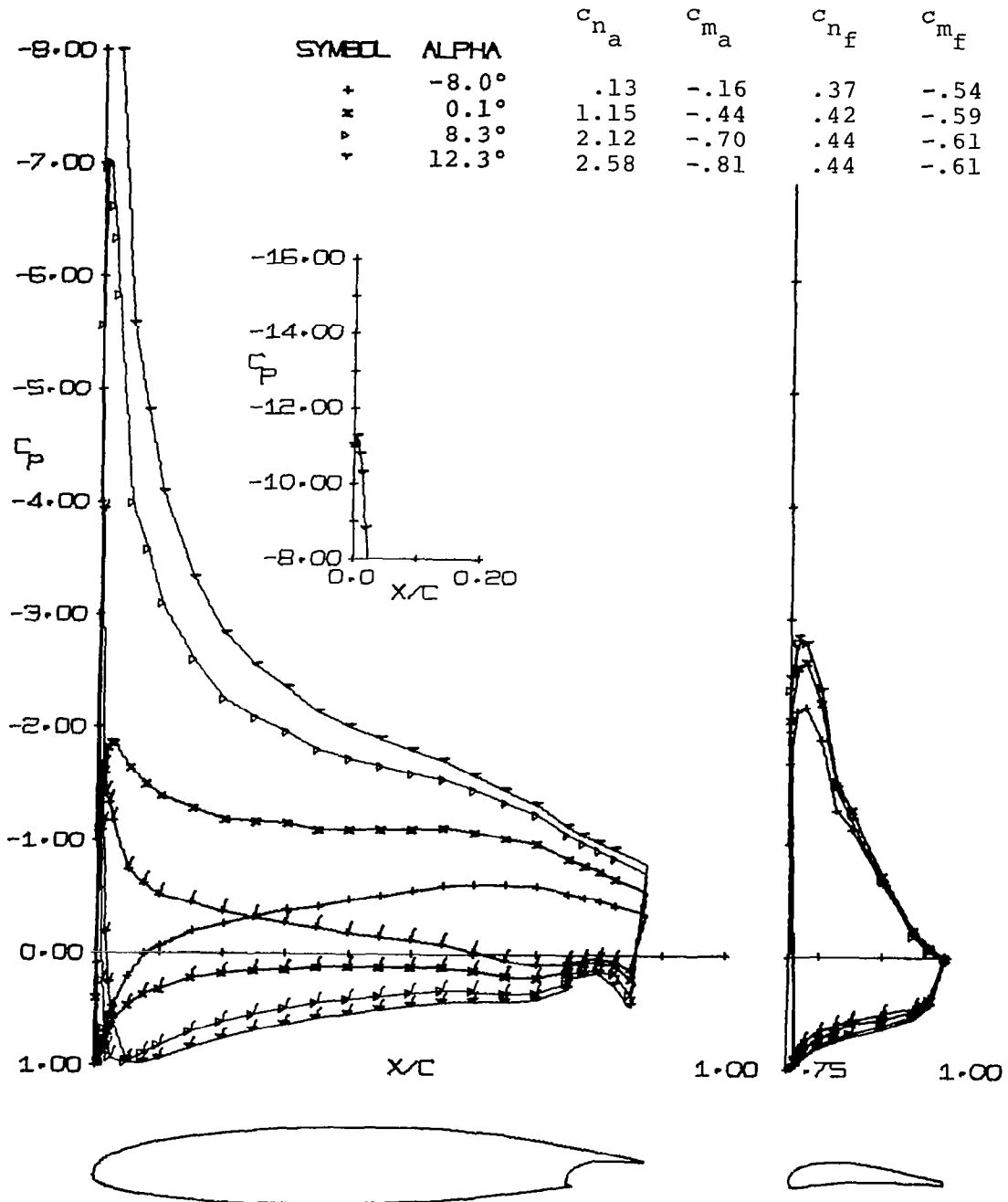
(f) FLAP DEFLECTION = 20.0 DEGREES, HIGH α'S
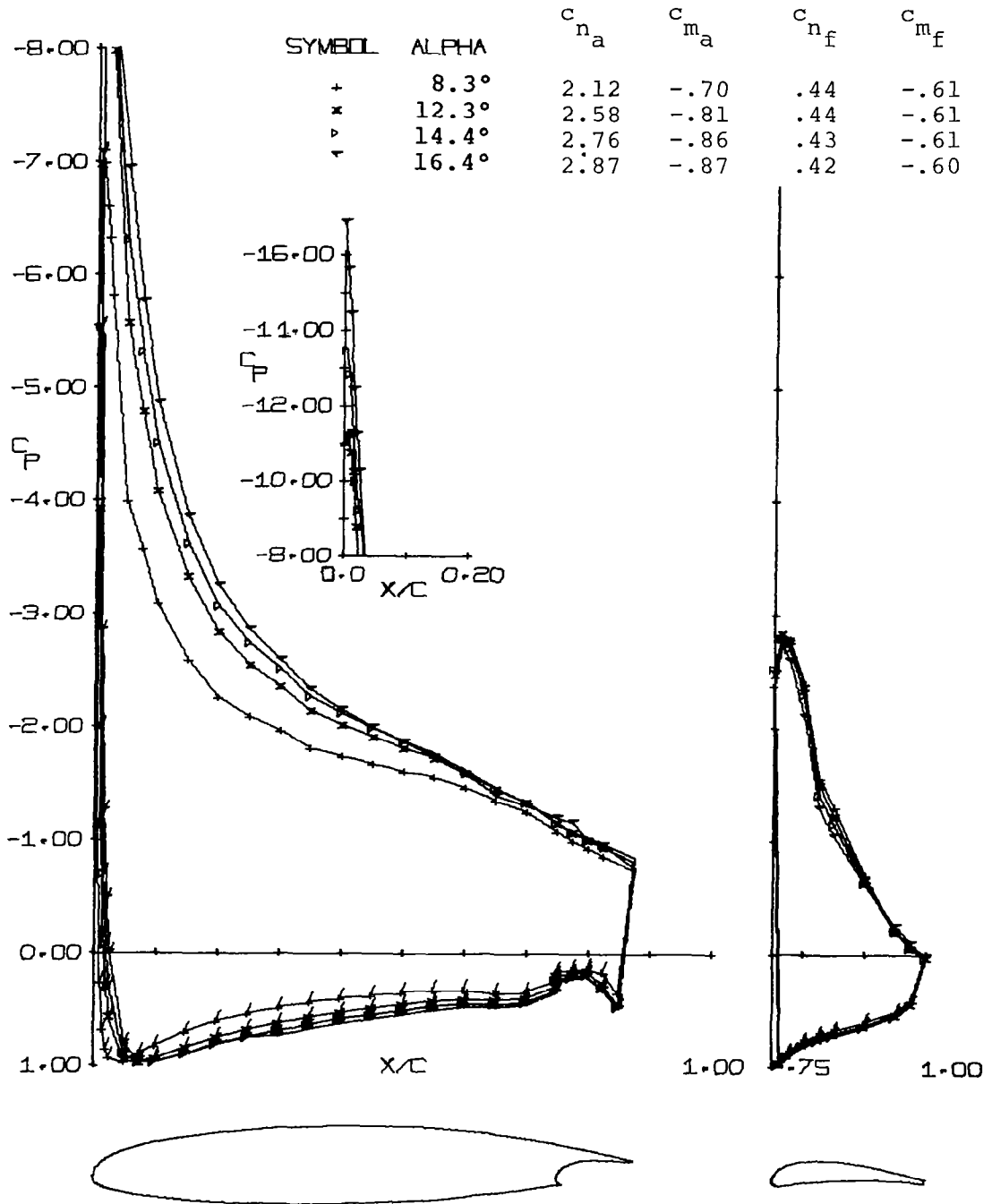
MACH NO. = 0.13

REYNOLDS NO. = 2.2 E 06

SYMBOL	ALPHA	c_{n_a}	c_{m_a}	c_{n_f}	c_{m_f}
+	8.3°	2.12	-.70	.44	-.61
×	12.3°	2.58	-.81	.44	-.61
▷	14.4°	2.76	-.86	.43	-.61
▼	16.4°	2.87	-.87	.42	-.60

Figure 10 - Continued.

52

(g) FLAP DEFLECTION = 30.0 DEGREES, LOW α'S

MACH NO. = 0.13

REYNOLDS NO. = 2.2 E 06

SYMBOL	ALPHA	c_{n_a}	c_{m_a}	c_{n_f}	c_{m_f}
+	−8.0°	.60	−.36	.46	−.62
×	0.2°	1.58	−.62	.46	−.62
▷	8.3°	2.56	−.88	.47	−.64
▼	12.4°	2.97	−.98	.46	−.64

Figure 10 – Continued.

53

(h) FLAP DEFLECTION = 30.0 DEGREES, HIGH α'S

MACH NO. = 0.13

REYNOLDS NO. = 2.2 E 06

SYMBOL	ALPHA	c_{n_a}	c_{m_a}	c_{n_f}	c_{m_f}
+	8.3°	2.56	−.88	.47	−.64
x	12.4°	2.97	−.98	.46	−.64
▷	14.4°	3.04	−.97	.43	−.63
▼	16.2°	1.85	−.67	.31	−.58

Figure 10 - Continued.

54

SYMBOL	ALPHA	c_{n_a}	c_{m_a}	c_{n_f}	c_{m_f}
+	-8.0°	.73	-.41	.47	-.62
×	0.2°	1.72	-.67	.46	-.63
▷	8.3°	2.72	-.94	.46	-.64
▼	12.4°	3.08	-1.02	.47	-.66

Figure 10 - Continued.

55

(j) FLAP DEFLECTION = 35.0 DEGREES , HIGH α'S

MACH NO. = 0.13

REYNOLDS NO. = 2.2 E 06

SYMBOL	ALPHA	c_{n_a}	c_{m_a}	c_{n_f}	c_{m_f}
+	8.3°	2.72	-.94	.46	-.64
x	12.4°	3.08	-1.02	.47	-.66
▷	14.4°	3.12	-1.01	.43	-.63

Figure 10 - Continued.

56

(k) FLAP DEFLECTION = 40.0 DEGREES, LOW α'S

MACH NO. = 0.13

REYNOLDS NO. = 2.2 E 06

SYMBOL	ALPHA	c_{n_a}	c_{m_a}	c_{n_f}	c_{m_f}
+	-8.0°	.68	-.39	.46	-.64
✕	0.2°	1.71	-.68	.43	-.61
▷	8.3°	2.70	-.93	.44	-.62
▼	12.4°	3.15	-1.05	.47	-.65

Figure 10 - Continued.

57

(1) FLAP DEFLECTION = 40.0 DEGREES, HIGH α'S
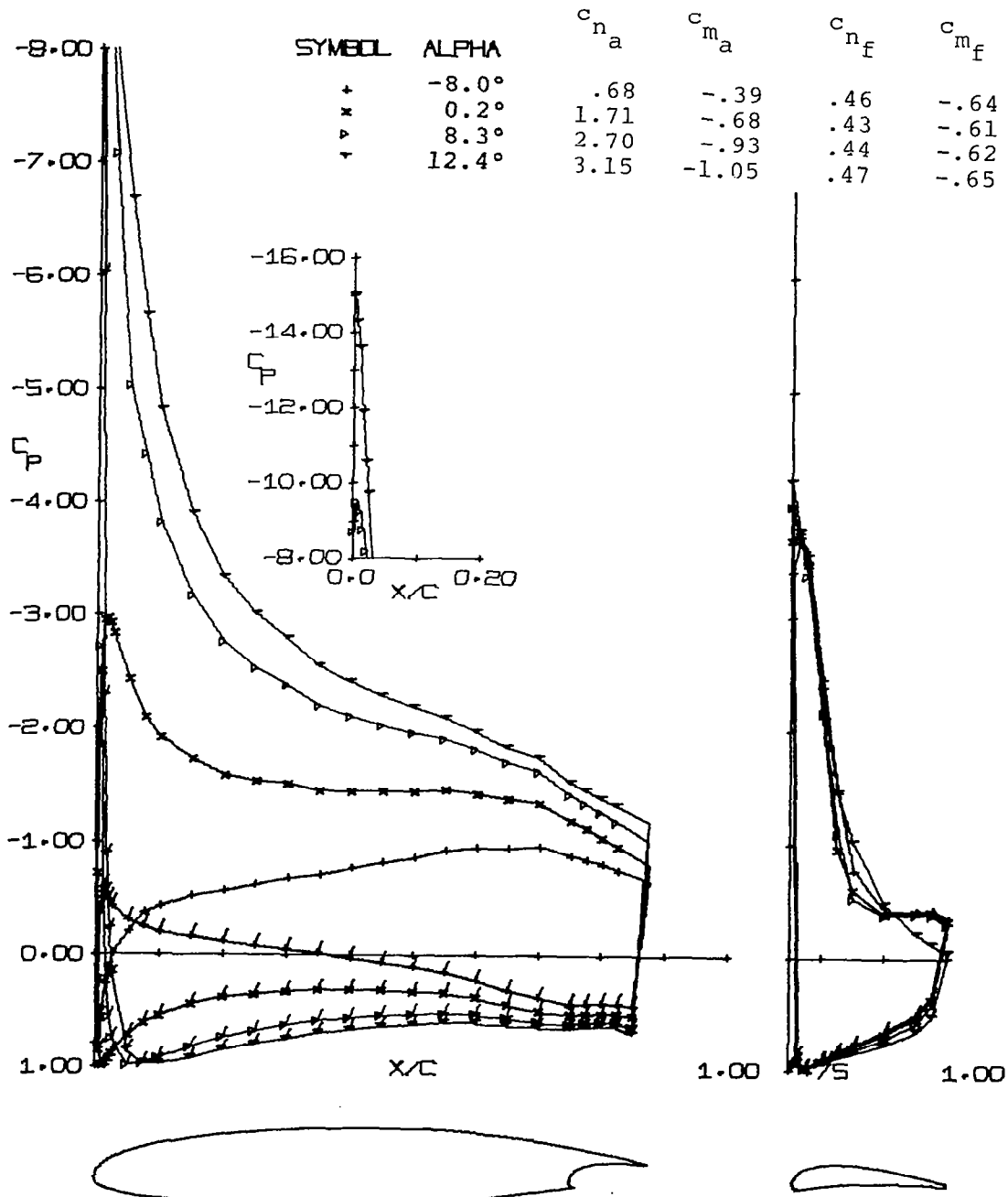
MACH NO. = 0.13

REYNOLDS NO. = 2.2 E 06

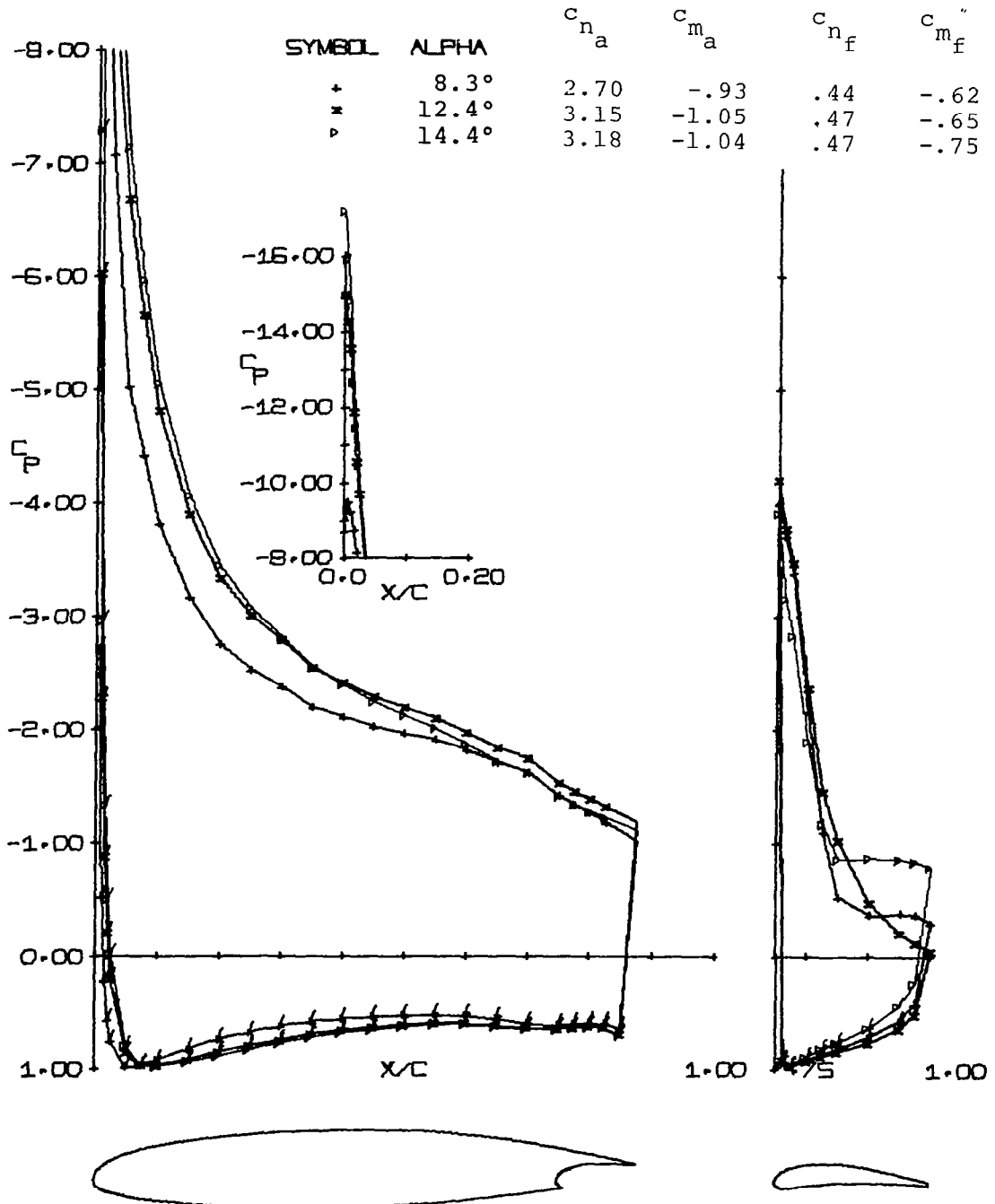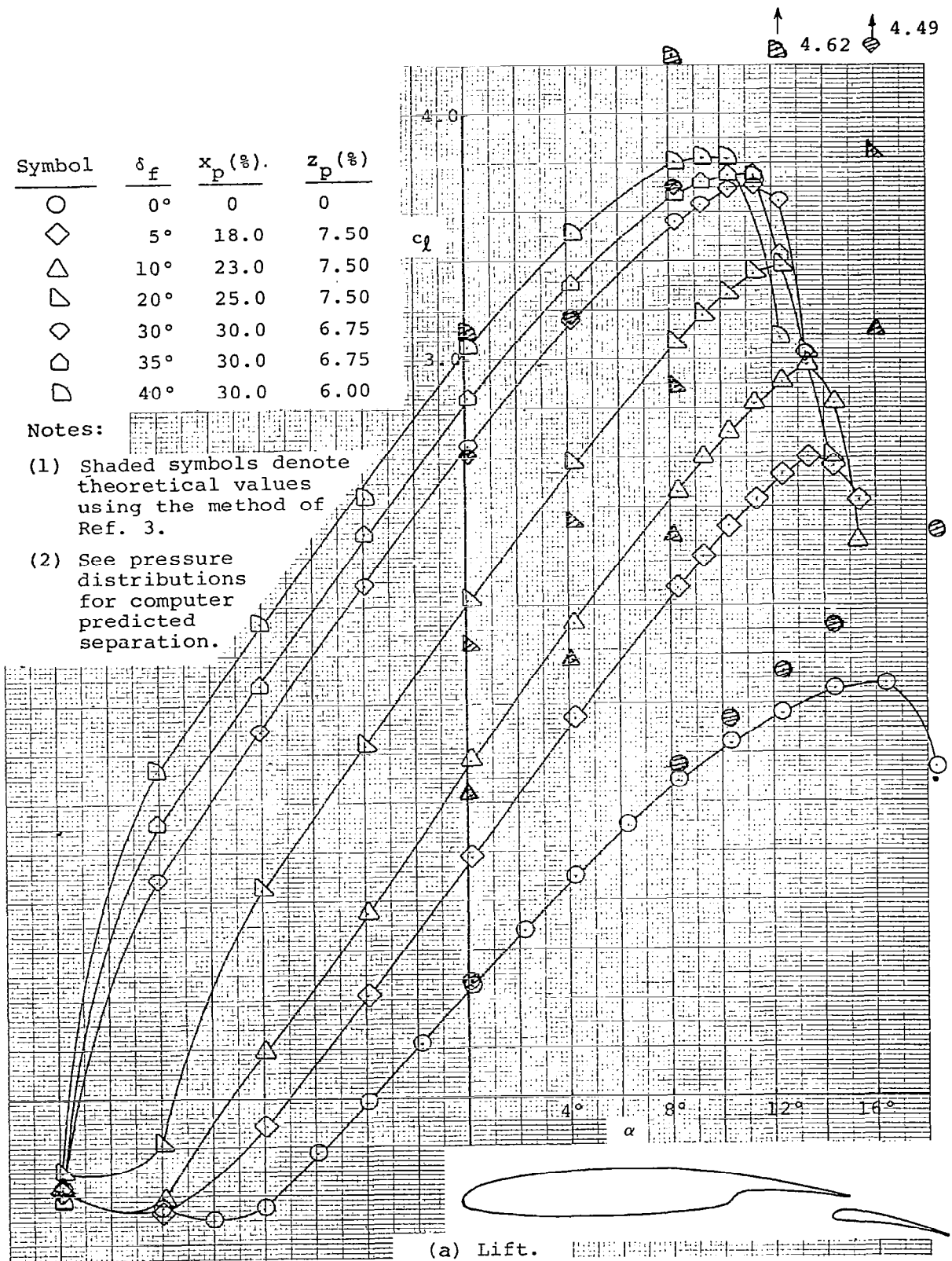| SYMBOL	ALPHA	c_{n_a}	c_{m_a}	c_{n_f}	c_{m_f}''
+	8.3°	2.70	−.93	.44	−.62
x	12.4°	3.15	−1.05	.47	−.65
▷	14.4°	3.18	−1.04	.47	−.75

Figure 10 – Concluded.

58

4.62 4.49

Symbol	δ_f	$x_p(\%)$	$z_p(\%)$
◯	0°	0	0
◇	5°	18.0	7.50
△	10°	23.0	7.50
◁	20°	25.0	7.50
◇	30°	30.0	6.75
⬠	35°	30.0	6.75
⬡	40°	30.0	6.00

Notes:
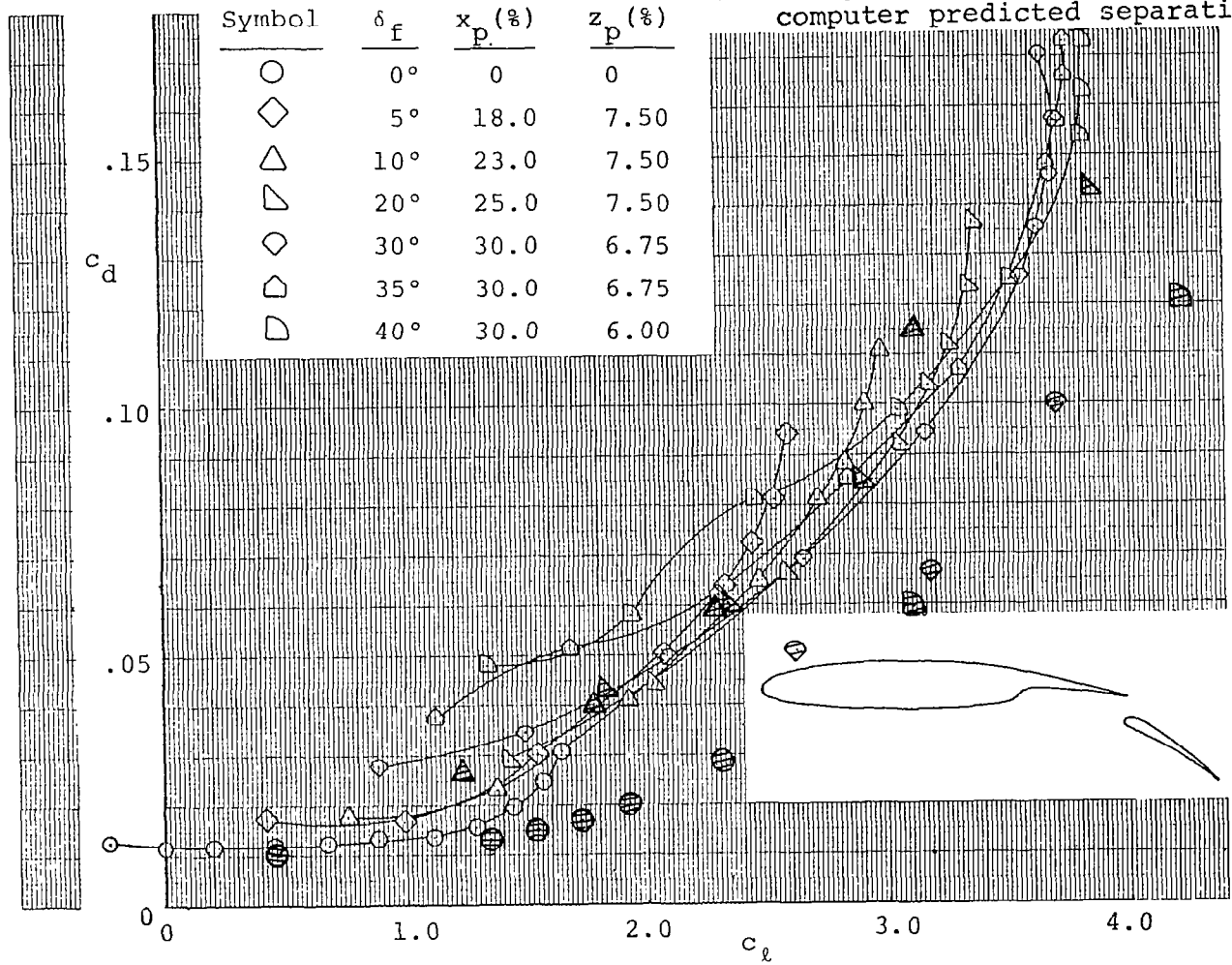
(1) Shaded symbols denote theoretical values using the method of Ref. 3.

(2) See pressure distributions for computer predicted separation.

c_l

4.0

3.0

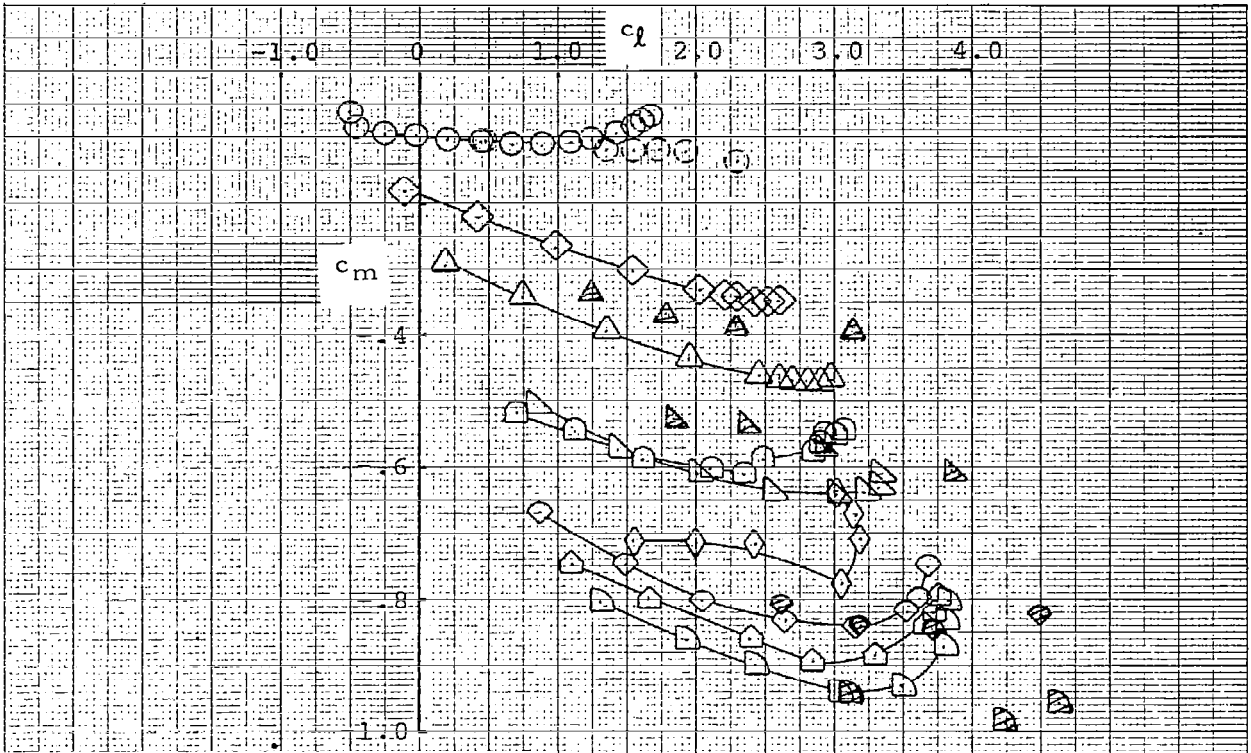4°   8°   12°   16°

α

(a) Lift.

Figure 11 - Theoretical and Experimental Force Characteristics.
with 30% Fowler Flap.

59

Notes: (1) Shaded symbols denote theoretical values using the method of Ref. 3.

(2) See pressure distributions for computer predicted separation.

Symbol	δ_f	$x_p.(\%)$	$z_p.(\%)$
◯	0°	0	0
◇	5°	18.0	7.50
△	10°	23.0	7.50
◹	20°	25.0	7.50
◇	30°	30.0	6.75
⬠	35°	30.0	6.75
◺	40°	30.0	6.00

(b) Drag.

Figure 11- ·Continued.

Symbol	δ_f	x_p (%)	z_p (%)
○	0°	0	0
◇	5°	18.0	7.50
△	10°	23.0	7.50
◺	20°	25.0	7.50
◇	30°	30.0	6.75
⬠	35°	30.0	6.75
◖	40°	30.0	6.00
◇	50°	27.0	8.00
⬠	60°	28.0	8.75

Notes:

(1) Shaded symbols denote theoretical values using the method of Ref. 3.

(2) See pressure distributions for computer predicted separation.
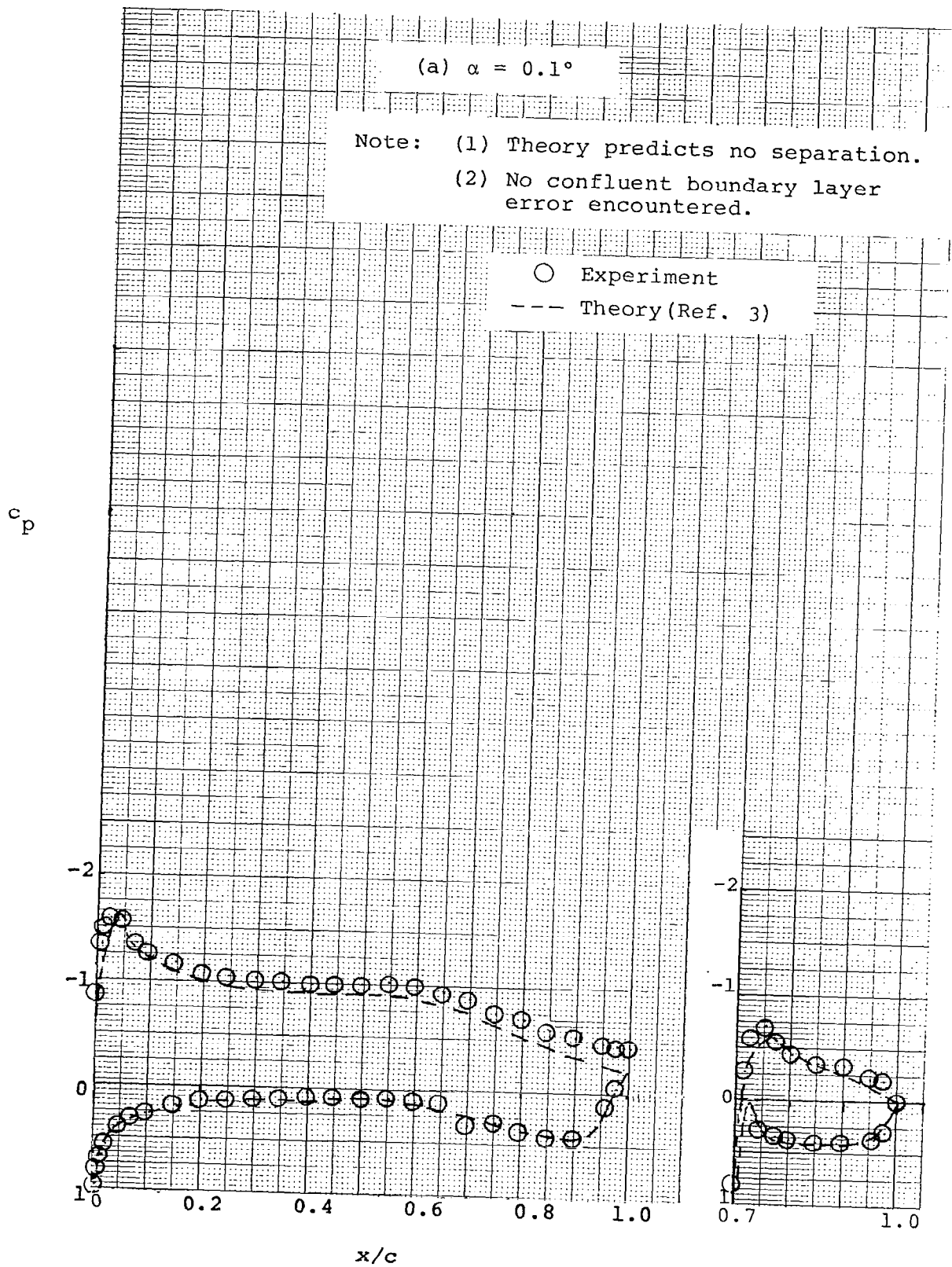
(c) Moment.

Figure 11 - Concluded.

61

(a) $\alpha = 0.1°$

Note: (1) Theory predicts no separation.

(2) No confluent boundary layer error encountered.

○   Experiment

– – – Theory(Ref. 3)

x/c

Figure 12 - Pressure Distributions with
30% Fowler Flap, 10° Flap Deflection.

62

Figure 12- Continued.

63

(c) $\alpha = 8.3°$

Note: (1) Theory predicts no separation.
      (2) No confluent boundary layer
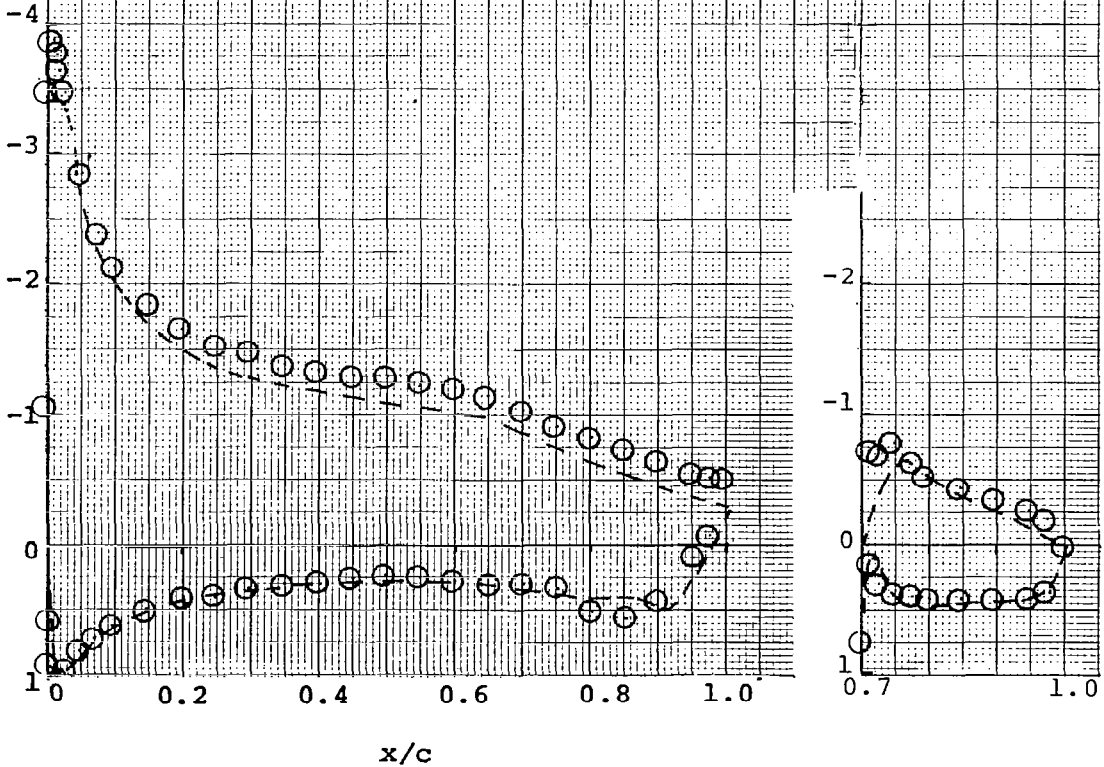   error encountered.

◯ Experiment
--- Theory(Ref. 3)

Figure 12- Continued.
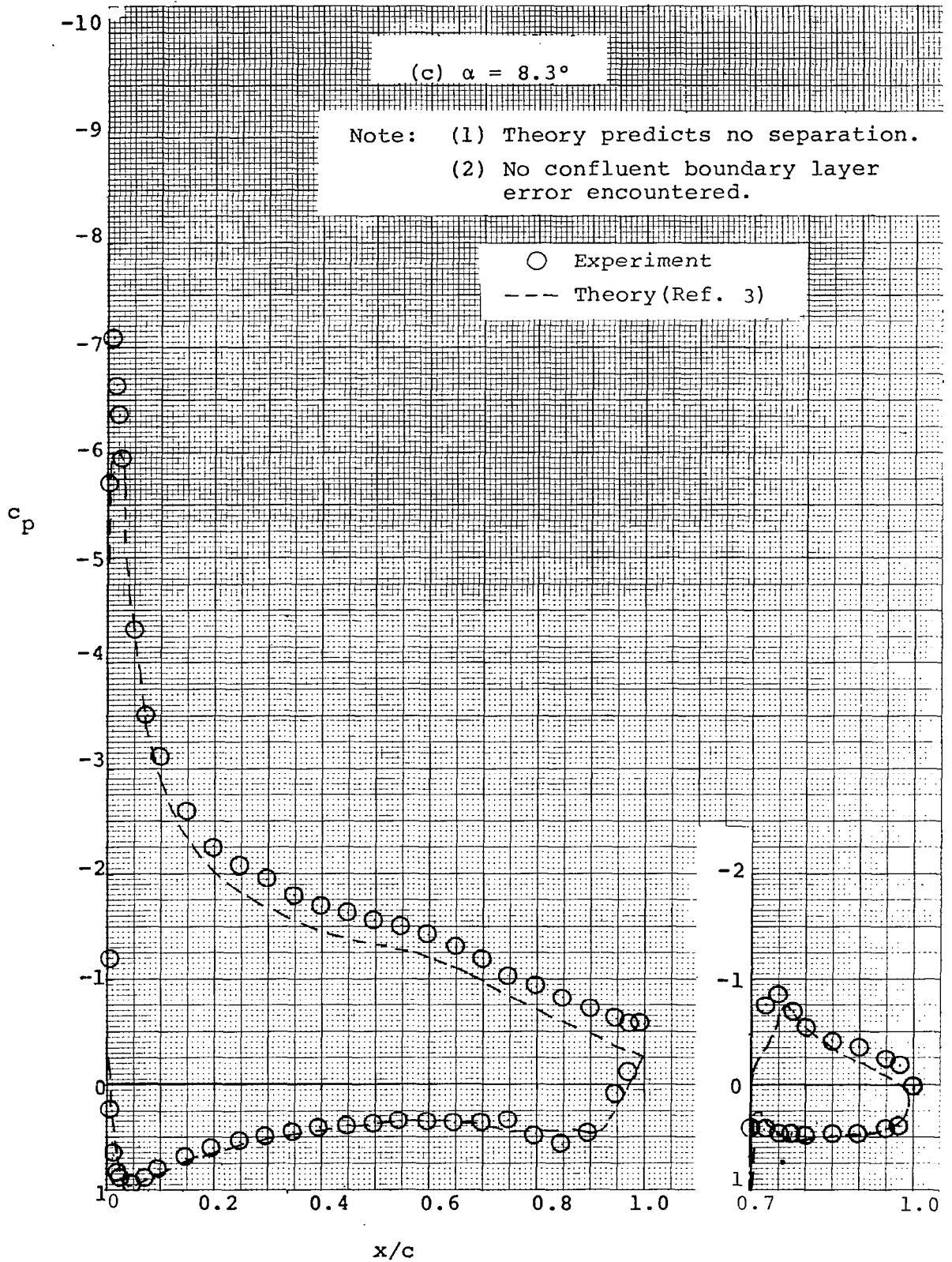
(d) α = 16.1°

Note: (1) Theory predicts separation at
x/c = .92 (upper surface).

(2) No confluent boundary layer
error encountered.

○ Experiment
--- Theory(Ref. 3)

Figure 12- Concluded .

(a) $\alpha = 0.1°$

Note: (1) Theory predicts no separation.
(2) No confluent boundary layer error encountered.

◯ Experiment
– – – Theory (Ref. 3)

Figure 13 – Pressure Distributions with
30% Fowler Flap, 20° Flap Deflection.

66

(b) $\alpha = 4.2°$

Note: (1) Theory predicts no separation.
(2) No confluent boundary layer error encountered.

○ Experiment
— — — Theory(Ref. 3)

c_p

x/c

Figure 13- Continued.

(c) α = 8.3°

Note: (1) Theory predicts no separation.

(2) No confluent boundary layer error encountered.

○ Experiment

— — — Theory (Ref. 3)

x/c

Figure 13- Continued.

$c_{p_{min}} = -21.35$ (d) $\alpha = 16.1°$

Note: (1) Theory predicts separation at
x/c = .95 (upper surface).

(2) No confluent boundary layer
error encountered.

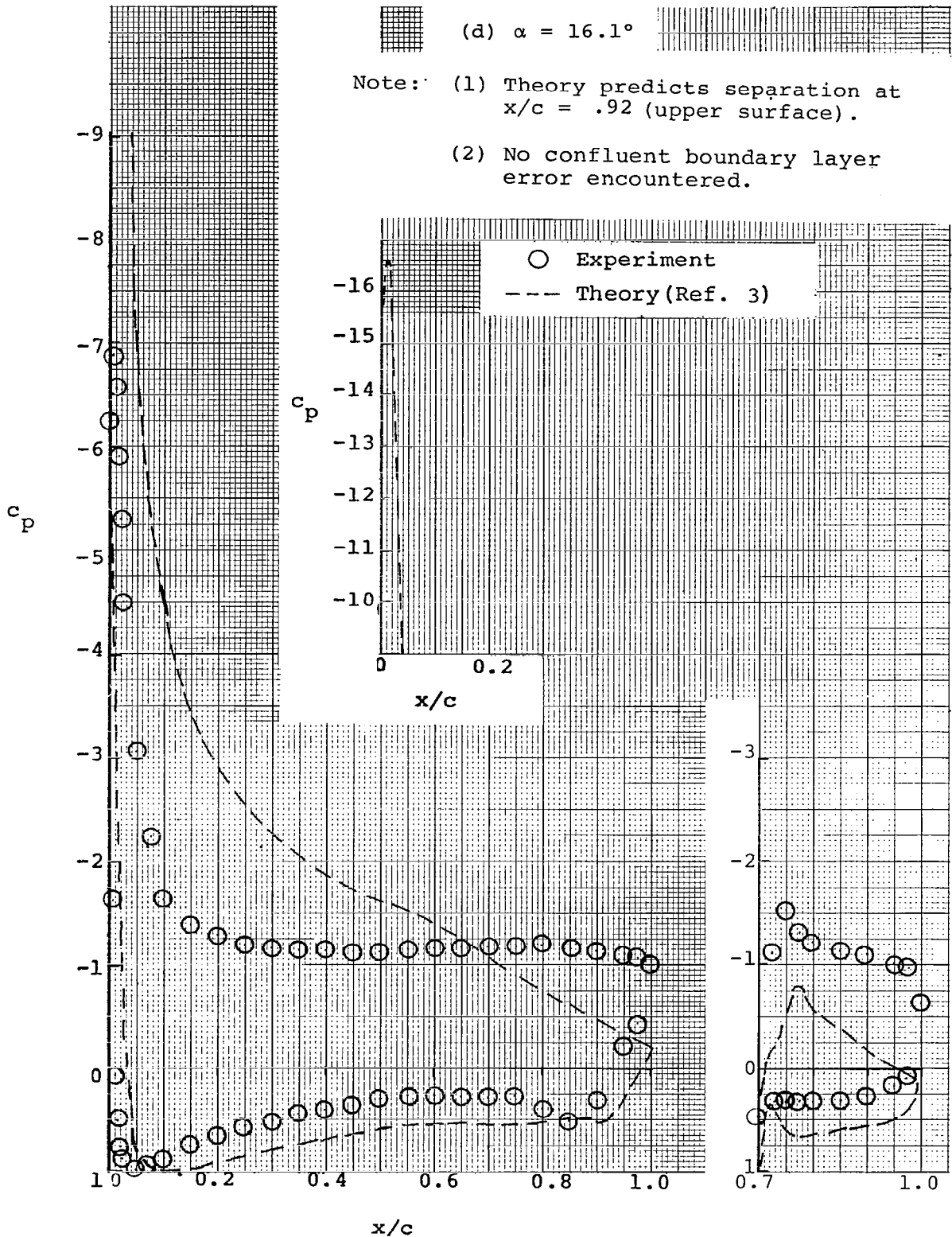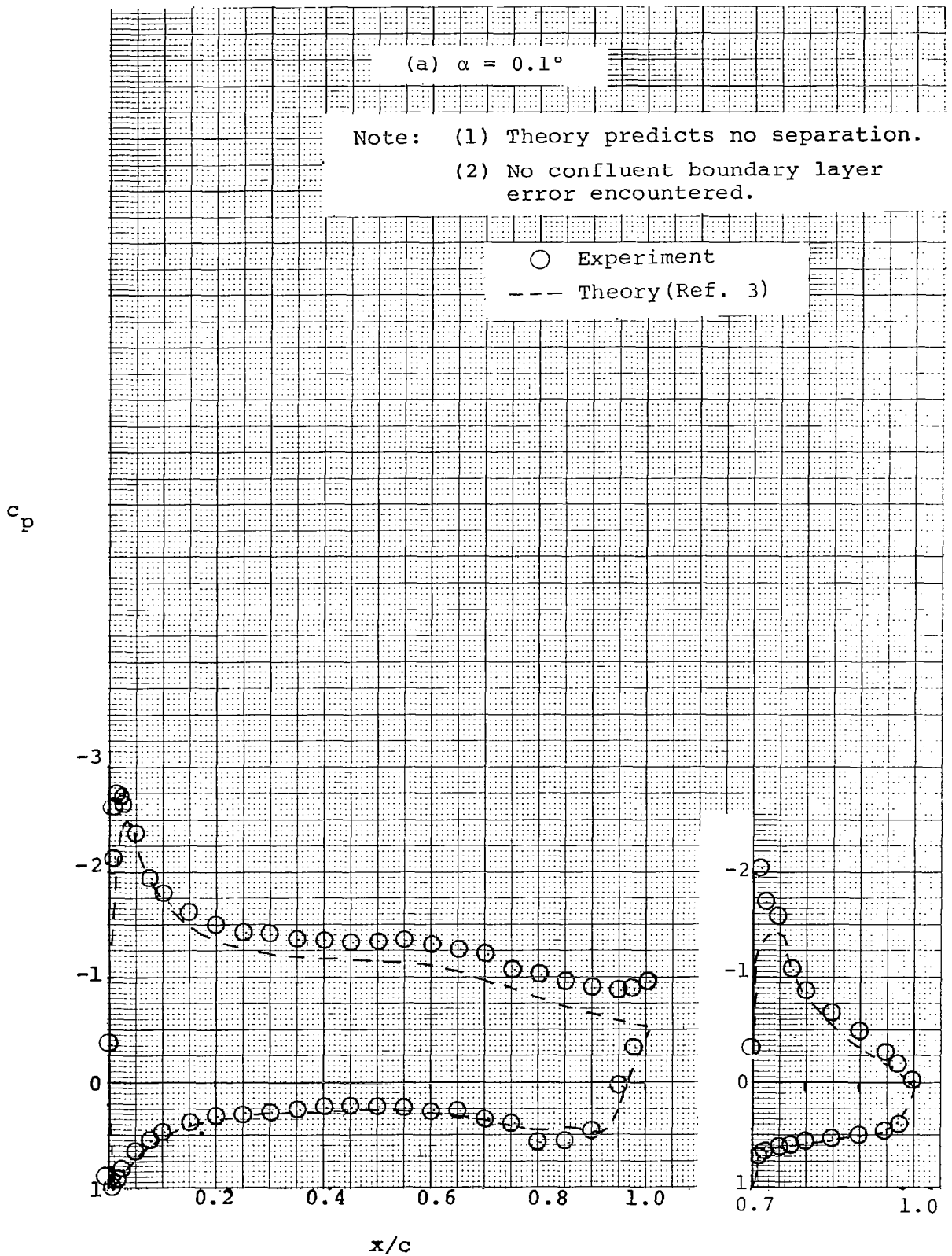○ Experiment
--- Theory(Ref. 3)

x/c
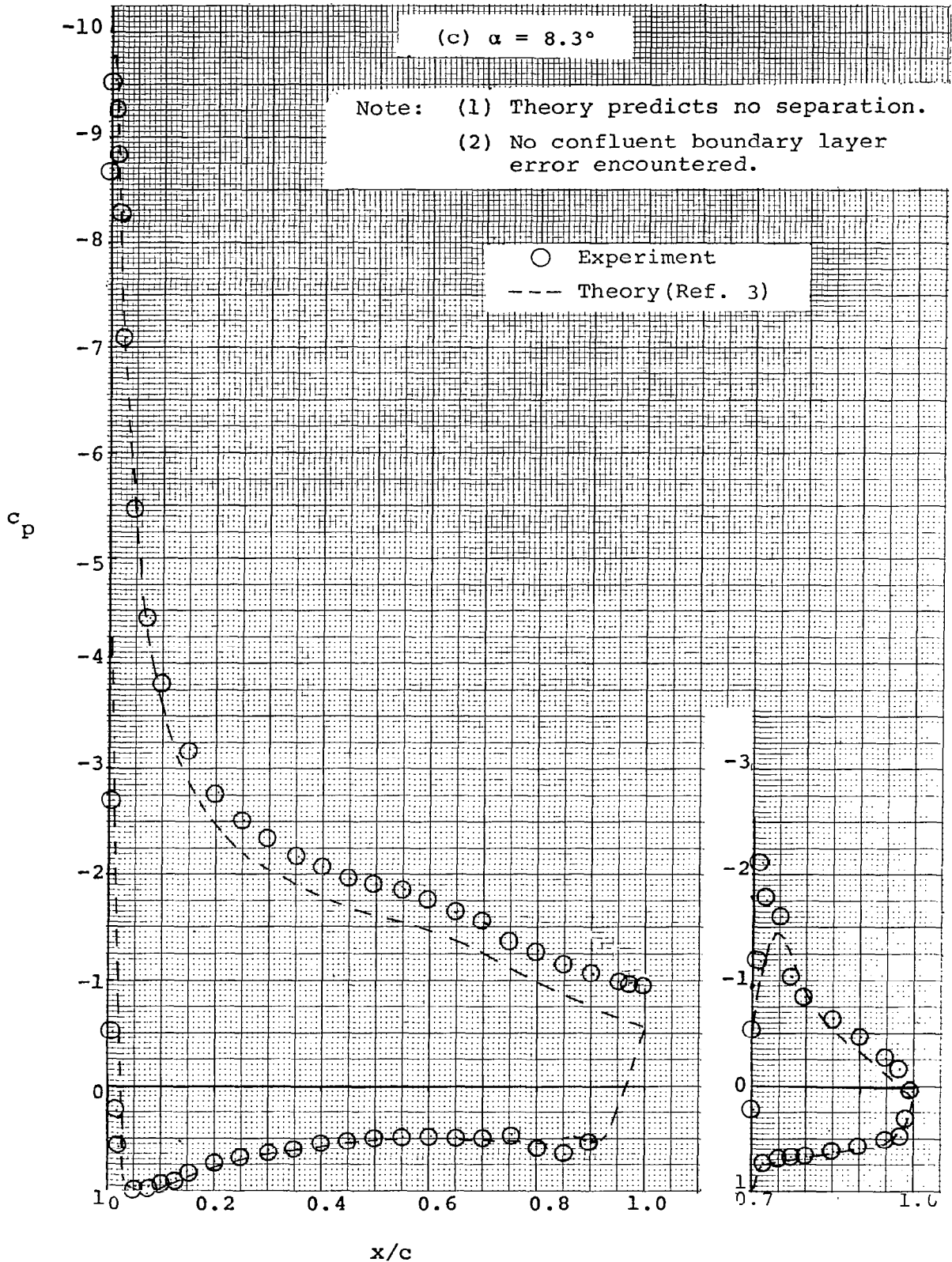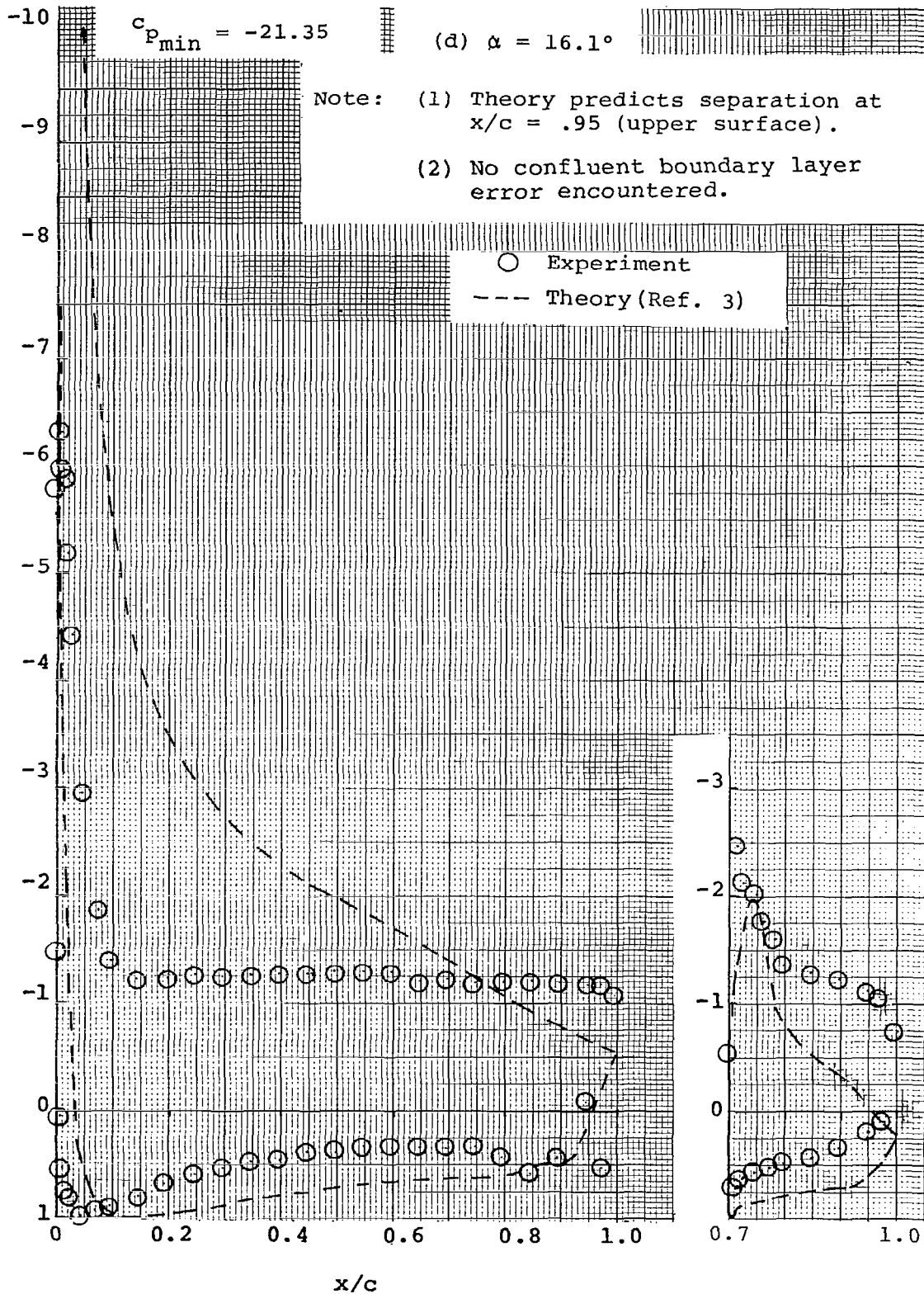
Figure 13 - Concluded.

69
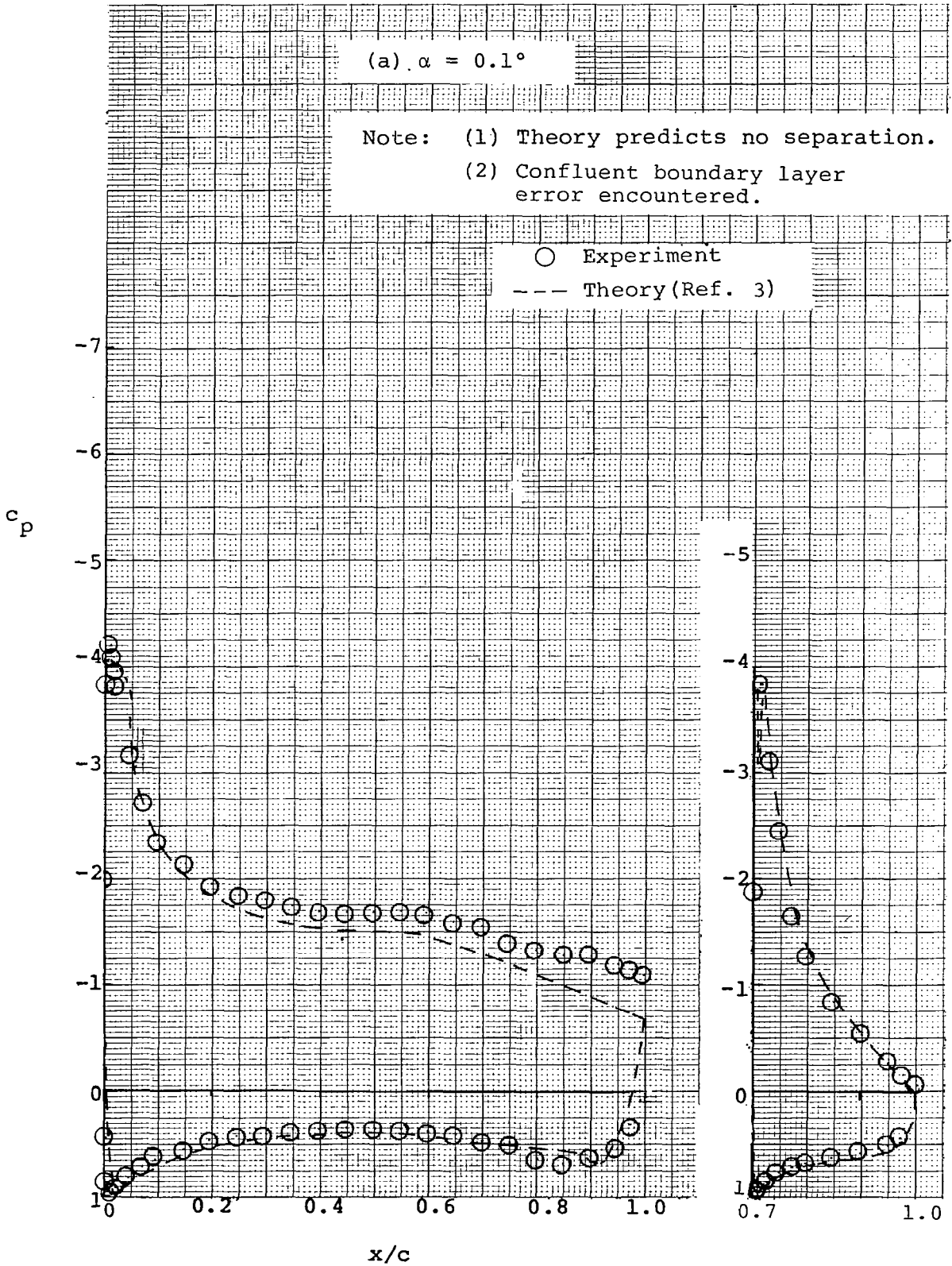
Figure 14 - Pressure Distributions with
30% Fowler Flap, 30° Flap Deflection.

(b) $\alpha = 4.1°$

Note: (1) Theory predicts no separation.

(2) Confluent boundary layer error encountered.
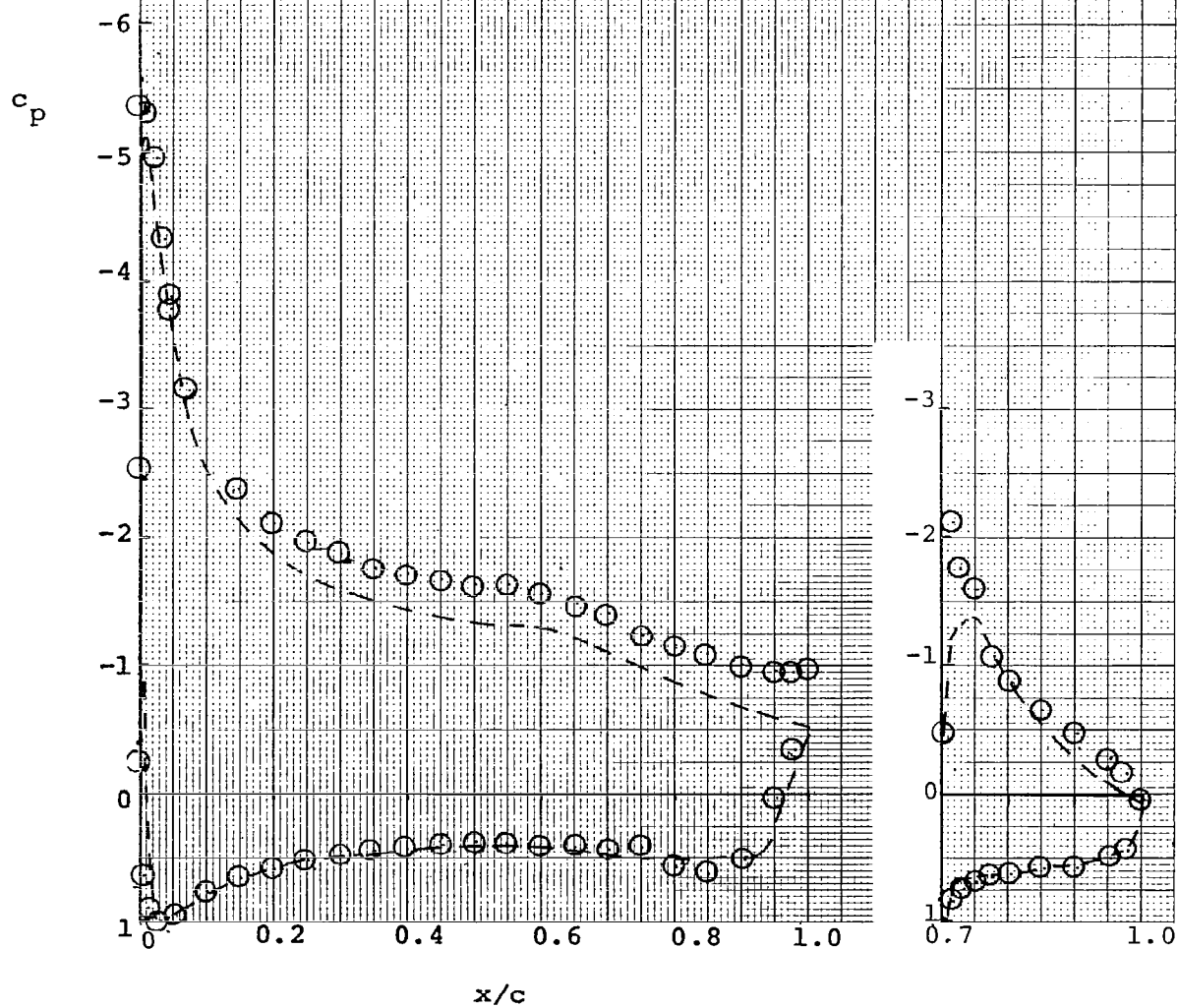
○ Experiment

– – – Theory (Ref. 3)

Figure 14 - Continued.

71

(c) α = 8.2°

Note: (1) Theory predicts no separation.

(2) Confluent boundary layer error encountered.

○ Experiment

– – – Theory(Ref. 3)

Figure 14 - Continued.

72

Figure 14 - Concluded.

(a) $\alpha = 0.1°$

○   Experiment
— — — Theory(Ref. 3)

Note: (1) Theory predicts separation at
               x/c = .95 (lower surface).

          (2) Confluent boundary layer error
               encountered.

c_p

x/c
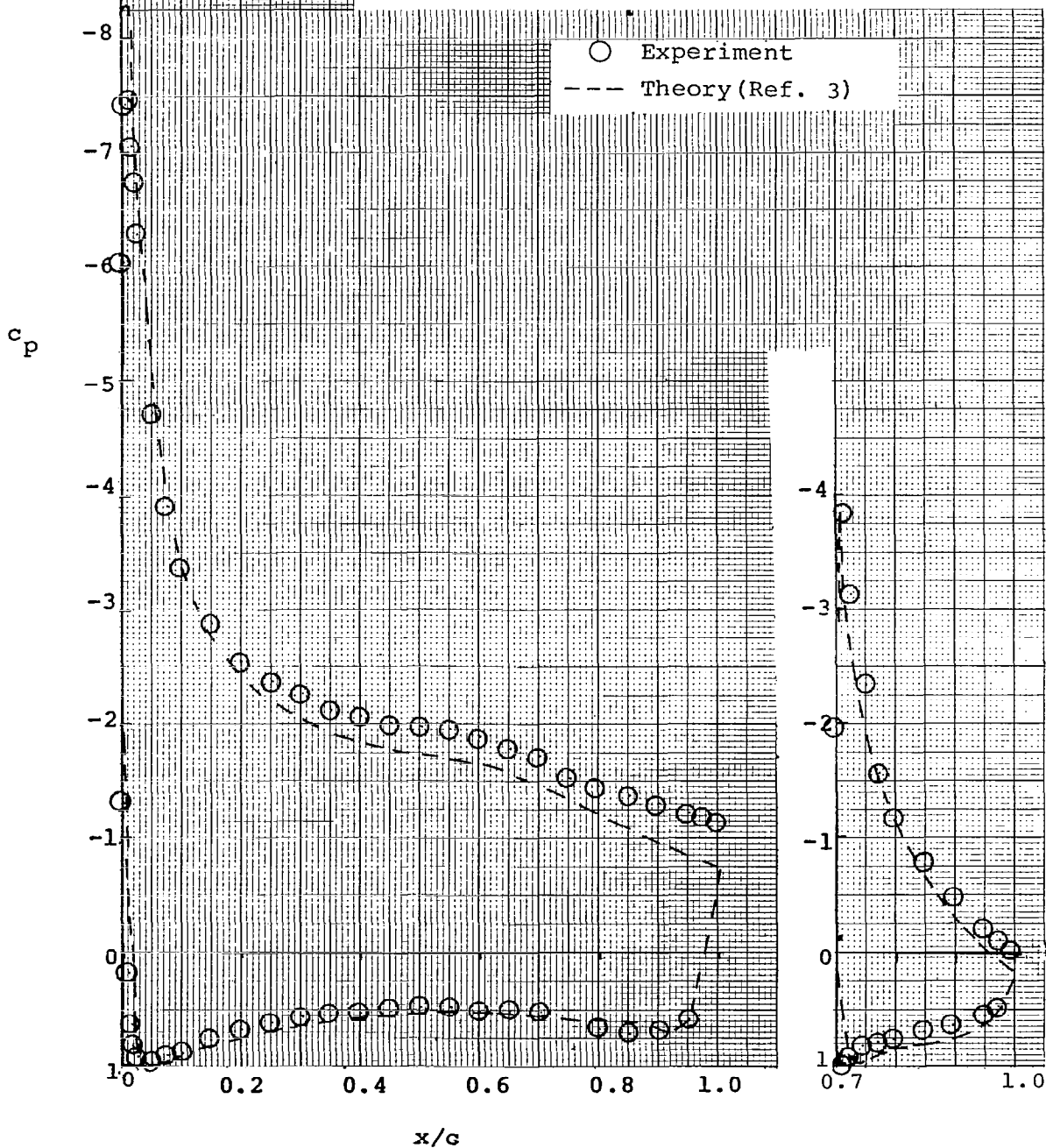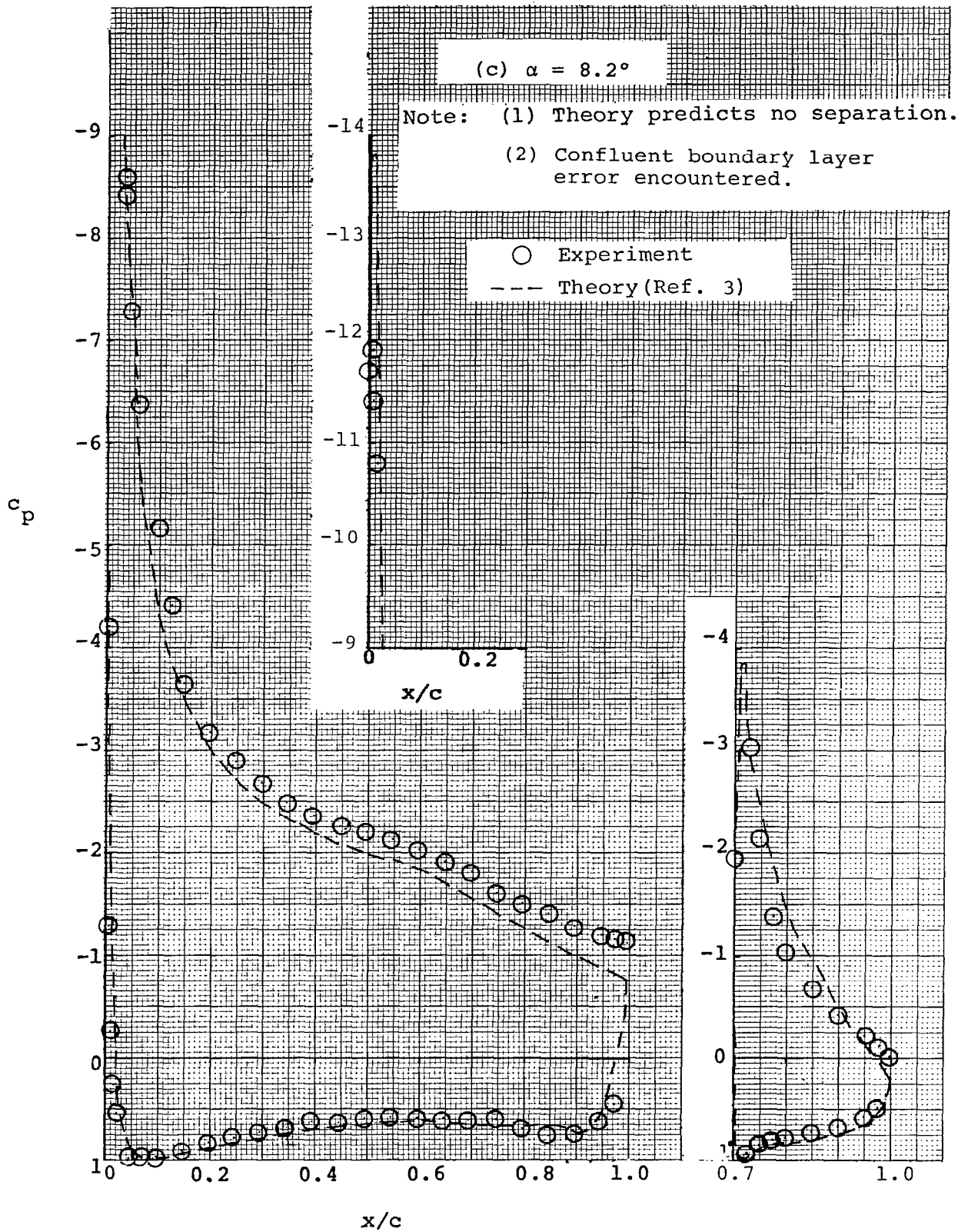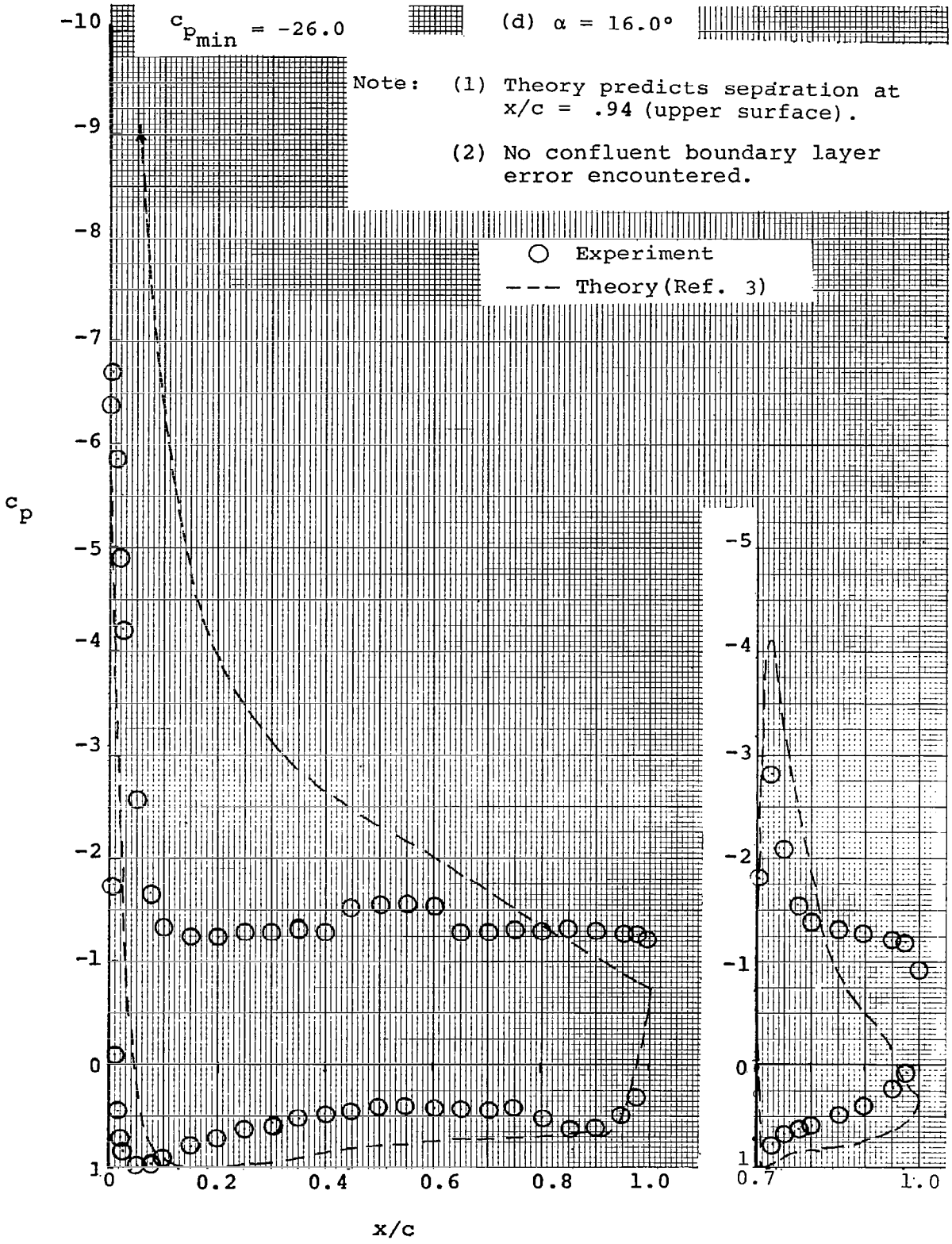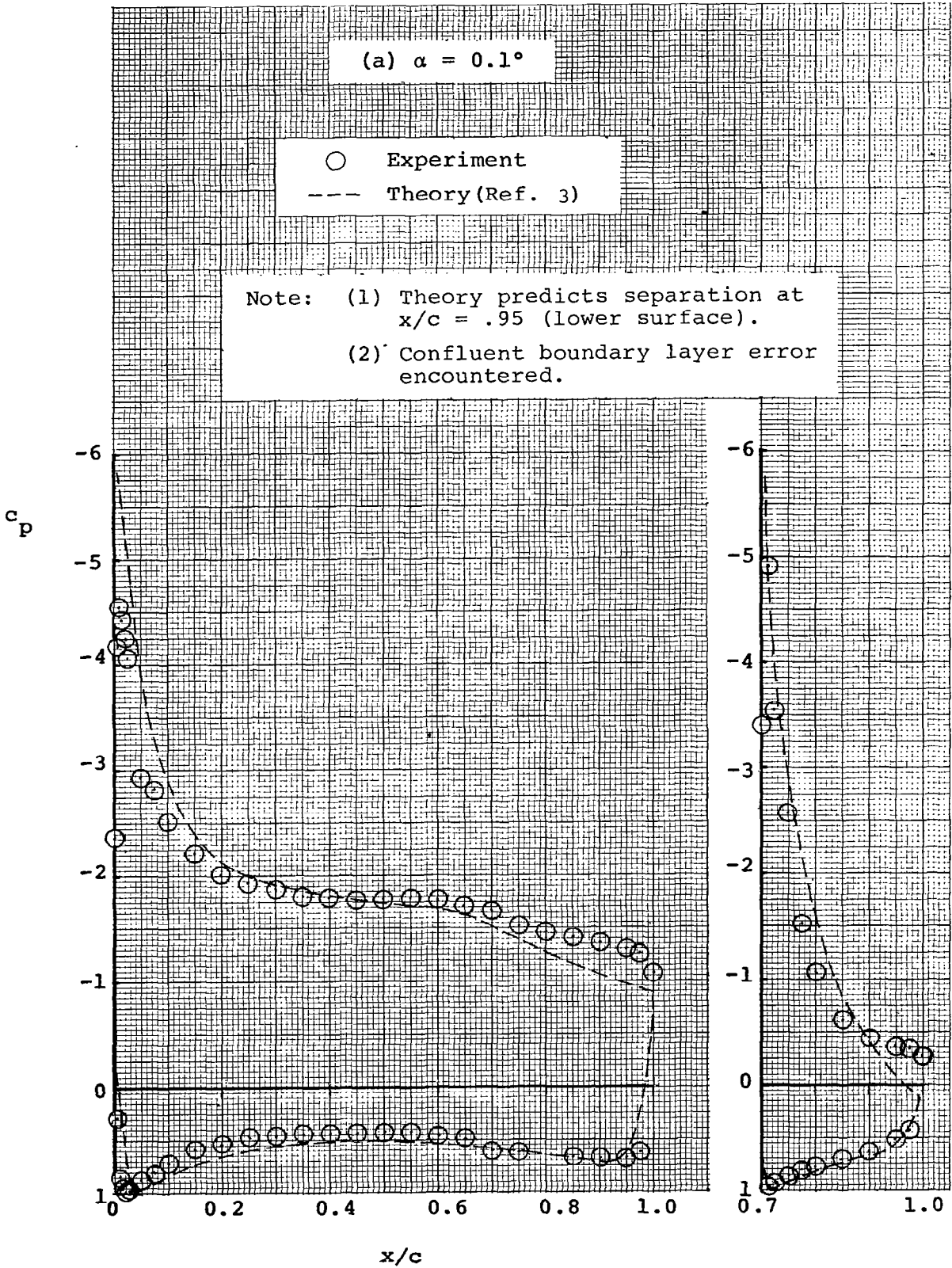
Figure 15- Pressure Distributions with
30% Fowler Flap, 40° Flap Deflection.

74

(b) α = 8.2°

○ Experiment
--- Theory (Ref. 3)

Note: (1) Theory predicts separation at x/c = .96 (lower surface).

(2) Confluent boundary layer error encountered.

Figure 15- Continued.

75

(c) $\alpha = 12.3°$

○   Experiment
---   Theory(Ref. 3)

Note: (1) Theory predicts separation at
              $x/c = .97$ (lower surface).
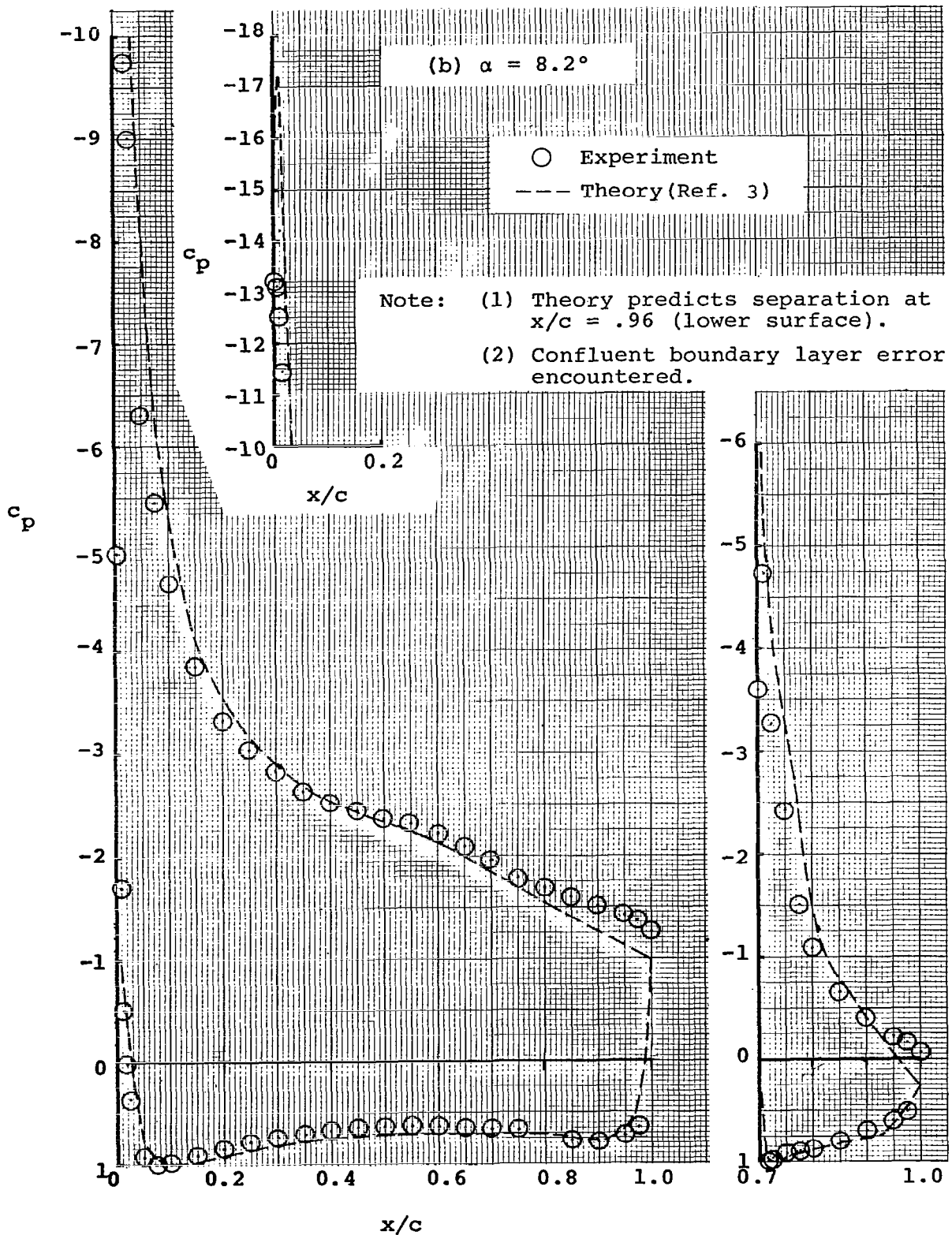
        (2) Confluent boundary layer error
              encountered.
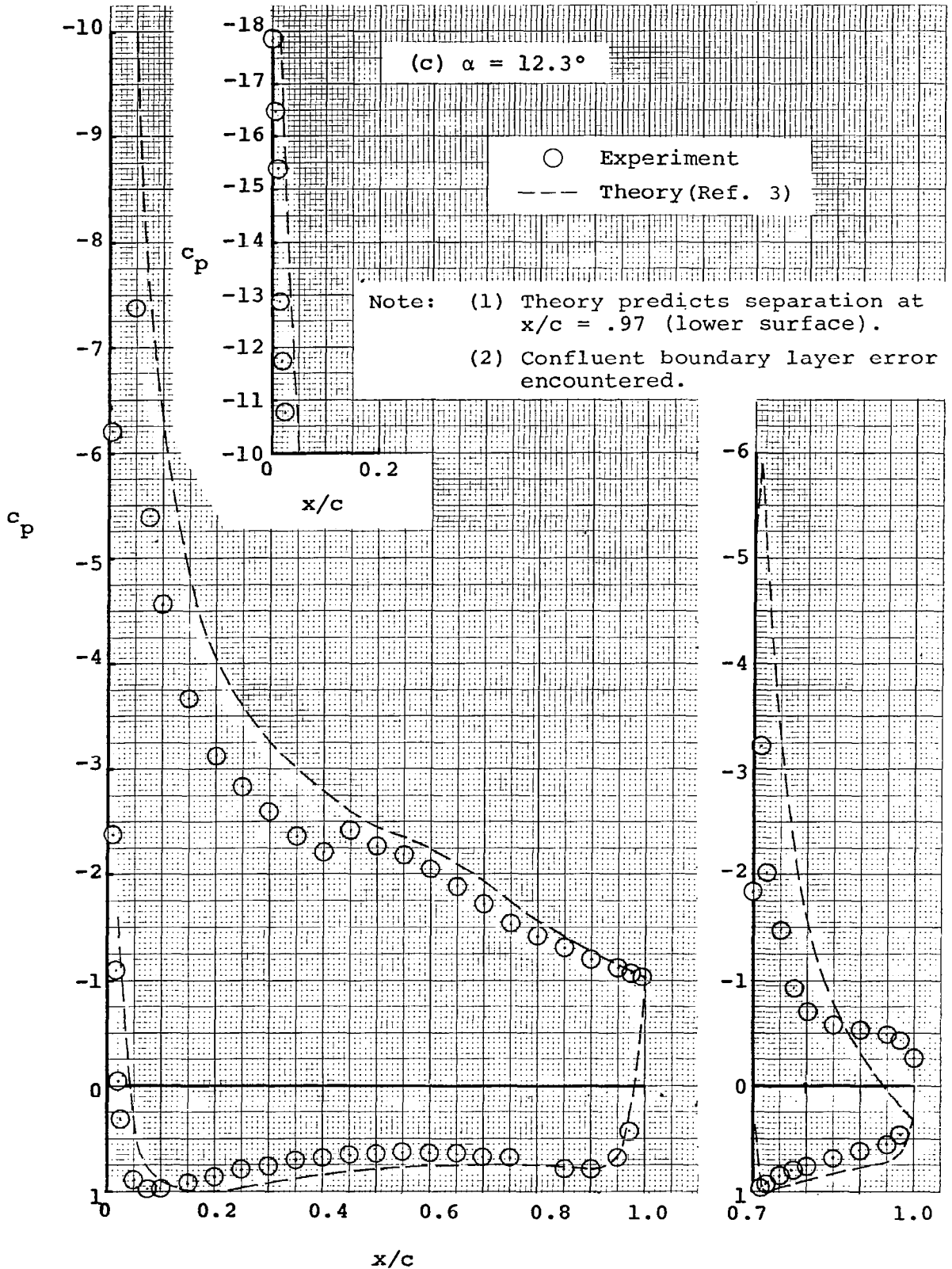
Figure 15 - Concluded.

(a) FLAP DEFLECTION = 5.0 DEGREES

MACH NO. = 0.13

REYNOLDS NO. = 2.2 E 06

SYMBOL	ALPHA	c_{n_a}	c_{m_a}	c_{n_f}	c_{m_f}
+	0.2°	.87	−.39	.13	−.24
×	4.2°	1.42	−.54	.16	−.28
▶	8.3°	1.93	−.68	.20	−.33
▼	12.3°	2.35	−.77	.24	−.39
◀	16.2°	1.71	−.64	.35	−.58

Flagged Symbols Denote
Lower Surface Pressures

C_P

X/C
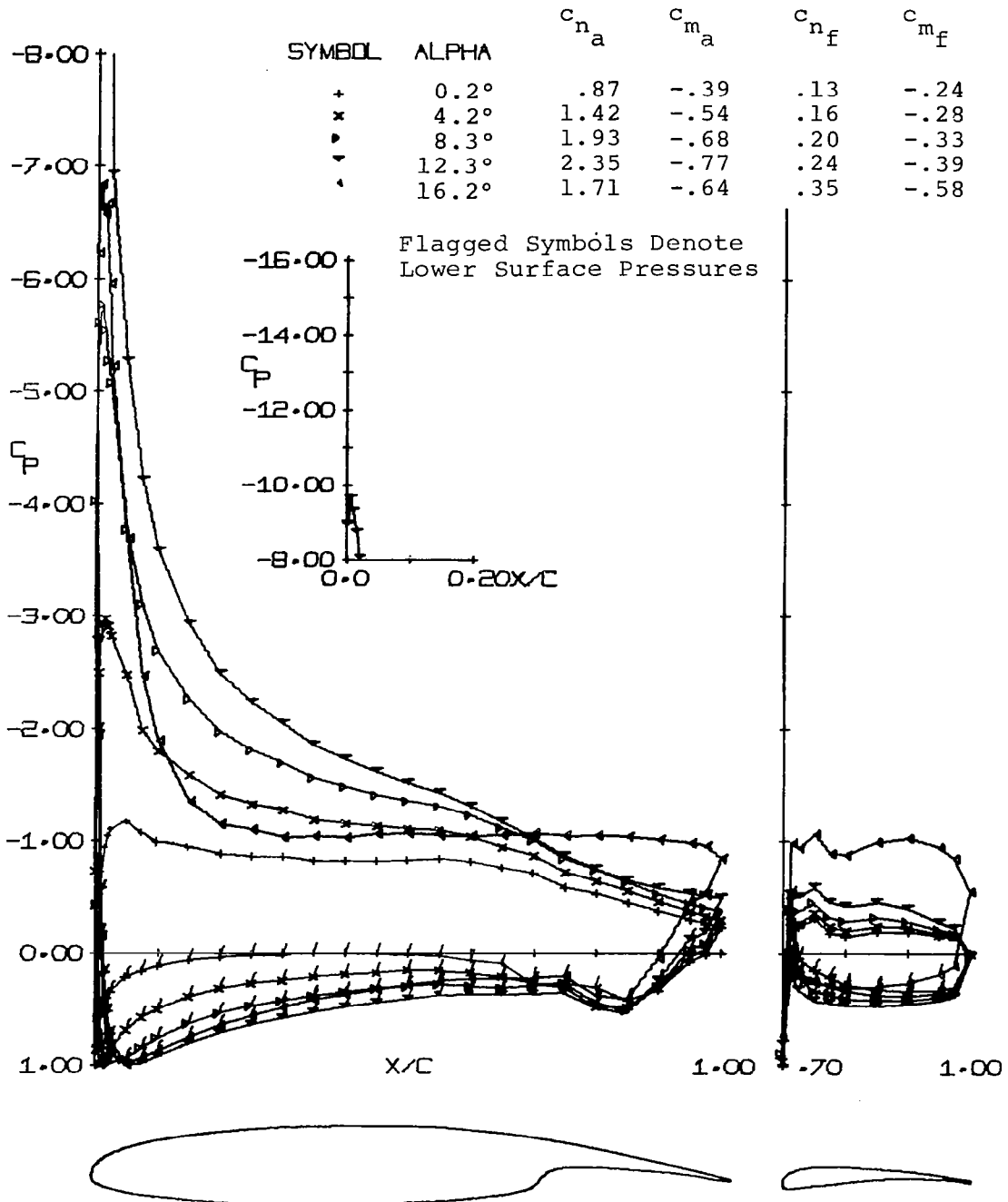
Figure 16 - Experimental Pressure Distributions with 30% Fowler Flap.

SYMBOL	ALPHA	c_{n_a}	c_{m_a}	c_{n_f}	c_{m_f}
+	0.1°	1.17	−.52	.22	−.34
x	4.2°	1.74	−.68	.25	−.37
▶	8.3°	2.28	−.82	.28	−.41
▼	12.3°	2.71	−.93	.31	−.44
◀	16.1°	1.81	−.73	.42	−.66

Figure 16 - Continued.

78

MACH NO. = 0.13

REYNOLDS NO. = 2.2 E 06

SYMBOL	ALPHA	c_{n_a}	c_{m_a}	c_{n_f}	c_{m_f}
+	0.1°	1.70	-.73	.39	-.50
×	4.2°	2.28	-.90	.41	-.52
▷	8.3°	2.80	-1.04	.41	-.53
▼	12.3°	3.15	-1.10	.41	-.54
◀	16.1°	1.88	-.79	.53	-.77

Figure 16 - Continued.

79
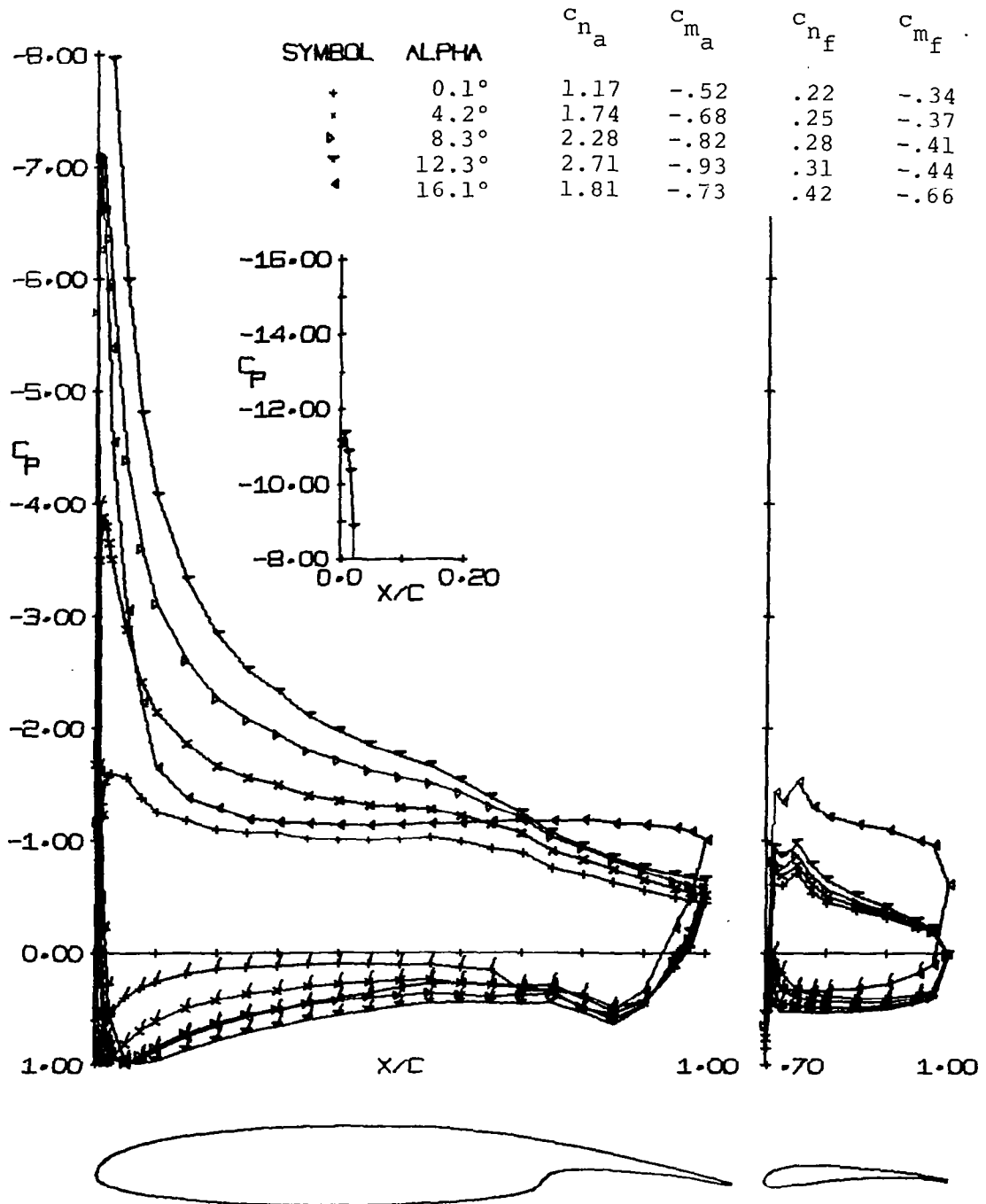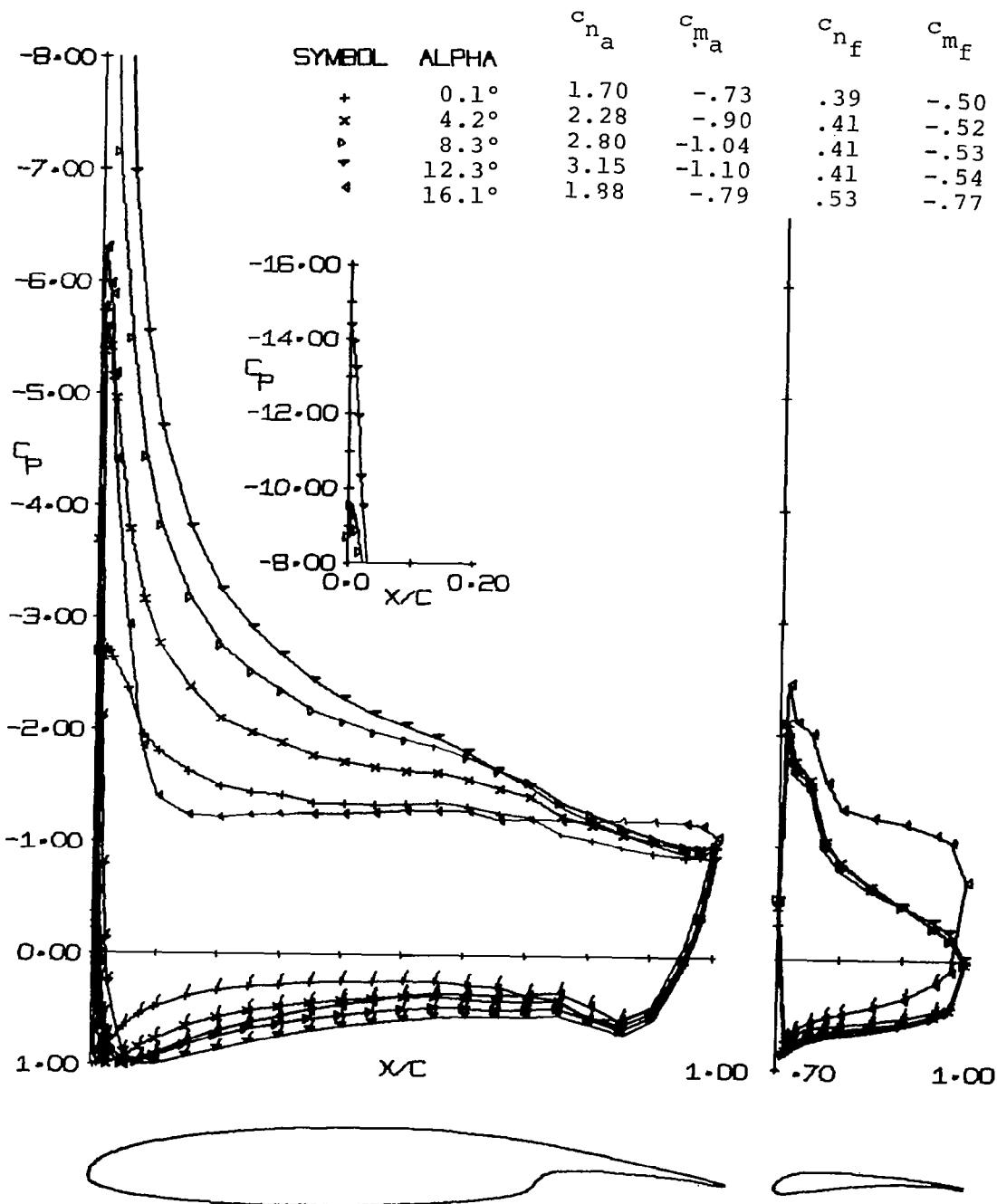
(d) FLAP DEFLECTION = 30.0 DEGREES

MACH NO. = 0.13

REYNOLDS NO. = 2.2 E 06

SYMBOL	ALPHA	c_{n_a}	c_{m_a}	c_{n_f}	c_{m_f}
+	0.1°	2.27	-1.00	.53	-.61
×	4.1°	2.83	-1.16	.53	-.61
▶	8.2°	3.31	-1.28	.51	-.60
▼	12.3°	3.51	-1.28	.45	-.58
◀	16.0°	2.06	-.93	.60	-.83
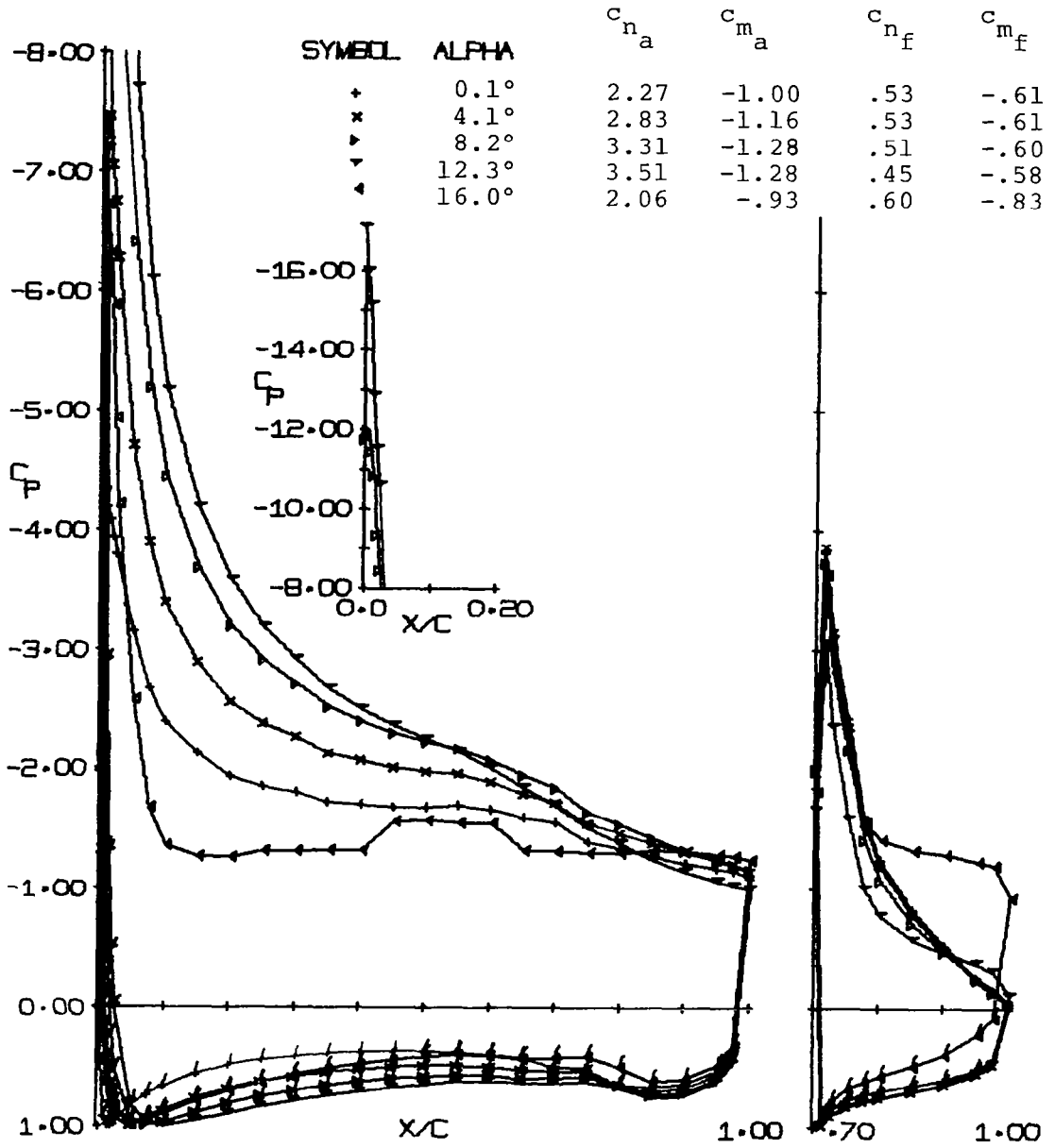
Figure 16 - Continued.

(e) FLAP DEFLECTION = 40.0 DEGREES
MACH NO. = 0.13
REYNOLDS NO. = 2.2 E 06

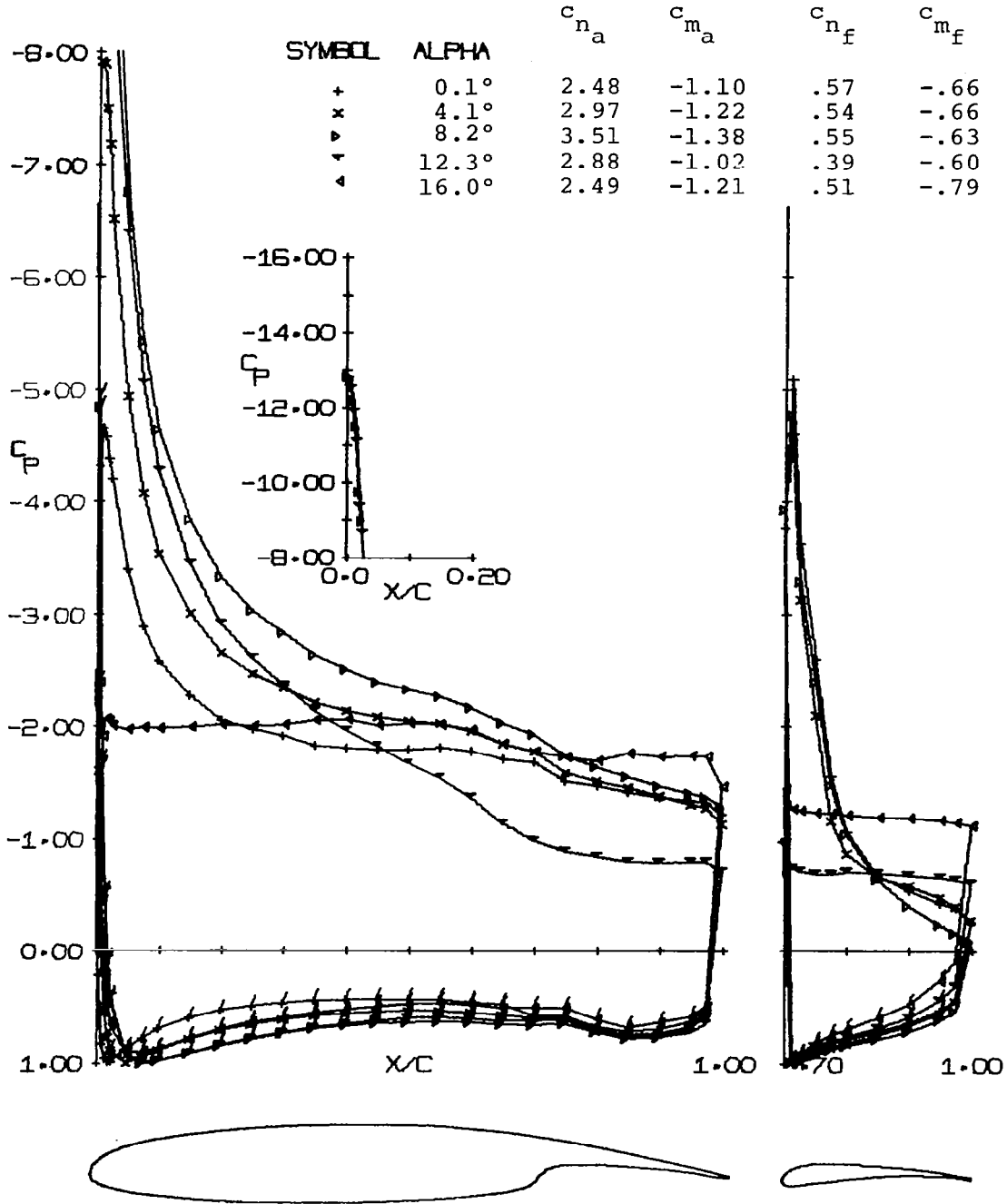| SYMBOL	ALPHA	c_{n_a}	c_{m_a}	c_{n_f}	c_{m_f}
+	0.1°	2.48	−1.10	.57	−.66
×	4.1°	2.97	−1.22	.54	−.66
▷	8.2°	3.51	−1.38	.55	−.63
▼	12.3°	2.88	−1.02	.39	−.60
◀	16.0°	2.49	−1.21	.51	−.79

Figure 16 - Concluded.

81

1. Report No. NASA CR-2948	2. Government Accession No.	3. Recipient's Catalog No.
4. Title and Subtitle Pressure Distributions for the GA(W)-2 Airfoil With 20% Aileron, 25% Slotted Flap and 30% Fowler Flap		5. Report Date February 1978
		6. Performing Organization Code
7. Author(s) W. H. Wentz, Jr. and K. A. Fiscko		8. Performing Organization Report No. AR 76-3
9. Performing Organization Name and Address Wichita State University Wichita, Kansas 67208		10. Work Unit No. 505-06-33-10
		11. Contract or Grant No. NSG 1165
12. Sponsoring Agency Name and Address NASA Langley Research Center Hampton, Virginia 23665		13. Type of Report and Period Covered Contractor Report
		14 Sponsoring Agency Code

15. Supplementary Notes

Langley technical monitor: Robert J. McGhee
Topical Report

16. Abstract

Surface pressure distributions have been measured for the 13%-thick GA(W)-2 airfoil section fitted with 20% aileron, 25% slotted flap and 30% Fowler flap. All tests were conducted at a Reynolds number of 2.2×10^6 and a Mach number of 0.13. Pressure distribution and force and moment coefficient measurements are compared with theoretical results for a number of cases. Agreement between theory and experiment is generally good for low angles of attack and small flap deflections. For high angles and large flap deflections where regions of separation are present, the theory is inadequate. Theoretical drag predictions are poor for all flap-extended cases.

17. Key Words (Suggested by Author(s)) Low-speed Experiment Airfoil Theory Aileron High-lift Pressure distributions		18. Distribution Statement FEDD Distribution Subject Category 02		
19. Security Classif. (of this report) Unclassified	20. Security Classif. (of this page) Unclassified		21. No. of Pages 85	22. Price* $6.00

*Available from NASA's Industrial Application Centers